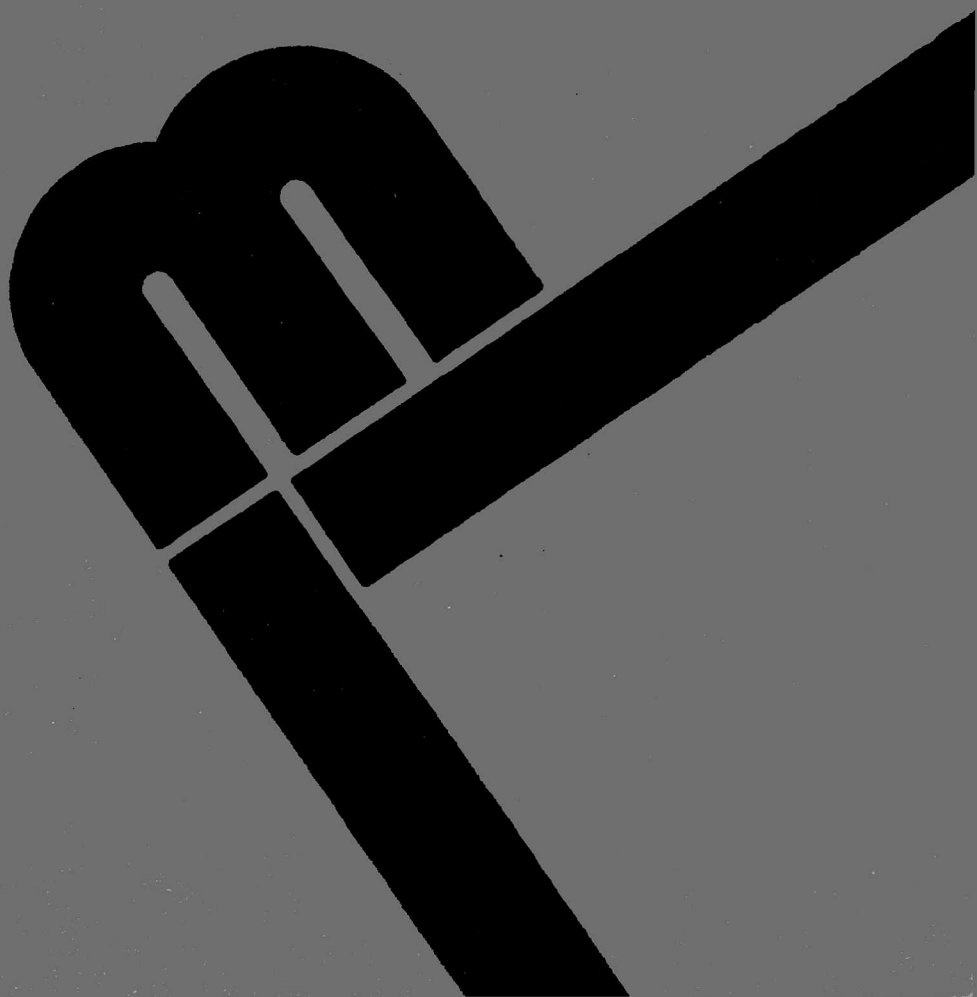


Jan Misiewicz

Optical excitations in zinc phosphide (Zn_3P_2)

Wrocław 1989



PRACE NAUKOWE POLITECHNIKI WROCLAWSKIEJ

**Scientific Papers of the Institute of Physics
of the Technical University of Wrocław**

No. 28

No. 28

Monographs

No. 17

1989

Jan MISIEWICZ

Optical excitations in zinc phosphide (Zn_3P_2)

Prace Naukowe Instytutu Fizyki
Politechniki Wrocławskiej

28

Seria:
Monografie

17



Jan Misiewicz

**Optical excitations
in zinc phosphide (Zn_3P_2)**



Wydawnictwo Politechniki Wrocławskiej · Wrocław 1989

Recenzenci

Robert R. GAŁAZKA
Jerzy GINTER
Janusz M. PAWLIKOWSKI

Opracowanie redakcyjne

Danuta SOWIŃSKA

Weryfikacja językowa i korekta

Hanna BASAROWA

© Copyright by Wydawnictwo Politechniki Wrocławskiej, Wrocław 1989

WYDAWNICTWO POLITECHNIKI WROCŁAWSKIEJ
Wybrzeże Wyspiańskiego 27, 50-370 Wrocław

ISSN 0370-0828

Nakład 150 + 75 egz. Ark. wyd. 8,25. Ark. druk. 63/4. Papier offset. kl. IV, 70 g. B1.
Oddano do druku w maju 1989 r. Druk ukończono w czerwcu 1989 r.
Zakład Graficzny Politechniki Wrocławskiej. Zam. nr 871/89 — Cena zł 500,-

Interband transitions, selection rules, birefringence, dichroism, reflectivity, absorption, photoluminescence, photoconductivity, optical constants, lattice modes, defect related transitions, acceptor and donor energies

Jan MISIEWICZ*

OPTICAL EXCITATIONS IN ZINC PHOSPHIDE (Zn_3P_2)

Electromagnetic wave interaction with Zn_3P_2 crystal within 0.003-11 eV energy range was investigated. As a result of the analysis of the reflectivity and Raman scattering spectra one-phonon energies were determined. Energies of two- and three-phonon excitations were obtained using absorption and Raman spectra. The symmetry of phonon branches as well as the selection rules of the overtones and combinations were derived and applied to describe observed multiphonon transitions. Optical excitations present in absorption, photoconductivity and photoluminescence spectra within 0.15-1.45 eV at 295 K and up to 1.66 eV at low temperatures, were ascribed to defect related levels. Acceptor levels at energies of 0.05, 0.17, 0.27, 0.36 eV were found. The deep levels were noticed at 0.55, 0.66 and 0.85 eV. Native defects were taken as origin of these levels existence. Excitations observed in absorption, reflectivity and photoconductivity spectra within 1.5-11 eV were ascribed to interband transitions. Analysing the spectra at polarized light and applying derived selection rules for interband transitions, anisotropic model of the band structure at Γ point was proposed. Direct energy gap was determined as 1.60 eV at E1c; crystal field and spin-orbit splitting of the valence band as 0.03 eV and 0.11 eV, respectively. Lin-Chung pseudocubic band structure model was successfully adopted to describe sequence of transitions for the energies higher than 4.5 eV.

*

Institute of Physics, Technical University of Wrocław, Wybrzeże Wyspiańskiego 27, 50-370 Wrocław, Poland.

1. INTRODUCTION

Zinc phosphide (Zn_3P_2), always p-type tetragonal semiconductor, has received growing attention in the last ten years as a possible candidate for many applications. The main interest connected with this material is solar energy conversion, so far. The essential factors necessary for the application of Zn_3P_2 in such devices are well fulfilled:

1. Location of the optical absorption edge at 1.4–1.6 eV, which is the optimum range for solar energy conversion predicted by simple estimations (Loferski 1956),

2. Minority carrier diffusion length $\approx 10 \mu\text{m}$.

3. Both constituent elements are abundant and inexpensive.

There are a lot of papers devoted to preparation and investigations of solar energy converters based on Zn_3P_2 . The extensive review of these studies has recently been made by Pawlikowski (1988). Thin Zn_3P_2 films were also used to produce ultraviolet detectors. Moreover, a distinct photodichroism observed on metal- Zn_3P_2 (oriented single crystal) junction was applied for light polarization step indicator.

A short review of the papers on application studies of Zn_3P_2 is included as Appendix.

Zn_3P_2 seems to be an interesting compound, not only because of its possible applications, but also because its fundamental properties are still relatively little known.

Experimental band structure investigations are based mainly on the fundamental absorption and reflectivity spectra as well as on photoemission spectra analysis.

Fundamental absorption edge in Zn_3P_2 was measured in several works. Pawlikowski et al. (1979) presented results of absorption measurements performed on the single crystals in the range of 10^0 – $5 \times 10^3 \text{ cm}^{-1}$. Absorption of single crystals was also measured by Fagen (1979) in the range of 10^0 – $1.5 \times 10^3 \text{ cm}^{-1}$ and by Źdanowicz et al. (1980) in the 3×10^0 – $2 \times 10^2 \text{ cm}^{-1}$. The paper by Sobolev and Syrbu (1974) brought the absorption edge in the range 3×10^0 – $1.5 \times 10^3 \text{ cm}^{-1}$ but the curve is displaced almost parallelly towards lower energies of about 90 meV. Absorption coefficient was measured for thin Zn_3P_2 films in wide energy range (up to 2.3 eV) an $\alpha \approx 7 \times 10^5 \text{ cm}^{-1}$ by Fagen (1979) and by Źdanowicz et al. (1980) in the energy range 1.55–2.0 eV. Absorption of the Zn_3P_2 films was also measured in 1.5–2.3 eV energy range by Murali et al. (1986).

For the first time, fundamental absorption edge was measured for oriented samples in polarized light for the absorption coefficient range 3×10^0 – $6 \times 10^2 \text{ cm}^{-1}$ by Misiewicz and Gaj (1981).

Very preliminary reflectivity spectra of Zn_3P_2 in the 1.5–5 eV energy range were presented by Misiewicz et al. (1980). Some data on reflectivity plots of Zn_3P_2 were also published by Sobolev and Syrbu (1974), Fagen (1979), and Pawlikowski et al. (1979). The results of reflectivity measurements in the 1.5–5 eV energy range performed on oriented Zn_3P_2 single crystals at polarized light were presented by Misiewicz et al. (1984a). Valence band structure of Zn_3P_2 was investigated using photoemission technics by Domashevskaya et al. (1980). In that paper, there are also some data on the conduction band structure.

The aim of the first part of the present work (Section 3) is to contribute to a better understanding of the band structure of Zn_3P_2 . Band-to-band optical transitions are discussed using the results of wide range spectral measurements of fundamental absorption, photoconductivity and reflectivity. The measurements were performed for the oriented single crystals using polarized light within the 1.4–5 eV energy range. Reflectivity measurements were also made in 5–11 eV energy range in unpolarized light. Additional source of information was birefringence measurements.

The basis of the analysis of the experimental results has been the energy band structure of Zn_3P_2 calculated theoretically for the pseudocubic crystal structure by Lin-Chung (1971).

The selection rules for the optical transitions derived by us and determined using group theory for the real crystal structure has been applied to analyse band-to-band transitions at polarized light. On the basis of these considerations a model of the band structure at Γ point is proposed.

The second part of this work (Section 4) is devoted to Zn_3P_2 lattice vibrations. Till now, only a few works contain results on this problem. Chronologically, the first infrared transmission measurement in the 400–750 cm^{-1} energy range was made by Radautsam et al. (1977) at room temperature. A few lattice bands were found in this region with very small resolution. The absorption spectra in the 500–1000 cm^{-1} energy range were measured by Misiewicz et al. (1986a) at 295 and 80 K. Twelve absorption bands were observed. Reststrahlen spectrum of Zn_3P_2 at room temperature and multiphonon absorption measurements in 40–700 cm^{-1} energy range were presented by Misiewicz et al. (1988, 1988a).

In this part, the analysis of electromagnetic wave interaction with the lattice of Zn_3P_2 crystal is presented. The group theory methods are used in these considerations. Critical point analysis and compatibility relations allow us to determine the symmetry of phonon dispersion curves. Two-phonon selection rules for infrared and Raman active

modes are determined on the base of Kronecker symmetrized square and Kronecker product reductions. Theoretical predictions in an analysis of experimental results are used. Fundamental reflectivity spectra were measured at room and at liquid helium temperatures in the 40-450 cm^{-1} energy range. Absorption spectra in the region of multiphonon transitions (380-1200 cm^{-1}) were measured at room and at low temperatures. The Raman scattering was measured in the range of 25-500 cm^{-1} at room temperature. From the reflectivity results the set of infrared active one-phonons are determined. The main transitions in Raman spectra are ascribed to one-phonon branches at Γ point as well. The other Raman transitions and singularities in absorption spectra are interpreted in terms of overtones and two-phonon combination modes.

The third part of this work (Section 5) is devoted to the optical characterization of the levels located within the energy gap. The knowledge of such levels is the important indicator of the material quality and then its potential applicability.

Several works on this field have been published until now. The results of electrical transport measurements were presented by Żdanowicz and Henkie (1964), Shevchenko et al. (1975), Müller et al. (1979), Catalano and Hall (1980), Wang et al. (1982), Sierański and Szatkowski (1986), and Szatkowski and Sierański (1987). Some data were also included in the papers of Misiewicz et al. (1986b) and Misiewicz (1989). DLTS measurements of the $\text{Mg-Zn}_3\text{P}_2$ diodes were performed and analysed by Suda and Bube (1984) and Suda and Kuroyanagi (1986). Photoluminescence investigations were made within 0.4-1.2 eV energy range by Sundström et al. (1980); 0.9-1.7 eV by Huldé et al. (1979); 1.25-1.4 eV by Briones et al. (1981), Kurbatov et al. (1976), Misiewicz et al. (1988), and 1.5-1.7 eV by Misiewicz (1988). Optical absorption of the deep levels was measured in the 0.1-1.4 eV energy range and discussed for the first time by Misiewicz et al. (1986a) and more details in the next paper by Misiewicz (1989). Photoelectrical spectra of metal- Zn_3P_2 contacts were used to investigate deep levels by Radautsan et al. (1976), Volodina et al. (1977), Syrbu et al. (1980), Wang and Bube (1982), and Misiewicz (1988).

In the present work, the results of optical absorption measurements in the energy range of 0.1-1.5 eV at room temperature and at liquid nitrogen, photoconductivity spectra measured within 0.65-1.5 eV energy range at room temperature and in the 1.45-1.6 eV range at 80 K, low temperature photoluminescence spectra measured in the 1.15-1.7 eV energy range, are collected. Within the energy range of 1.4-1.6 eV the derivatives of absorption plots at 295, 90 and 10 K were also deter-

mined. All these measurement results allowed us to determine a set of acceptor levels in Zn_3P_2 and followed their basic parameters.

Well known Quantum Defect Method (Bebb 1969) was applied to describe acceptor levels parameters.

Zn_3P_2 single crystals used in our investigations were grown by using chemical transport method with iodine as an active carrier as well as by directed physical vapour methods (Misiewicz and Królicki 1985, and Misiewicz et al. 1986). By using the former technique, single crystals with dimensions of approx. $5 \times 3 \times 1 \text{ mm}^3$ were obtained, when the latter one gave single crystals with approx. 0.9 cm in diameter and 1-2 cm long.

An extensive review on the thermodynamics of Zn_3P_2 formation; methods of the preparation of Zn_3P_2 and growth of crystals was published by Misiewicz and Królicki (1985).

2. Zn_3P_2 CRYSTAL STRUCTURE

Zn_3P_2 is one of four crystallographically similar semiconductors of the $A_3^{II}B_2^V$ type, the others being Cd_3P_2 , Zn_3As_2 and Cd_3As_2 (Żdanowicz and Żdanowicz 1975). The first two of them are strictly isostructural (Pistorius et al. 1977) similarly to the other ones. According to the papers by Stackelberg and Paulus (1935) and Pistorius et al. (1977), the Zn_3P_2 lattice is of tetragonal symmetry, belonging to space group D_{4h}^{15} ($P4/nmo$). The unit cell dimensions are: $a = b = 8.0889 \text{ \AA}$ and $c = 11.4069 \text{ \AA}$ (Pistorius et al. 1977), with eight formula units and 40 atoms. The crystal structure of Zn_3P_2 may be regarded as a Na_2O lattice to the first approximation (or antiferrofluoride lattice) in which one quarter of the metal sites are vacant. As in the hypothetical antiferrofluoride structure, cations and anions occupy alternate planes normal to the c axis. In this case, however, cation vacancies occur in pairs along all four body diagonals of the antiferrofluoride subcell. The ordering of cation vacancies makes the volume of Zn_3P_2 unit cell four times larger than the volume of the antiferrofluoride cell, causes lowering of the symmetry. Because of the existence of vacancies, some distortion can be found in the crystal structure. The Zn atoms are tetrahedrally coordinated with phosphorous atoms, being their nearest neighbours at the corners of a distorted tetrahedron. Every phosphorous atom is surrounded by zinc atoms located on six corners of a slightly distorted cube. Zn_3P_2 crystal structure is schematically presented in Fig 1a, whereas Fig. 1b shows basic defect antiferrofluoride structure.

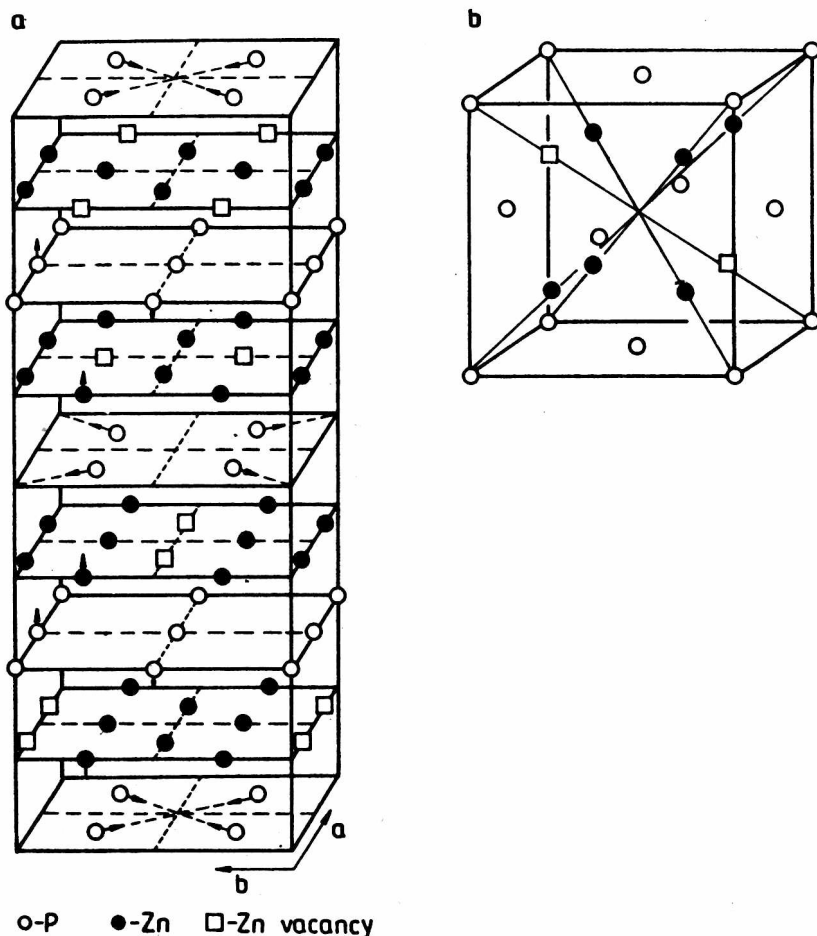


Fig. 1. Zn_3P_2 crystal structure (from Stackelberg and Paulus 1935): tetragonal unit cell (a) c-axis is two times elongated, basic defect antiperfluorite cell (b). Arrows denote atomic distortion directions

Rys. 1. Struktura krystaliczna Zn_3P_2 (Stackelberg i Paulus 1935): a - tetragonalna komórka elementarna, oś c jest dwukrotnie wydłużona, b - zdefektowana komórka typu antyfluoruru. Strzałki oznaczają kierunki dystorsji atomów

Zyubina et al. (1977) reported high symmetry of O_h type ($m\bar{3}m$) for Zn_3P_2 crystal from extensive X-ray analysis. This result indicates that Zn_3P_2 , although classified in the tetragonal structure, possesses a pseudocubic lattice with the reduced lattice parameter 11.45 \AA . This conclusion may be regarded to be consistent with the previous discussion since the c/a ratio is approximately equal to $\sqrt{2}$ and therefore,

the cube, which contains eight defect antiferro units can be constructed from the tetragonal cell along the face diagonal of the base and the c axis.

3. ENERGY BAND STRUCTURE OF Zn_3P_2

3.1. Theoretical considerations

3.1.1. Bondings

Anion sublattice in Zn_3P_2 is nearly close-packed (fcc) as it is visible in Fig. 1. The bondings, however, of all compounds of II_3V_2 group are expected to be different from those of III-V and II-VI groups. In contrast to the four valence electrons per atoms for the III-V and II-VI compounds, there are only seven electrons per every two atoms for II_3V_2 compounds. Compounds of III-V type normally have tetrahedral bondings with only four of the eight tetrahedral sites in the fcc structure occupied. For II_3V_2 , six of the eight such sites are occupied. Such a structure, more tightly filled by the metal atoms, enhances the interaction between them and increases the metallic contribution to the bond. The smaller energy band gaps in II_3V_2 materials in comparison with those of III-V ones with the same anion may be an example that more metallic contribution actually affects the physical properties.

The average number of valence electrons per bond is $4/3$ rather than 2 electrons as it is in conventional tetrahedrally coordinated semiconductors. This relative deficiency of bonding electrons results in a distribution of equilibrium bond lengths. Figure 2 presents the distribution for all 96 bonds in the unit cell, calculated from the crystallographic coordinates given by Pistorius et al. (1977) and sorted into $0.05\text{-}\text{\AA}$ -wide bins. Most of the bond lengths (56) remain very close to the sum of covalent radii for tetrahedral coordination (2.41 \AA). The remaining 40 bond lengths are placed in the range of $2.6\text{-}2.8\text{ \AA}$, i.e., below the sum of ionic radii (2.86 \AA). The value of fractional ionicity of Zn_3P_2 , $f_1 = 0.19$, was determined from crystallographic data by an extension of Phillip's spectroscopic model, and $f_1 = 0.17$ estimated from X-ray absorption edge shift by Adhyapak and Nigavekar (1978). The chemical bond for Zn_3P_2 is therefore a complex ionic-metallic-covalent bond.

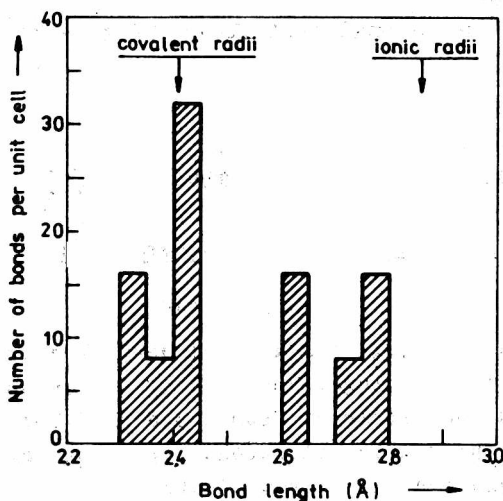


Fig. 2. Distribution of bond lengths in unit cell of Zn_3P_2 calculated from crystallographic data, given by Pistorius et al. (1977), and rounded to the nearest 0.05 Å

Rys. 2. Rozkład długości wiązań w komórce elementarnej Zn_3P_2 obliczony wg danych krystalograficznych z pracy Pistoriusa i in. (1977)

3.1.2. Quasi-cubic energy band structure model

The theoretical calculation of the energy band structure of Zn_3P_2 has been a difficult task because of the large number of atoms present in the tetragonal unit cell. Despite the complexities, Lin-Chung (1971) carried out a calculation by means of pseudopotential method. A pseudocubic, antiferrofluoride-like structure of Zn_3P_2 was taken into account by an effective vacancy potential superpose on the zinc atomic pseudopotential assumed in the ideal antiferrofluoride structure. It should be mentioned that the calculations were based on O_h^5 symmetry, and the spin-orbit and crystal field interactions as well as the presence of d-electrons of Zn were neglected. Those calculations showed a triply degenerated valence band maximum at the zone center, and the conduction band minima at the same point. The energy gap was determined as equal to 1.89 eV. The energy band structure obtained by Lin-Chung (1971) is presented in Fig. 3. According to the Lin-Chung calculations the lowest valence is a phosphorous s-like level. The second band is a Zn s-like band. The third and fourth bands are s-like mainly-Zn and p-like mainly-P atoms.

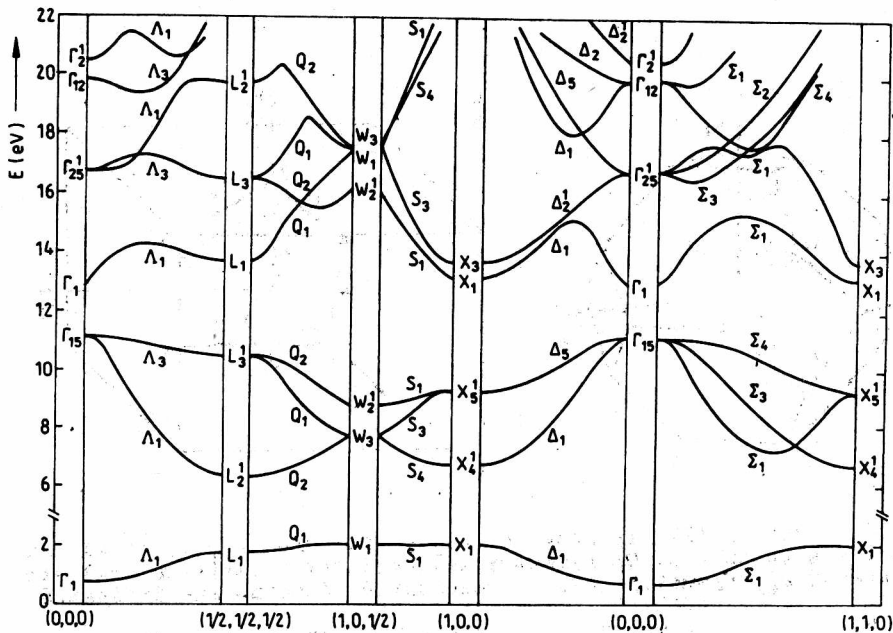


Fig. 3. Energy band structure of Zn_3P_2 for hypothetical crystal structure with O_h^5 symmetry and first Brillouin zone, as in Fig. 4a, calculated by Lin-Chung (1971)

Rys. 3. Struktura pasm energetycznych Zn_3P_2 obliczona dla hipotetycznego modelu sieci krystalicznej o symetrii O_h^5 (Lin-Chung 1971)

The first Brillouin zone for the hypothetical antiferrofluoride crystal structure, for which the above calculations have been performed, is shown in Fig. 4a. Real-symmetry analysis gives first Brillouin zone volume as only 1/8th of that of antiferrofluoride structure and with completely different form (Fig. 4b). These notations of the points and axes are commonly used for O_h^5 and D_{4h}^{15} structure, respectively. Thus, we do not change the marking. To avoid ambiguity it will be always made clear which of the Brillouin zones is taken into account in further parts of the present paper.

The problem is what changes can be expected coming out of the Lin-Chung model to the band structure in the real crystal. A small potential, which is the difference between the potential used in calculations and the potential of the real crystal, should be expected. Such potential should be small and it is rather difficult to evaluate it quantitatively. We can only state that its symmetry is D_{4h}^{15} . This potential will affect the electrons tending to mix states, which have the numbers differing from each other by the reciprocal lattice vectors of the real structure. The potential will have the main influence on the states with small energy differences. The most important effect of

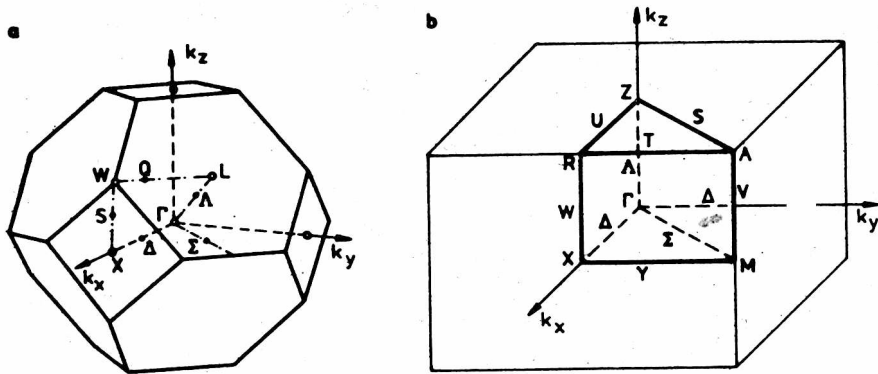


Fig. 4. First Brillouin zone of Zn_3P_2 for the hypothetical anti-fluoride structure of O_h^2 symmetry (a), and for real tetragonal structure of D_{4h}^{12} symmetry (b). Representation domains are indicated

Rys. 4. Pierwsza sfera Brillouina dla hipotetycznej sieci krystalicznej o symetrii O_h^2 (a) i dla realnej sieci krystalicznej o symetrii D_{4h}^{12} (b). Zaznaczone podstawowe obszary sfery Brillouina

its existence is mixing the states associated with Γ and X points in anti-fluoride structure. As a result, we expect the conduction band minima at Γ point to be lowered and the valence band Γ_{15} to be raised, so the energy at Γ point should be smaller than that calculated by Lin-Chung as 1.89 eV. Additional conduction band above Γ_1 coming out from the X_1 and/or X_3 states should occur (see Fig. 3). The residual potential and the spin-orbit interaction will lift the degeneracy of maximum of valence band Γ_{15} . When the potential acts, there will also be interactions between the levels Γ_{15} and X_5' , so the interband energy $X_1, X_5' \rightarrow X_1$ will increase. Similarly, the interband energy $L_3' \rightarrow L_1$ will decrease.

3.1.3. Spin-orbit and crystal field effects

In order to obtain reasonable energy band model at the Γ point, theoretical considerations including spin and crystal field effects connected with real tetragonal symmetry of the crystal are necessary. This indicates an analysis of the value of crystal field splitting and spin-orbit splitting to be necessary.

At first, it is possible to estimate the spin-orbit splitting in a simple anti-fluoride structure by means of well-known formula (see Cardona 1977):

$$\Delta_{so} = A \left[\lambda \Delta_{so}^{Zn} + (1 - \lambda) \Delta_{so}^P \right] \quad (1)$$

where λ is the ionicity of the compounds, and Δ_{so}^{Zn} and Δ_{so}^P are spin-orbit splitting values of free atoms. The A constant is very close to 1 for different semiconductors, so we have taken $A = 1$. $\lambda = 0.18$ has been taken from Adhyapak and Nigaveakar (1978). According to the small value of ionicity, correlated with the asymmetry in distribution of bonds, one can expect non-ionized or at most single ionized zinc and phosphorous atoms. Thus, we obtain $\Delta_{so} = 0.07$ eV for the former and 0.09 eV for the latter case. The last value is in a good agreement with the value of 0.11 eV calculated on the base of Lin-Chung model by Dowgialko-Plenkiewicz and Plenkiewicz (1978). In the last paper, a value of crystal field splitting was also given, as 0.03 eV. The same value was found by Cisewski (1982) from the lattice deformation analysis. The data of $\Delta_{so} = 0.21$ and $\Delta_{cf} = 0.04$ eV were obtained by Pawlikowski (1982a).

For the O_h^5 symmetry group, that of antiferrofluoride cell, the levels of X, Y and Z symmetry transform according to the three-fold degenerate Γ_{15} representation. For the D_{4h}^{15} group, the states of X and Y symmetry transform according to Γ_5^- representations and the states of Z symmetry according to the Γ_2^- representation. Due to the spin-orbit interaction, the Γ_5^- state will split into Γ_7^+ and Γ_7^- and the Γ_2^- state becomes Γ_7^- . Finally, because of the residual tetragonal potential and spin-orbit interactions, the three-fold degenerated valence band maximum will be splitted into three levels Γ_7^+ , Γ_7^+ , Γ_7^- . The lowest conduction band in quasi-cubic Lin-Chung model, Γ_1 , will transform as Γ_6^+ in D_{4h}^{15} structure.

The sequence of subbands can be determined experimentally, for example, by using the selection rules of the optical transitions.

3.1.4. Selection rules for direct optical transitions in real crystal structure of Zn_3P_2

The knowledge of the selection rules is necessary to interpretation of the optical measurements. First, in some cases band-to-band transitions can be forbidden. Furthermore, in the physical system which has low symmetry, the selection rules can depend on the polarization of light. In the case of the D_{4h}^{15} space group, the perturbing operator for direct optical transitions transforms as Γ_5^- for the light polarized perpendicular to c-axis and as Γ_2^- for the light polarized parallel to c-axis. Thus, the selection rules for Zn_3P_2 depend on the polarization direction of the light.

Table 1

Direct optical transitions for Zn_3P_2 crystal allowed both for $E \perp c$ and $E \parallel c$ light polarizations

| | | |
|---|----------------------------------|---------------------------------------|
| $\Gamma_1^{\pm} \longrightarrow \Gamma_j^{\pm}$ | $1, j = 6, 7$ | |
| $Q_1 \longrightarrow Q_1$ | $1 = 6, 7$ | $Q = \Lambda, V$ |
| $Q_5 \longrightarrow Q_5$ | $Q = Z, M, \Sigma, \Delta, U, W$ | |
| $Q_1 \longrightarrow Q_j$ | $1 = 3, 5 \quad 1 \neq j$ | $Q = \Delta\Sigma, US, X, R$ |
| $Q_1 \longrightarrow Q_1$ | $1 = 3, 4$ | $Q = \Lambda\Delta, YW, \Delta\Sigma$ |

Table 2

Direct optical transitions for Zn_3P_2 crystal allowed either for the light polarization $E \perp c$, or for $E \parallel c$

| $E \perp c$ | | |
|---|---------------|---------------------------------------|
| $\Gamma_1^{\pm} \longrightarrow \Gamma_j^{\mp}$ | $1, j = 6, 7$ | |
| $A_1^{\pm} \longrightarrow A_1^{\pm}$ | $1 = 5, 6$ | |
| $A_1^{\pm} \longrightarrow A_j^{\pm}$ | $1, j = 5, 6$ | |
| $Q_1 \longrightarrow Q_1$ | $1 = 3, 4$ | $Q = X, R, \Delta\Sigma, US$ |
| $Q_1 \longrightarrow Q_j$ | $1, j = 6, 7$ | $Q = \Lambda, V$ |
| $Q_1^{\pm} \longrightarrow Q_1^{\pm}$ | $1 = 2, 3$ | $Q = T, S, Y$ |
| $Q_1 \longrightarrow Q_j$ | $1 = 3, 4$ | $Q = \Lambda\Delta, YW, \Delta\Sigma$ |
| $E \parallel c$ | | |
| $A_1^{\pm} \longrightarrow A_1^{\mp}$ | $1 = 5, 6$ | |
| $Q_2^{\pm} \longrightarrow Q_2^{\mp}$ | $Q = T, S, Y$ | |

The first Brillouin zone of Zn_3P_2 real structure is presented in Fig. 4b, with the points and lines of symmetry indicated.

By using the characters of the representation of the points and lines of the symmetry as given in Fig. 4b, the respective selection rules, taking into account the spin, may be obtained. Table 1 presents a list of the direct optical transitions allowed for both the light polarizations. The common notations is used, see, e.g., Olbrychski (1965) and Plenkiewicz and Dowgiałko-Plenkiewicz (1979).

Table 2 presents a list of the transitions which are permitted at the $E \perp c$ polarization.

There are only a few transitions possible solely at $E \parallel c$ polarization: $A_1^+ \rightarrow A_1^+$, $i = 5, 6$, $G_2^+ \rightarrow G_2^+$, $Q = T, S, Y$.

3.2. Interband optical transitions - experiment

The samples of the appropriate thickness were cut out from the boules and mechanically polished using alumina powder with 1, 0.3 and 0.05 μm grain size. After polishing, the samples were degreased in acetone and methanol and then etched in 1.5-2% bromine methanol solution. For reflectivity measurements, there were also used single crystals obtained by chemical transport growth with mirror-like as-grown surfaces. Absorption measurements were performed for the samples with different thicknesses, from 5 mm to $\approx 10 \mu m$. The thinnest samples were prepared by mechanical polishing up to $\approx 100-150 \mu m$ and finally by careful etching in bromine methanol solution. For photoconductivity measurements, the samples were of the dimensions of $8 \times 3 mm^2$ and thicknesses within the range of 100-300 μm . Electrical contacts were made on the extremities of the samples using gold chloride solution.

3.2.1. Fundamental absorption edge

Absorption coefficient spectra were determined by means of the transmission and reflectivity measurements in 1.35-1.66 eV energy range. Standard Cary-14 system as well as the equipment based on GDM-1000 monochromator were applied. The latter was described by Gumieny and Misiewicz (1982). The obtained absorption edge is presented in Fig. 5. In this figure, there are also presented absorption plots measured using thin films in the range of $10^3-2 \times 10^4 cm^{-1}$ by Fagen (1979), in the range of $4 \times 10^3-1.5 \times 10^4 cm^{-1}$ by Zdanowicz et al. (1980), and $5 \times 10^3 cm^{-1}-2 \times 10^4 cm^{-1}$ by Murali et al. (1986).

In the 1.4-1.58 eV energy range nearly exponential increase of absorption is found. Below 1.4 eV there is visible an absorption which origin

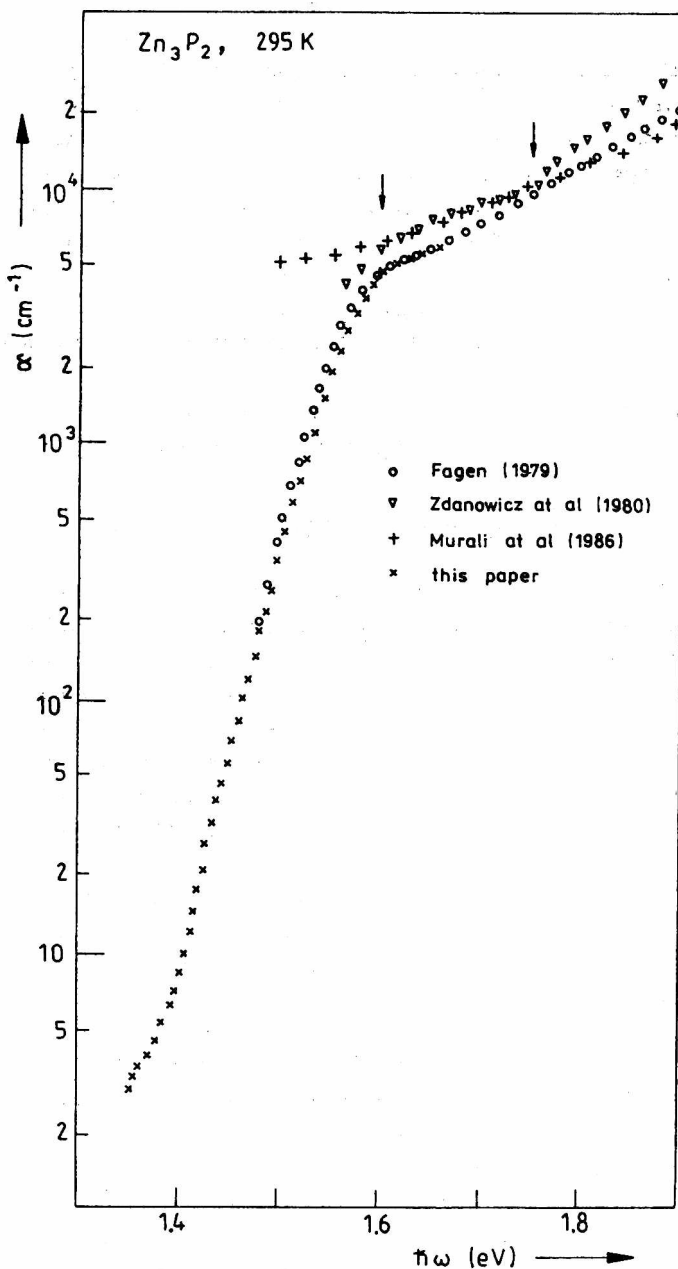


Fig. 5. Fundamental absorption edge of Zn_3P_2 measured for single crystals. The data for thin films are also included. Arrows denote transition energies (see Tab. 3)

Rys. 5. Krawędź absorpcji podstawowej Zn_3P_2 zmierzona dla monokryształów. Zamieszczono również dane literaturowe dla cienkich warstw. Strzałki oznaczają energie przejść (patrz tab. 3)

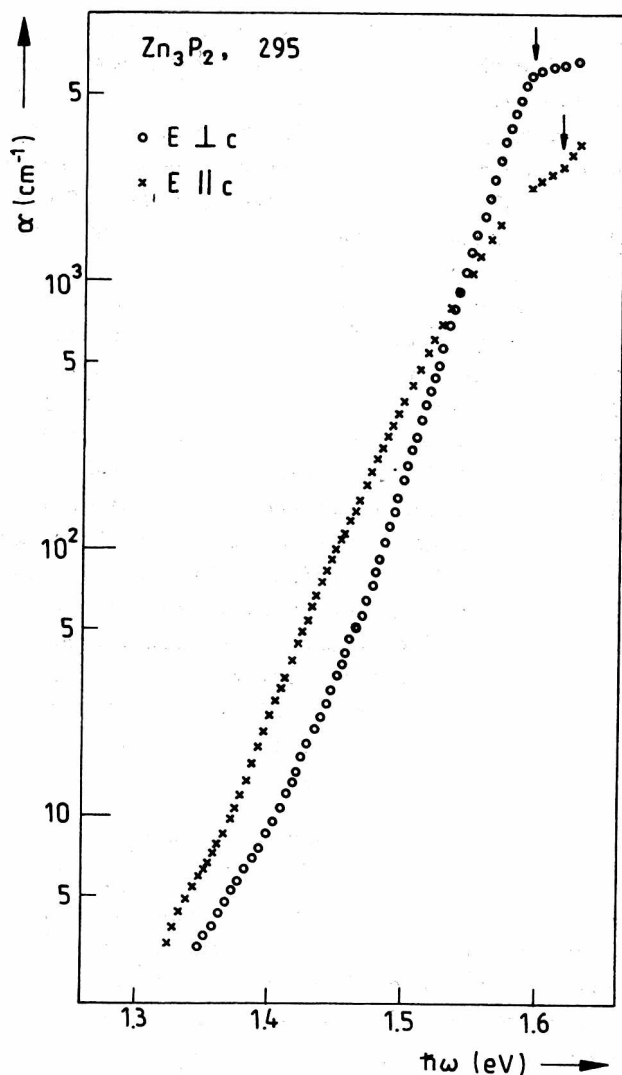


Fig. 6. Fundamental absorption edge measured in polarized light for oriented single Zn_3P_2 crystals. Distinct changes in absorption curves slope at 1.59 eV and 1.62 eV for polarizations $E \perp c$ and $E \parallel c$, respectively (marked by arrows) denote energies of allowed direct transitions. A change in the slope within 1.57-1.60 eV for $E \parallel c$ corresponds to forbidden direct transition

Rys. 6. Krawędź absorpcji podstawowej Zn_3P_2 dla światła spolaryzowanego i zorientowanych próbek. Wyraźne zmiany na krzywych absorpcji zaznaczone strzałkami dla energii 1.59 eV i 1.62 eV, gdy polaryzacja światła jest odpowiednio $E \perp c$ i $E \parallel c$, określają energie dozwolonych przejść prostych. Zmiana nachylenia widoczna na krzywej absorpcji dla $E \parallel c$ w obszarze 1.57-1.60 eV odpowiada prostemu przejściu wzbronionemu

has not been determined unambiguously. In the 1.58-1.62 eV energy region, the absorption coefficient is being slightly changed with the apparent change of the slope of the curve at approx. 1.6 eV. For thin film spectra, besides the change in slope at 1.6 eV there is also another one at approx. 1.75 eV.

As Zn_3P_2 is a tetragonal material, it is necessary to perform the optical measurements using polarized light and oriented samples. For our measurements, the light was polarized by means of Carl Zeiss Jena polarizers with a polarization grade higher than 99%. Zn_3P_2 single crystals were oriented using standard X-ray technique. Figure 6 presents absorption edges obtained for the light polarized parallelly and perpendicularly to the c-axis. For the absorption coefficient values smaller than 10^3 cm^{-1} the lower-energy absorption plot is related to polarization $E \parallel c$, whereas the higher energy plot to the $E \perp c$ ones. The absorption plots cross at the energy of approx. 1.55 eV, corresponding to absorption coefficient values of 10^3 cm^{-1} approx. Such crossing of the plots was expected from taking into account the data published previously (Misiewicz and Gaj 1981, and Misiewicz et al. 1984a). Above the cross the absorption plot for $E \perp c$ have the same slope at both lower and higher energies, whereas the absorption plot for $E \parallel c$ increases much slower above the cross. Absorption coefficient for $E \perp c$ saturates for the energies higher than 1.6 eV. For $E \parallel c$ there is a small change of the slope at 1.57-1.60 eV and more prominent one at 1.62 eV. Absorption for $E \perp c$ in the range of 1.58-1.62 eV is distinct stronger than for $E \parallel c$.

3.2.2. Photoconductivity spectra

To perform photoconductivity measurements, a standard experimental equipment described elsewhere (Misiewicz 1988) was applied. Figure 7 shows representative plot of photoconductivity in the 1.45-2.7 eV energy range measured in unpolarized light. A few distinct singularities at the energies 1.6-1.63, 1.74, 1.86, 2.07 and 2.55 eV are visible in this spectrum.

Photoconductivity of the oriented samples, using polarized light in 1.45-1.95 eV energy range was also measured (see Fig. 8). Similarly to the absorption plot, two edges can be observed, one for $E \parallel c$ and the other for $E \perp c$. They cross each other at the energy of 1.56 eV approx. Distinct changes in the slopes of photoconductivity curves are observed at 1.6 eV and at 1.63 eV for the $E \perp c$ polarization. At the same polarization there is also a step visible on the photoconductivity slope at 1.75 eV and a slight change of the slope in the 1.83-1.9 eV range. For $E \parallel c$, there are changes in photoconductivity plot

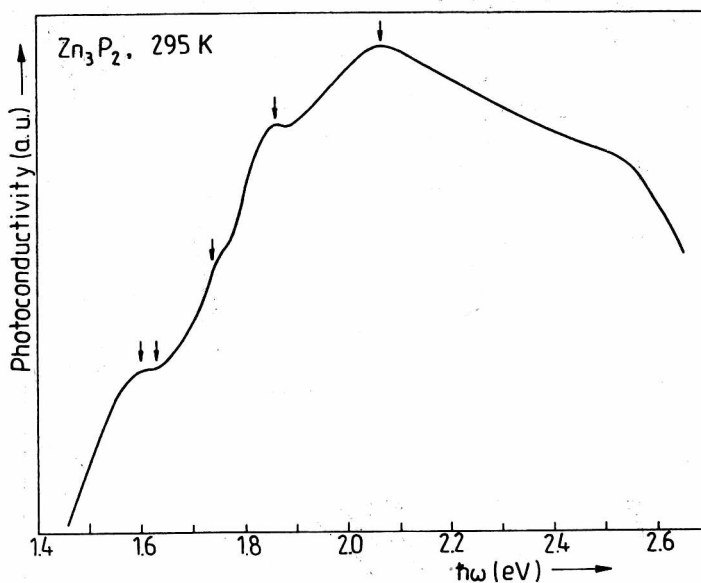


Fig. 7. Photoconductivity spectrum of Zn_3P_2 crystal in unpolarized light. Arrows indicate energies of band-to-band transitions

Rys. 7. Widmo fotoprzewodnictwa Zn_3P_2 w świetle niespolaryzowanym. Strzałki oznaczają energie odpowiadające przejściom międzypasmowym

in the range of 1.55–1.65 eV and next more prominent change at 1.86 eV.

3.2.3. Reflectivity spectra

Reflectivity measurements were performed by using two different set-ups. One was based on the SPM-2 and MDR-2 monochromators and allowed to measure absolute value of reflectivity coefficient in the 1.3–6 eV energy range (details see Becla et al. 1978). In the 4–11 eV energy range experimental equipment was based on a vacuum ultraviolet monochromator MV-8 with a hydrogen discharge lamp (details see Misiewicz et al. 1989). In the 1.3–4.6 eV energy range, the measurements were performed also for the oriented samples and in the polarized light.

Typical fundamental reflectivity spectrum of Zn_3P_2 in the whole measured energy range is presented in Fig. 9. The spectrum consists of a few distinguishable bands. Below the first one, at approx. 2.6 eV, there are two small changes of the slope of the reflectivity curve at

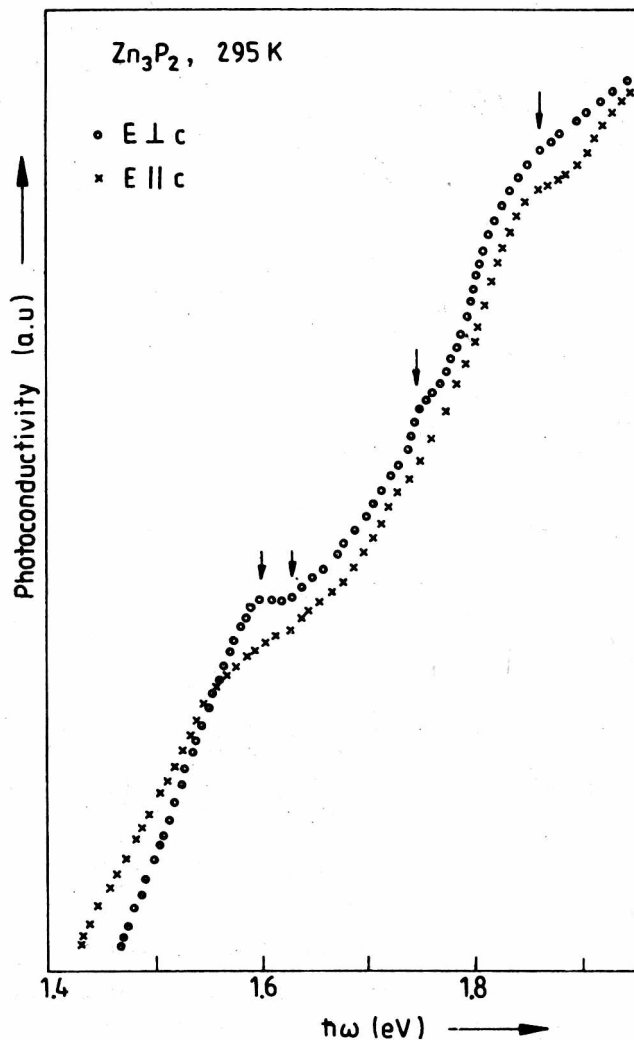


Fig. 8. Photoconductivity spectrum of Zn_3P_2 crystal at two different light polarizations. Arrows indicate energies of the transitions connected with Γ point in Brillouin zone (see also Tab. 3 and caption of Fig. 6)

Rys. 8. Widmo fotoprzewodnictwa Zn_3P_2 dla dwóch różnych polaryzacji światła. Strzałki oznaczają energie przejść w punkcie Γ strefy Brillouina

1.5-1.6 eV and at 1.86-1.88 eV. The second band in the energy range of 4-5 eV is splitted into two subbands. The third distinct peak is located at 5.25 eV. The main band placed within 5.5-8 eV consists of two peaks at 6.25 eV and 6.8 eV and two thresholds on the left and

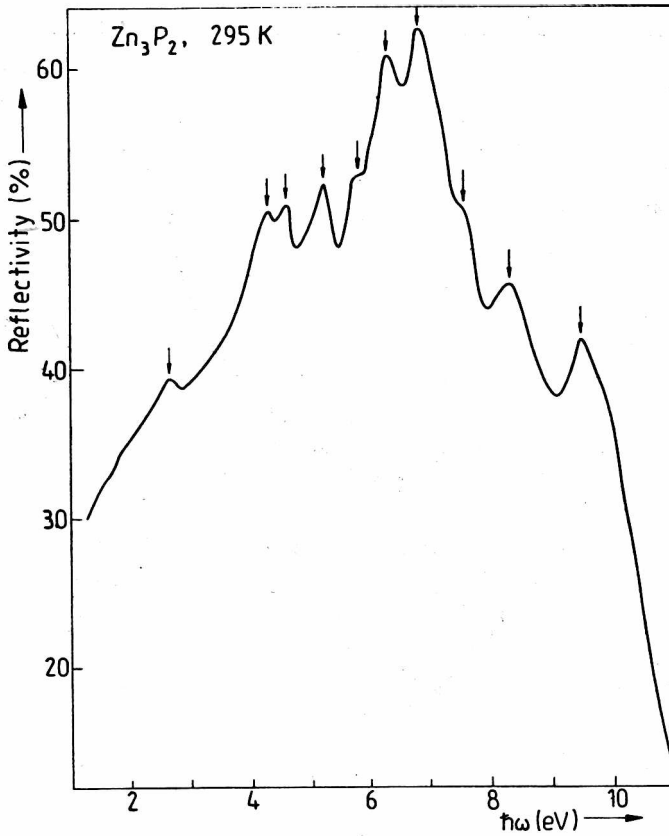


Fig. 9. Reflectivity spectrum of Zn_3P_2 crystal in unpolarized light
 Rys. 9. Widmo odbicia Zn_3P_2 dla światła niespolaryzowanego

right sides of the band. The highest energy peaks are located at 8.3 and 9.5 eV.

Figure 10 presents reflectivity plots obtained in polarized light. Both plots, obtained in different polarizations, are relatively similar. We observed two main transitions located at nearly the same energies for both polarizations. The maximum at 4.3 eV is much prominent for $E \parallel c$ polarization in comparison with the $E \perp c$ one. Transitions at 1.88 and 4.12 eV are more visible for $E \parallel c$, and transition at 4.58 eV is stronger for $E \perp c$ polarization. Figures 11 a-c present the details of the plots within 1.4-1.7 eV range (a) and the main maxima (b, c). For the $E \perp c$ polarization a small maximum is located at 1.59 eV and a change in reflectivity curve slope can be

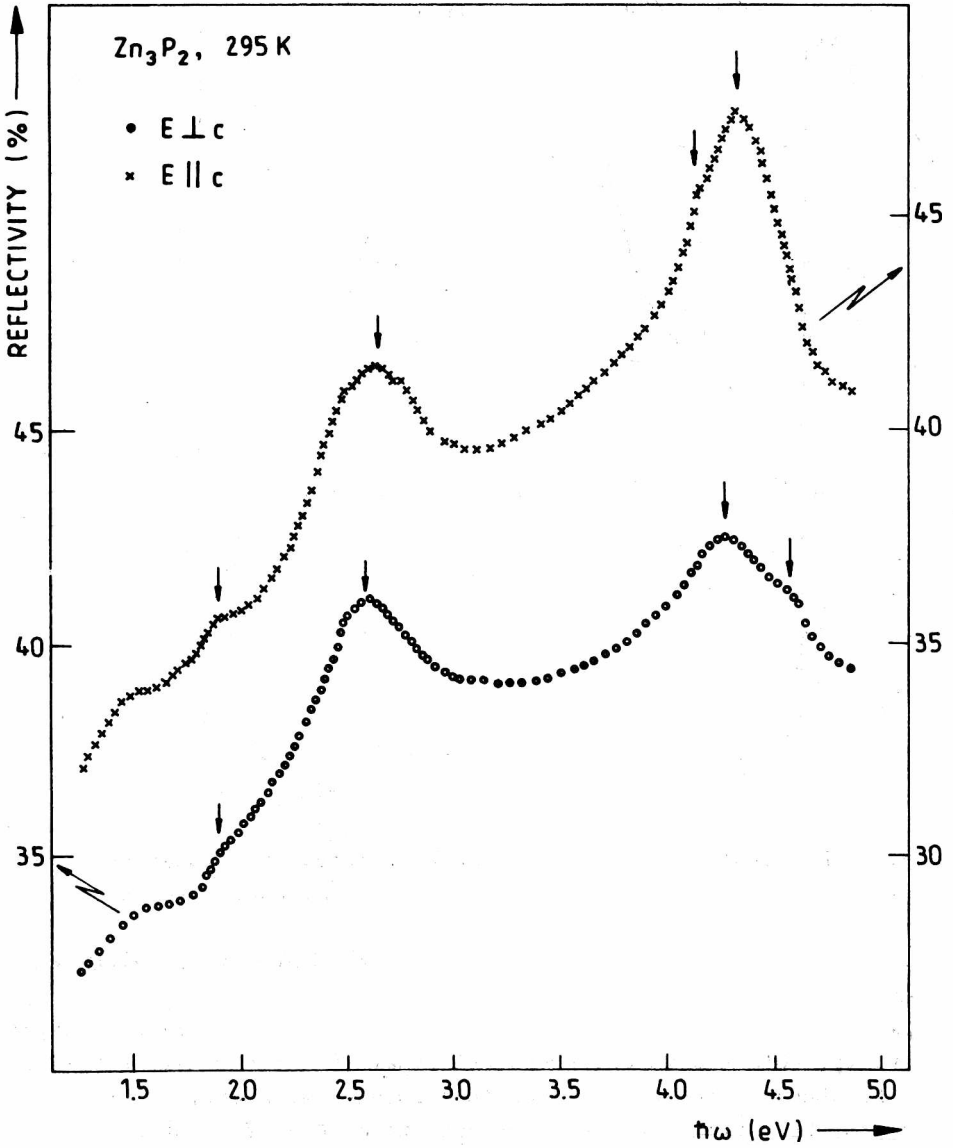


Fig. 10. Reflectivity spectrum of Zn_3P_2 crystal for two different light polarizations. Arrows denote the characteristic energies

Rys. 10. Widmo odbicia Zn_3P_2 dla dwóch polaryzacji światła. Strzałki oznaczają energie charakterystyczne

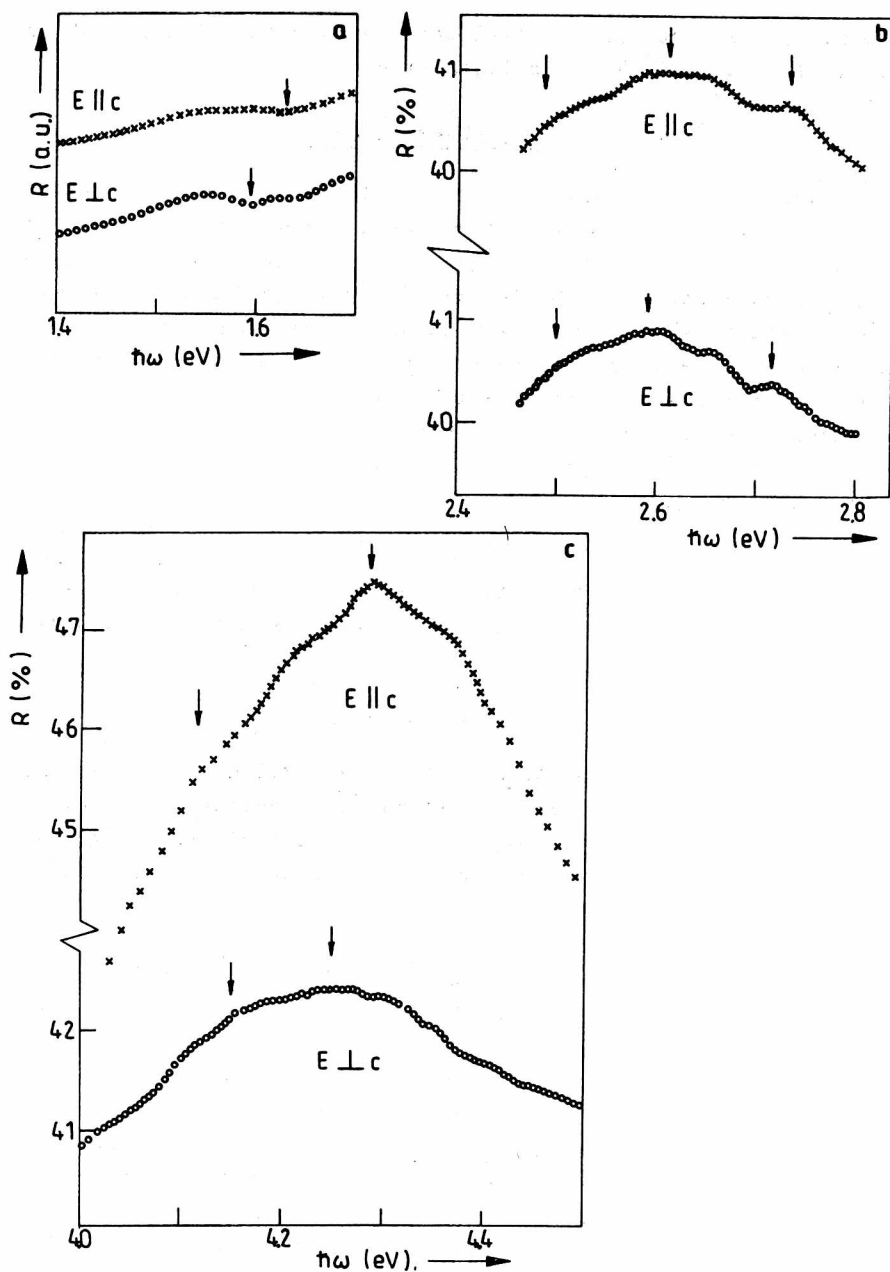


Fig. 11. Details of the reflectivity spectrum at room temperature in the three most important regions. Arrows denote the transition energies. The energy values are collected in Tables 3 for (a) and 5 for (b) and (c) cases

Rys. 11. Szczegóły widma odbicia Zn_3P_2 w temperaturze pokojowej w trzech najważniejszych regionach. Strzałki oznaczają energie przejść

seen at 1.65 eV approx. A small minimum in reflectivity plot is also seen at 1.63 eV for $E \parallel c$ polarization.

3.3. Birefringence

In tetragonal crystals, there is a difference between refractive indices for the light polarized parallelly and perpendicularly to the optical axis c . Zn_3P_2 birefringence was measured using two methods described extensively by Wardzyński (1970), and Gumienny and Misiewicz (1985). Figure 12 presents typical plots measured within 0.5–1.45 eV energy range both at room temperature and at 80 K. Birefringence spectrum is almost energy independent below 0.8 eV. For higher energies a distinct increase of birefringence value occurs. For Zn_3P_2 it was found that $n_{\parallel} > n_{\perp}$ (where \parallel and \perp means $E \parallel c$ and $E \perp c$).

The birefringence

$$\delta n = n_{\parallel} - n_{\perp} \quad (2)$$

is related to the dichroism, i.e., the difference between absorption coefficient for the light polarized parallelly and perpendicularly to the c -axis

$$\delta \alpha = \alpha_{\parallel} - \alpha_{\perp}. \quad (3)$$

The measurement of birefringence is equivalent to determining the difference between real part of dielectric constants which are connected with the difference of imaginary parts of dielectric constants, and further with dichroism. The Kramers-Kronig formula gives relation (see Gaj 1973)

$$\delta n(E) = \frac{\hbar c}{\pi} \int_0^{\infty} \frac{\delta \alpha(x)}{x^2 - E^2} dx \quad (4)$$

where E is a photon energy, and \hbar, c are universal constants.

By measuring the birefringence, one can obtain information about the dichroism plot in the photon energy range not attainable (or very difficult to reach) in transmission measurement. It makes possible to analyse optical transitions at such energies.

From Equation (4), assuming Delta-type function model of the dichroism, one obtains

$$\delta n(E) = \frac{\hbar c}{\pi} \frac{A}{E_0^2 - E^2} \quad (5)$$

where A is a fitting constant, and E_0 is the characteristic energy.

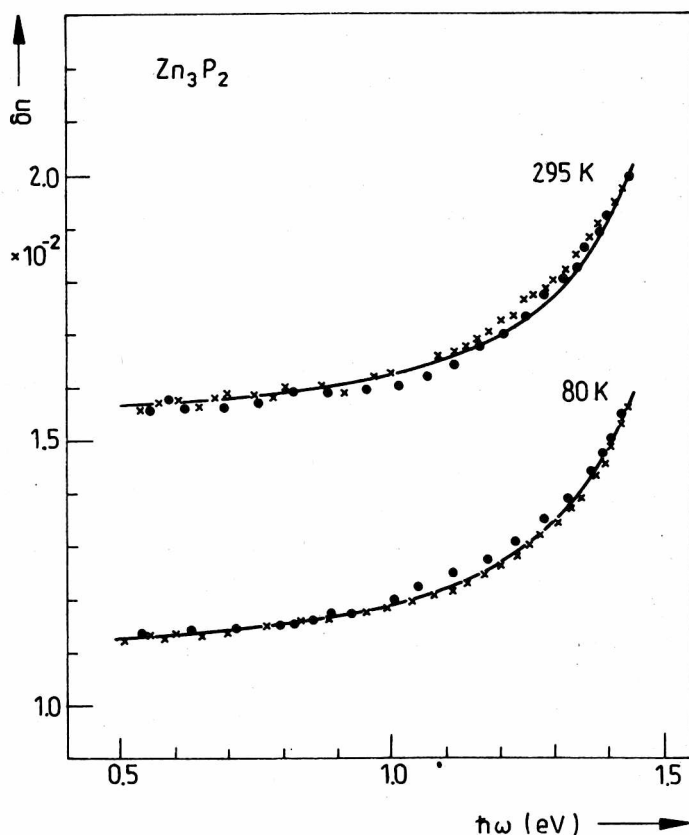


Fig. 12. Birefringence dependence for Zn_3P_2 crystal determined for two different samples marked by crosses and circles (from Misiewicz and Gaj 1981). Solid line; theoretical model, with energy gap equal to 1.60 eV at room temperature and 1.65 eV at 80 K for minimized standard deviation value (Misiewicz et al. 1984)

Rys. 12. Dwójłomność kryształu Zn_3P_2 dla dwóch różnych próbek oznaczonych krzyżykami i kółkami (z pracy Misiewicza i Gaja 1981). Linia ciągła oznacza model teoretyczny z wartościami energii progowej 1,60 eV w temperaturze pokojowej i 1,65 eV w 80 K. Dopasowanie otrzymane dla minimum odchylenia średniokwadratowego

By fitting the relation (5) to the experimentally obtained birefringence spectrum (see solid line in Fig. 12) one can determine characteristic energy E_0 . This energy usually corresponds to the smallest band-to-band distance (Gaj 1973). In the case of Zn_3P_2 , the values of E_0 are equal to 1.6 eV and 1.65 eV at room temperature and at 80 K, respectively.

3.4. Interband optical transitions - a model

3.4.1. Optical transitions at the center of Brillouin zone

As Figure 5 shows, there occurs an exponential-like increase of the absorption coefficient of Zn_3P_2 crystal within 1.4–1.58 eV energy range.

The data from absorption curve in Fig. 5 can be well fitted over almost entire three decade absorption range by the relation (Urbach 1953)

$$\alpha(\hbar\omega) = \alpha'_0 \exp \frac{\hbar\omega}{kT_0}, \quad (6)$$

with $\alpha'_0 \approx 7 \times 10^{-22} \text{ cm}^{-1}$ and $T_0 = 315 \text{ K}$. The value of fitting constant T_0 is in a relatively good agreement with the temperature of measurements, according to Urbach's original observations. Such dependence (Eq. (6)) is commonly accounted for by the existence of density of states tail and by the optical transitions to such tail of conduction band (in the case of p-type material). In the Dow-Redfield (1972) model, such an exponential absorption tail arises from exciton ionization by localized internal electric fields, i.e., field-induced tunneling of the photogenerated electrons away from the photogenerated holes. The physical origin of these internal fields may result from phonons, impurities, dangling bonds, or from any other sources of potential fluctuation.

In ionic crystals, it is common to correlate exponential behaviour of absorption edge with the role of the LO phonons in creation active fields. In ordinary covalent semiconductors, the fields arise primarily from charged impurities. Considering the predominantly covalent character of the material, the impurities are expected to play a significant role in the field creation.

To determine direct gap from absorption edge one can use simple "classic" dependence for absorption

$$\alpha \hbar\omega = A(\hbar\omega - E_g)^{1/2} \quad (7)$$

where A is a constant.

By using this dependence a direct gap value of Zn_3P_2 at 300 K was determined on bulk samples as 1.51 eV (Pawlikowski et al. 1979). Using the same formula (7) Zdanowicz et al. (1980) have found the energy value of 1.52 eV, and additional transitions at 1.66 eV and 1.82 eV; Murali et al. (1986) have found transition at the energy of 1.66 eV and next transitions at 1.75 eV and 1.82 eV. The analysis performed

by Żdanowicz et al. (1980) and Murali et al. (1986) concerned absorption of thin films only. Combining the results of measurements for bulk material and thin films, Fagen (1979) obtained a gap value of 1.55–1.60 eV and the next transitions at 1.9 eV and 2.05 eV. Pawlikowski (1982) obtained a set of transitions at 1.51 eV, 1.55 eV and 1.72 eV, fitting three-bands Kane-type model to the absorption plot combined from single crystal and thin films measurements.

For wide gap semiconductors, the influence of excitons on the absorption is to be expected, due to the Coulomb interaction of the electron and the hole produced in the transition process (Elliot 1957). Because of the small binding energy of exciton (≤ 10 meV) we can see excitonic peaks in absorption only at very low temperatures. At room temperature, due to the exciton influence on band-to-band transitions, the energy gap is expected to be placed just above the exponential part of the absorption edge. The energy of abrupt bending of the absorption plot is very close to the energy gap of the semiconductor (see, e.g., Sturge 1962).

Until now, in the case of Zn_3P_2 , for the energies higher than 1.55 eV the absorption results have been available only for thin films. The present paper brings about absorption data for single crystals much more appropriate to analyse band-to-band transitions. As we can see in Fig. 5, the distinct change of absorption edge slope takes place at 1.60 eV (± 0.02 eV). In the light of discussion presented above, we may take this value as the energy gap value of Zn_3P_2 at room temperature.

Regarding the results of measurement in polarized light, i.e., the absorption results (see Fig. 6) and those of photoconductivity within 1.4–1.65 eV energy range (see Fig. 8) two edges for different light polarizations are presented.

The increase of absorption for $E \parallel c$ is much slower and there is only slight change of its slope in the range of 1.57–1.60 eV. At about 1.62 eV there is also a change in absorption curve, occurring for both polarizations. Photoconductivity spectrum is of the similar behaviour. Besides singularities at 1.6 eV and 1.63 eV, there are also transitions at 1.86 eV occurring for both polarizations, and at 1.75 eV for $E \perp c$ polarization only.

Transitions at 1.59 and 1.63 eV visible in both absorption and photoconductivity spectra correspond to weak features observed in reflectivity (see Fig. 11a). Such features in reflectivity are usually correlated with band-to-band transitions (Sell 1972).

Taking the Lin-Chung model as a base of the discussion we can find that the transitions for energies not much higher than 2 eV should be

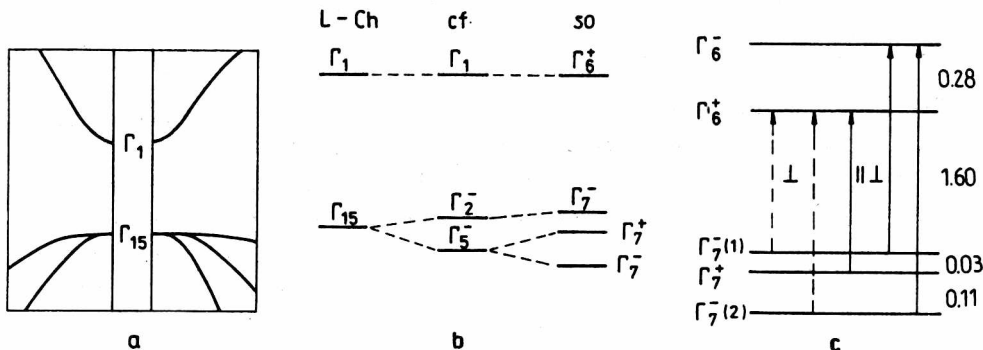


Fig. 13. Model of the band structure of Zn_3P_2 at Γ point, calculated by Lin-Chung (1971) for the pseudocubic crystal structure, $E_g = E(\Gamma_1) - E(\Gamma_{15}) = 1.89$ eV - (a); evolution of the bands from (a) due to the influence of tetragonal potential (cf) and spin-orbit interaction (so) - (b); model of the band structure at Γ point determined on the base of group theory analysis for D_{4h}^{2d} symmetry and experimental data at 295 K - (c), (energies in eV)

Rys. 13. Model struktury pasmowej Zn_3P_2 w punkcie Γ , obliczony przez Lin-Chung (1971) dla pseudokubicznej struktury krystalicznej, $E_g = E(\Gamma_1) - E(\Gamma_{15}) = 1.89$ eV (a); przekształcenie pasm z modelu (a) pod wpływem potencjału tetragonalnego (cf) i oddziaływania spin-orbita (so) (b); model struktury pasmowej w punkcie Γ wyznaczony na podstawie metod teorii grup i wyników eksperymentalnych w 295 K (c); (energia w eV)

connected only with Γ point and its close neighbourhood. Making such assumptions and taking into account evolution of the bands discussed in Sects. 3.1.2-3.1.4 and marked in Figs. 13a, b we may propose a band structure diagram for Γ point, shown in Fig. 13c. Valence band maximum consists of three sub-bands with symmetry Γ_7^- , Γ_7^+ and Γ_7^- . The lower conduction band is described by Γ_6^+ and the higher one, predicted in Sects. 3.1.2-3.1.4 should possess symmetry Γ_6^- . Transitions $\Gamma_7^- \rightarrow \Gamma_6^+$ from upper and lowest valence sub-bands are allowed only for $E \perp c$. Transition $\Gamma_7^+ \rightarrow \Gamma_6^-$ is forbidden in dipole approximation. The other possible transitions are allowed for both polarizations.

In Table 3, a comparison of the experimental data obtained in the present and other works is made, concerning optical transition in Zn_3P_2 . Theoretical description of the observed transitions in terms of the model shown in Fig. 13 is also presented in Tab. 3. The proposed model originates from group theory considerations and is confirmed by observations of optical absorption and photoconductivity for polarized light.

On the base of the above discussion, absorption and photoconductivity edges at $E \perp c$ correspond to $\Gamma_7^- \rightarrow \Gamma_6^+$ transition. The edge at $E \parallel c$ seems to be connected with $\Gamma_7^- \rightarrow \Gamma_6^+$ transition forbidden in dipole approximation as well as with $\Gamma_7^+ \rightarrow \Gamma_7^+$ transition allowed in both polarizations.

T a b l e 3

Optical transitions in Zn_3P_2 crystal within 1.5–2.1 eV energy range at 295 K and their assignments basing on group theory analysis for D_{4h}^{15} symmetry (α - absorption, PC - photoconductivity, B - birefringence, R - reflectivity; \perp - denotes $E \perp c$, \parallel - denotes $E \parallel c$), energy in eV

| Description | Model energy | α | PC | B | R | a | b | c | d |
|---|--------------|------------------------|------------------------|------|------------------------|-------------------|------|------|------|
| $\Gamma_7^-(1) \rightarrow \Gamma_6^+(\perp)$ | 1.60 | 1.59 \perp | 1.60 \perp | 1.60 | 1.59 \perp | 1.55–1.60 | | 1.55 | |
| $\Gamma_7^+ \rightarrow \Gamma_6^+(\perp \parallel)$ | 1.63 | 1.62 $\perp \parallel$ | 1.63 $\perp \parallel$ | | 1.63 \parallel | | 1.66 | | 1.66 |
| $\Gamma_7^-(2) \rightarrow \Gamma_6^+(\perp)$ | 1.74 | | 1.75 \perp | | | 1.77 [#] | 1.75 | 1.76 | |
| $\Gamma_7^-(1) \rightarrow \Gamma_6^-(\perp \parallel)$ | 1.88 | | 1.86 $\perp \parallel$ | | 1.88 $\perp \parallel$ | 1.9 | 1.82 | | 1.82 |
| $\Gamma_7^-(2) \rightarrow \Gamma_6^-(\perp \parallel)$ | 2.02 | | 2.07 | | | 2.05 [#] | | | |

- Visible as a change in absorption curve.

a - after Fagen (1979),

b - after Murali et al. (1986),

c - after Pawlikowski (1982),

d - after Zdanowicz et al. (1980).

Table 4

Energies (in eV) of the crystal field splitting, Δ_{cf} , and spin-orbit splitting, Δ_{so} ,
 (α - absorption, PC - photoconductivity, R - reflectivity, C - Cardona relation (1))

| | α | PC | R | C | a | b | c |
|--|----------|------|------|------|------|------|------|
| $\Delta_{cf} = E(\Gamma_7^-(1)) - E(\Gamma_7^+)$ | 0.03 | 0.03 | 0.04 | | 0.03 | 0.03 | 0.04 |
| $\Delta_{so} = E(\Gamma_7^+) - E(\Gamma_7^-(2))$ | | 0.11 | | 0.09 | 0.12 | 0.11 | 0.21 |

a - after Cisowski (1982),

b - after Dowgiałło-Plenkiewicz and Plenkiewicz (1978),

c - after Pawlikowski (1982).

On the basis of the absorption, photoconductivity, birefringence and reflectivity measurements performed in polarized light we can state that direct energy gap in Zn_3P_2 is equal to 1.6 eV at 300 K. The same value of energy gap in Zn_3P_2 was proposed by Domashevskaya et al. (1980) by using photoemission spectra, and Pawlikowski (1985) from absorption edge investigations of solid solutions of Cd_3P_2 - Zn_3P_2 . In photoemission investigations performed by Domashevskaya et al. (1980) there was also found a transition from valence band to the conduction band at energy of 2.2 eV. That transition seems to be correlated with the maximum at 2.07 eV observed by us in photoconductivity spectrum.

The crystal field splitting value $\Delta_{of} = E(\Gamma_7^-(1)) - E(\Gamma_7^+) = 0.03$ eV and spin-orbit splitting value $\Delta_{so} = E(\Gamma_7^+) - E(\Gamma_7^-(2)) = 0.11$ eV, determined in this work basing on the absorption, photoconductivity and reflectivity results, remain in a very good accordance with values obtained from other experiments as well as with those calculated theoretically by Dowgiałko-Plenkiewicz and Plenkiewicz (1978), see Tab. 4.

3.4.2. Analysis of the high-energy interband optical transitions

1. Anisotropic effects

There is a row of optical transition at energies higher than 2.2 eV, observed in reflectivity spectrum. At first, we will discuss results for the polarized light. As can be seen in Figs. 10 and 11, the influence of crystal orientation on the reflectivity spectra at differently polarized light is rather small.

The band with maximum at 4.3 eV is much more prominent in $E \parallel c$ polarization in comparison with the $E \perp c$ one. Transition at 4.12 eV is more prominent at $E \parallel c$, but transition for 4.58 eV is stronger for $E \perp c$. There are also small differences in the shape of reflectivity curve and energies of singularities, as it is shown in Fig. 11. The energies of transitions observed in polarized light are listed in Tab. 5. Furthermore, we can try to correlate the differences observed in the reflectivity plot with predictions of group theory analysis for real D_{4h}^{15} structure of Zn_3P_2 crystal. The selection rules for the direct optical transitions allowed at different polarization of light are presented in Tables 1 and 2. Group theory solves the problem of whether the matrix element of appropriate transition is zero or not. The intensity of allowed transitions may be different due to different values of matrix elements. A large part of the tetragonal Brillouine zone is occupied by lines and points, where optical transitions are possible for both polarizations of light (see Tab. 1). Thus, it is comprehensible that most of the thresholds and maxima occur on both plots in Fig. 10 for the same energies. As the reflectivity band at

Singularities in the reflectivity spectrum of Zn_3P_2 crystal
in polarized light

| Type of light polarization | Energy (eV) | | | | | |
|----------------------------|-------------|-------|-------|-------|-------|------|
| $E \parallel c$ | 2.48, | 2.62, | 2.73, | 4.12, | 4.28 | |
| $E \perp c$ | 2.50, | 2.60, | 2.72, | 4.15, | 4.25, | 4.58 |

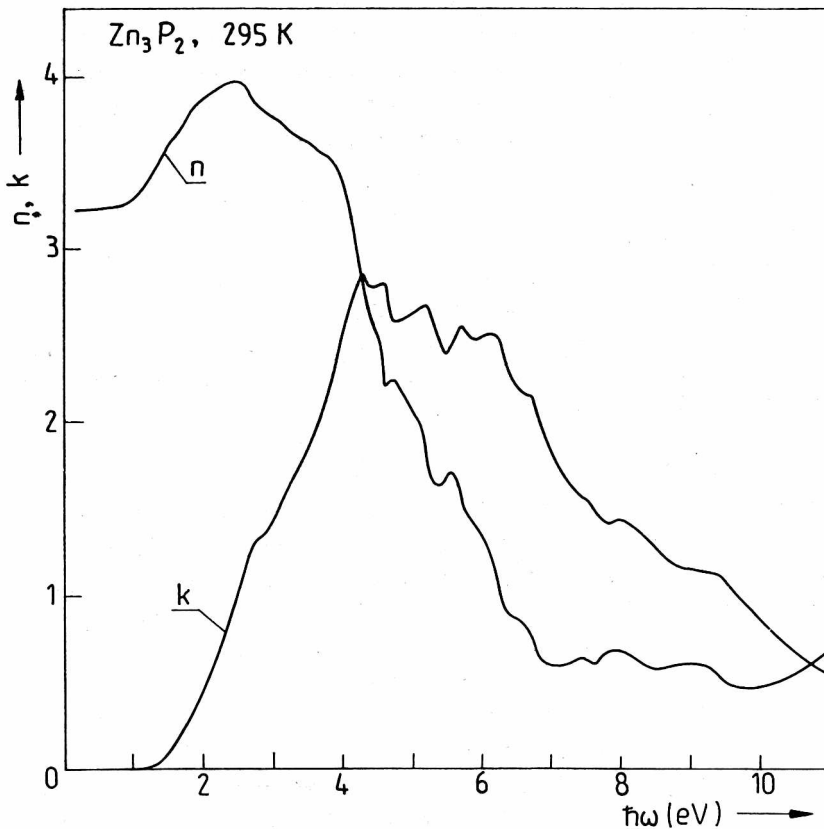


Fig. 14. Optical constants spectra of Zn_3P_2 (Misiewicz and Jezierski 1989), calculated by using the data of reflectivity spectrum (see Fig.9)

Rys. 14. Stałe optyczne Zn_3P_2 (Misiewicz i Jezierski 1989), obliczone na podstawie danych przedstawionych na rys. 9

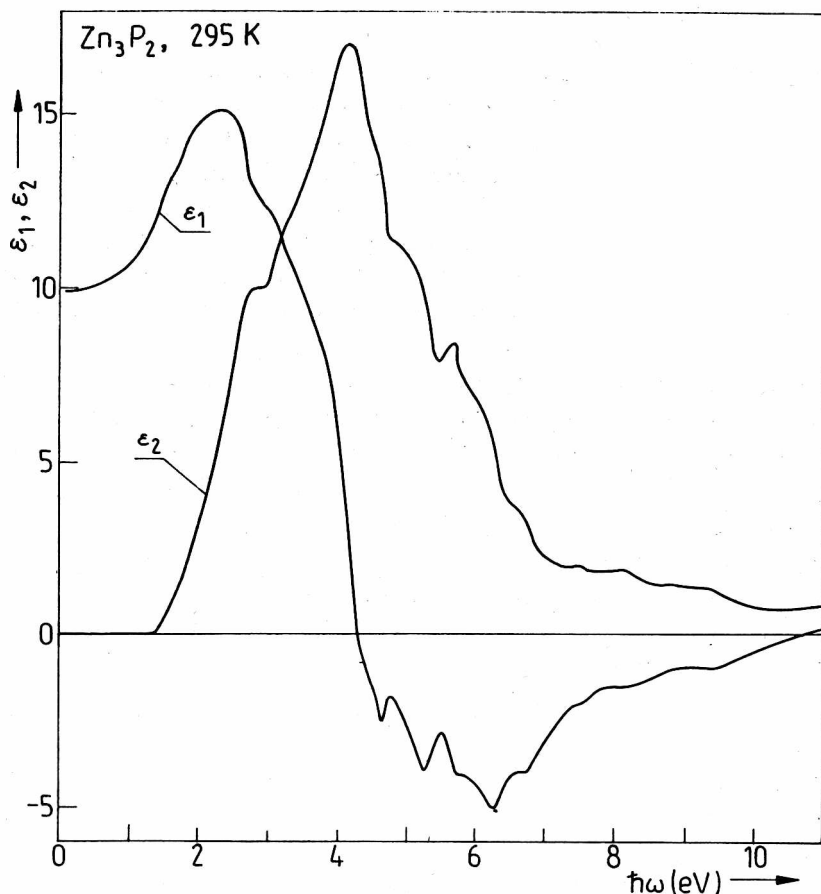


Fig. 15. Real and imaginary parts of dielectric constant for Zn_3P_2 (Misiewicz and Jezierski 1989), calculated by using the data of reflectivity spectrum (see Fig. 9)

Rys. 15. Rzeczywista i urojona część stałej dielektrycznej Zn_3P_2 (Misiewicz i Jezierski 1989), obliczone na podstawie danych z rys. 9

4.3 eV is more prominent for $E \parallel c$, one can expect the existence of an additional factor of the transitions at T, S, Y lines and at A point in tetragonal Brillouin zone. The transition at 4.58 eV may be connected with one of the transitions allowed only for $E \perp c$ polarization, listed in Tab. 2.

2. Optical constants

A Kramers-Kronig analysis of reflectivity curve was made to determine the spectra of the complex reflection index and the complex dielectric constant for Zn_3P_2 . As the reflectivity was measured in the range of 1.3–11 eV, beyond this region some extrapolations were

necessary. The linear-equations algorithm (Misiewicz et al. 1984) was applied to determine the low-energy extrapolation of the reflectivity curve. In this procedure, the agreement between the measured absorption edge (see Sect. 3.2.1) and low energy refractive index (see Sect. 4.2) was used to eliminate the extrapolation error. The high-energy extrapolation was used in the form of power-like function of energy with the parameters determined applying conditions of the continuity and the first derivative continuity of the measured and extrapolated reflectivity curves at last experimental point, i.e., at 11 eV. The high-energy extrapolation method is described in detail elsewhere (Jeziński and Misiewicz 1985). The optical constants spectra evaluated on the base of reflectivity spectrum taken from Fig. 9 are presented in Figs. 14 and 15.

3. Interpretation of the observed transitions in terms of quasi-cubic band structure model

The reflectivity spectrum as well as spectra of extinction coefficient, k , imaginary part of the complex dielectric constant, ϵ_2 , and quasi-joint density of states, DOS (see e.g., Phillips 1966)

$$\text{DOS} \sim \epsilon_2 \times E^2 \quad (8)$$

reflect approximately the real joint DOS function. The DOS energy distribution arises directly from energy band structure of the semiconductor.

From the dependence (8) (see Fig. 16) which reflects the DOS energy distribution, we can state that the main band-to-band optical transitions take place within 4-6 eV energy range with the local maxima at 4.25, 4.55, 5.05, 5.60 and 5.95 eV. The second group of transitions, less intensive, is located within 7-10 eV energy range with local maxima at 7.45, 8.0 and 9.15 eV. Between these two ranges there is also a transition at 6.60 eV.

It should be mentioned that the main band observed in photoemission spectrum presented by Domashevskaya et al. (1980) is also located within 4-6 eV, with sub-bands at 4.1 and 5.3 eV. It is not possible to see more details in that spectrum due to qualitatively and rather preliminary character of measurements. However, the general agreement between the result of Domashevskaya et al. (1980) and present work is very good. In the same paper (Domashevskaya et al. 1980) the energy position of the d-level was found at 9.7 eV below the top of valence band. That indicates that transitions correlated with existence of d-level may occur nearby the energy of 11.5 eV. The influence of d-electrons on the band structure of Zn_3P_2 was neglected in the Lin-Chung model.

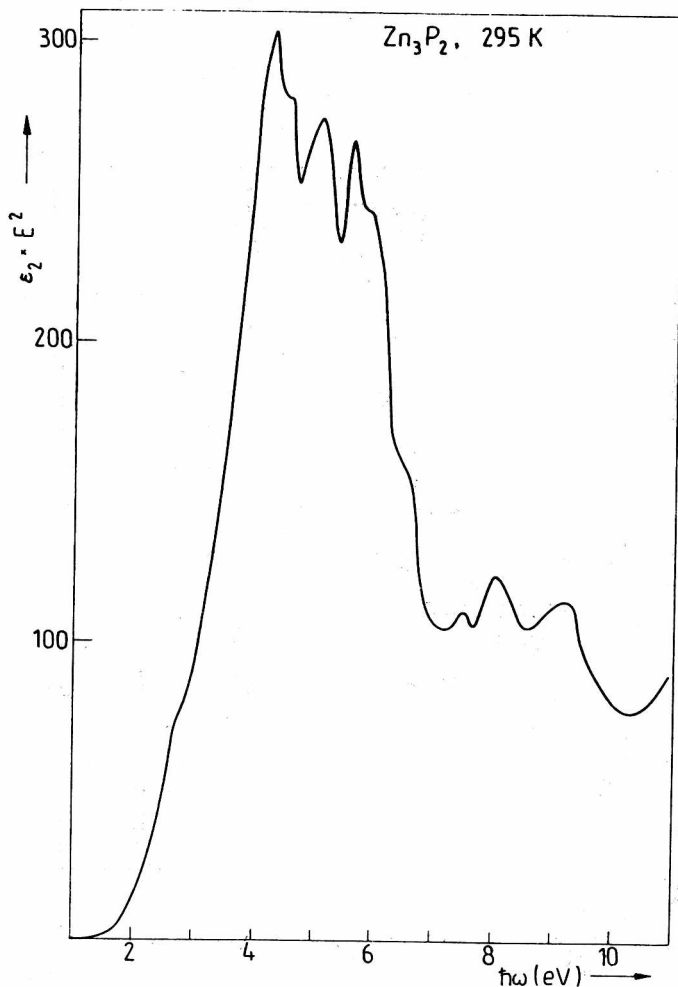


Fig. 16. Quasi-joint density of states function for Zn_3P_2 calculated by means of Kramers-Kronig analysis of reflectivity spectrum presented in Fig. 9 (Misiewicz and Jezierski 1989)

Rys. 16. Przybliżona funkcja łącznej gęstości stanów Zn_3P_2 wyznaczona za pomocą analizy Kramersa-Kroniga dla widma odbicia przedstawionego na rys. 9 (Misiewicz i Jezierski 1989)

By using the Lin-Chung model presented in Fig. 3, and by applying standard analysis with the critical-point line shapes method (M_0-M_3), see Phillips (1966), we may propose the types of critical points appropriate to the transitions observed in our spectra.

The first, relatively weak, band located at 2.65 eV can be correlated with the $L'_3 \rightarrow L_1$, $\Lambda_3 \rightarrow \Lambda_1$ transitions. Although the calculated energy of these transitions is 3.2 eV, but in the light of

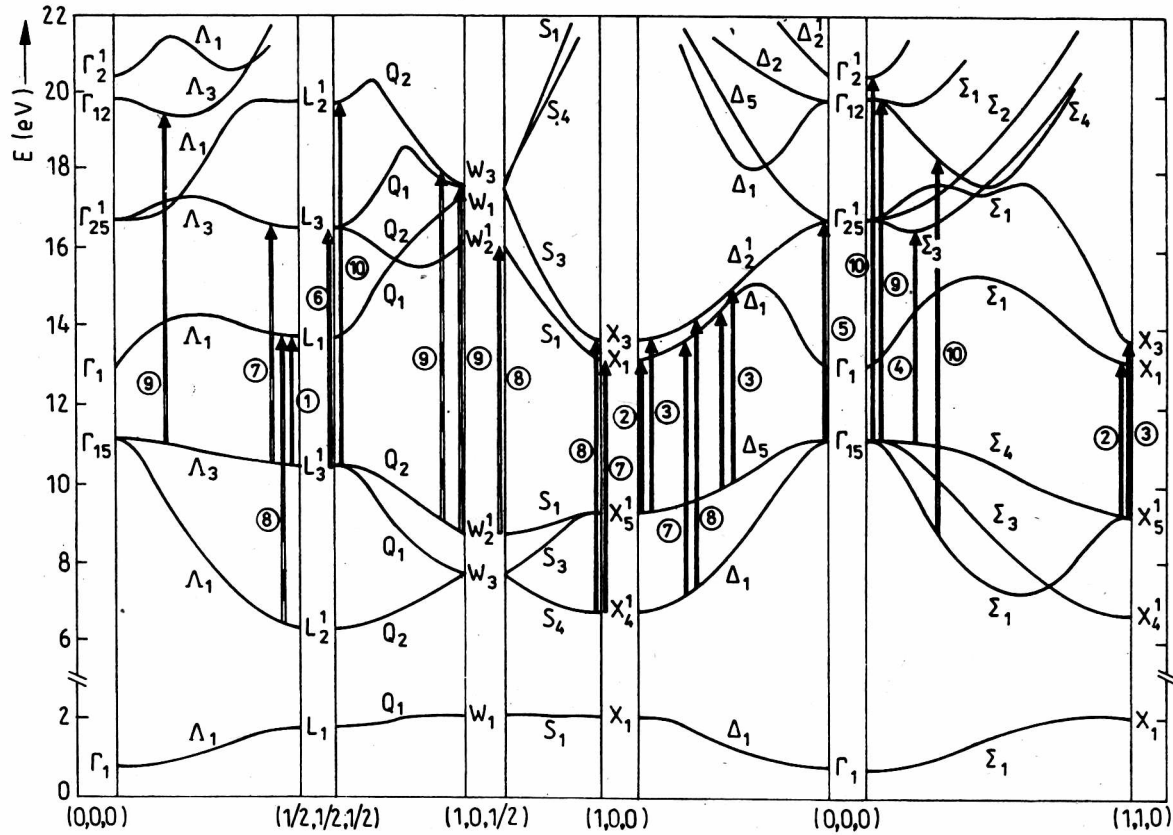


Fig. 17. Optical transitions observed in Zn₃P₂ crystal, marked by arrows on the pseudocubic energy band structure model (Lin-Chung 1971). Numbers are taken from Tab. 6 (Misiewicz i Jezierski 1989)

Rys. 17. Zaobserwowane w pomiarach przejścia optyczne w Zn₃P₂ zaznaczone strzałkami na tle pseudokubycznego modelu struktury pasmowej (Lin-Chung 1971). Numeracja przejść jak w tab. 6 (Misiewicz i Jezierski 1989)

Table 6

Energy (in eV) of the singularities in reflectivity spectrum measured for unpolarized light and calculated optical functions for Zn_3P_2 . The assignments are made on the base of Lin-Chung theoretical band structure model

| No. | R | k | ϵ_2 | $\epsilon_2 \times E^2$ | Theory | Assignment | Symmetry |
|-----|------|------|--------------|-------------------------|---------|---|----------------------|
| 1 | 2.65 | 2.75 | 2.8 | 2.7 | 3.2 | $L_3' \rightarrow L_1; \Lambda_3 \rightarrow \Lambda_1 (?)$ | $M_0 (M_1)$ |
| 2 | 4.28 | 4.3 | 4.10 | 4.25 | 4 | $X_5' \rightarrow X_1$ | $M_1 + M_2$ |
| 3 | 4.60 | 4.6 | 4.80 | 4.55 | 4.4-4.7 | $X_5' \rightarrow X_3; \Delta_5 \rightarrow \Delta_1, \Delta_2'$ | M_3 |
| 4 | 5.25 | 5.2 | 5.1 | 5.05 | 5.3 | $\Sigma_4 \rightarrow \Sigma_3$ | $M_1 + M_2$ |
| 5 | 5.75 | 5.7 | 5.65 | 5.60 | 5.6 | $\Gamma_{15} \rightarrow \Gamma_{25}$ | $M_1 + M_2$ |
| 6 | 6.25 | 6.2 | 6.2 | 5.95 | 6.1 | $L_3' \rightarrow L_3$ | M_3 |
| 7 | 6.80 | 6.75 | 6.7 | 6.6 | 6.5-6.9 | $\Lambda_3 \rightarrow \Lambda_3; X_4' \rightarrow X_1; \Delta_1 \rightarrow \Delta_1$ | $M_3, M_1 + M_2 (?)$ |
| 8 | 7.50 | 7.5 | 7.45 | 7.45 | 7.3-7.5 | $X_4' \rightarrow X_3; \Delta_1 \rightarrow \Delta_2'; W_2' \rightarrow W_2' (?); L_2' \rightarrow L_1$ | $M_1 + M_2$ |
| 9 | 8.30 | 8.0 | 7.95 | 8.0 | 8.2-8.6 | $\Lambda_3 \rightarrow \Lambda_3; \Gamma_{15} \rightarrow \Gamma_{12}; W_2' \rightarrow W_1, W_3; Q_2 \rightarrow Q_1, Q_2$ | $M_1 + M_2 (?)$ |
| 10 | 9.50 | 9.4 | 9.3 | 9.15 | 9.3-9.4 | $L_3' \rightarrow L_2'; \Gamma_{15} \rightarrow \Gamma_2'; \Sigma_1 \rightarrow \Sigma_4$ | $M_1 + M_2 (?)$ |

the discussion of residual tetragonal potential influence (see Sect. 3.1.2) one can expect a considerable decrease of its energy. The peak at 4.3 eV can be ascribed to $X'_5 \rightarrow X_1$ transition of energy ca 4 eV. In this case, residual potential makes the calculated energy increase. Thus, we can say that general agreement between theoretical predictions and experimental results for these two transitions is quite good. According to the discussion in Sect. 3.1.2, we should expect much less influence of the residual potential on the band structure for higher band-to-band energy distances. Thus, the agreement between theory and experiments is expected to be better. The last statement seems to be confirmed by the following analysis.

The peak in reflectivity spectrum at 4.6 eV may be attributed to $X'_5 \rightarrow X_3$ and/or $\Delta_5 \rightarrow \Delta_1, \Delta'_2$ transitions at the energy range of 4.4-4.7 eV. The next maximum at 5.25 eV seems to be connected with the transitions $\Sigma_4 \rightarrow \Sigma_3$ at energy 5.3 eV. The position of a small peak (or step) at 5.75 eV is in a good agreement with the value of 5.6 eV adequate to the transitions $\Gamma_{15} \rightarrow \Gamma_{25}$. The peak at 6.25 eV seems to correspond to the transitions at L point $L'_3 \rightarrow L_3$ (6.1 eV), and the second peak at 6.8 eV with $\Lambda_3 \rightarrow \Lambda_3$ and/or $X'_4 \rightarrow X_1, \Delta_1 \rightarrow \Delta_1$ possible ones. The joint density of states in Λ direction is high, as a consequence of nearly parallel alignments of both Λ_3 on the top of valence band and Λ_3 in the conduction band. To explain the step at the 7.5 eV we assume that the transitions $X'_4 \rightarrow X_3, \Delta_1 \rightarrow \Delta'_2, L'_1 \rightarrow L'_1$ and/or $W'_2 \rightarrow W_2$ occur. For the maximum placed at 8.3 eV, the possible locations in energy band model are as follows: $\Lambda_3 \rightarrow \Lambda_3$ (8.2 eV), $\Gamma_{15} \rightarrow \Gamma_{12}$ (8.6 eV), $W'_2 \rightarrow W_1, W_3$ (8.5 eV) and $Q_2 \rightarrow Q_1, Q_2$ (8.6 eV). We have no predictions allowing us to make a choice or to exclude any possibilities now. The last peak at 9.5 eV may be connected with transitions $L'_3 \rightarrow L'_2, \Gamma_{15} \rightarrow \Gamma'_2$ and $\Sigma_1 \rightarrow \Sigma_4$. All of them have the energy of 9.3-9.4 eV. The relatively high magnitude of the last two peaks may be explained by the coincidence of a few transitions taking place in the same energy region.

The propositions presented above supplemented with the critical points symmetry suggestions as well as by the singularity positions in R, k, ϵ_2 and $\epsilon_2 \cdot E^2$ are listed in Table 6, and marked on the Lin-Chung band structure model, see Fig. 17.

3.5. Conclusions on the band structure of Zn_3P_2

Optical and photoelectric methods were applied to investigate interband transitions in Zn_3P_2 at room temperature. Within 1.4-1.9 eV

energy range the fundamental direct transitions were investigated by using absorption, photoconductivity and reflectivity measurements performed for the oriented samples at the polarized light. From the results of these measurements the direct energy gap value was determined as 1.60 eV and valence band was found to be splitted into three sub-bands with crystal field splitting value equal to 0.03 eV and spin-orbit splitting value equal to 0.11 eV. The second conduction band was found at 0.28 eV above the lower one. Theoretical analysis of birefringence measurements in wide energy range gave also the value of fundamental optical transitions of 1.60 eV.

Reflectivity was used within the 2-11 eV energy range as a tool of experimental investigations, up to 5 eV applying polarized light, and at higher energies unpolarized light only. A good agreement between transitions observed experimentally in the 4.5-11 eV energy range and those possible in quasi-cubic Lin-Chung band structure model was found. This fact correlates with the results of group theory analysis performed for real D_{4h}^{15} symmetry of Zn_3P_2 crystal. This analysis predict that most of the possible transitions are allowed at both types of light polarization.

To obtain a qualitative agreement between the theory and the experimental results, for the transitions at the energies smaller than 4.5 eV, it was necessary to take into account an influence of tetragonal perturbation potential on the bands of Lin-Chung model. It should be mentioned that reflectivity data within 2-5 eV energy range indicate only a small anisotropy of optical transitions.

Complete disagreement between Lin-Chung pseudocubic model and experimental results was found at the Γ point. A distinct anisotropy for the transitions within 1.5-1.9 eV energy range was found. The analysis of the transitions possible to occur at Γ point, performed in terms of group theory analysis for the real symmetry of Zn_3P_2 structure, resulted in sequence of the bands consistent with the experimental data.

Finally, one may say that small distance effects, for large k-vectors in Brillouin zone, seem to be influenced by tetragonal symmetry not so much as the long distance ones. It means that anisotropy of Zn_3P_2 crystal influences more its properties at Γ point, than beyond it.

Band structure investigations were performed at room temperature. One should expect that decreasing the temperature mainly influences the interband distances, especially at Γ point, but does not considerably change the shape of bands. Thus, the main results of interband transitions investigations are valid, despite of the fact that they were performed at room temperature.

4. LATTICE VIBRATIONS IN Zn_3P_2

4.1. Theoretical analysis of lattice modes

4.1.1. Symmetry of one-phonon branches

Zn_3P_2 crystal composed of 40 atoms possesses 120 phonon branches, among them 117 are optical (oscillation), and 3 of them are acoustic modes, i.e., pure transitions. Only those phonons in each branch participate in optical processes which arise from regions in the Brillouin zone with a high density of phonon states per unit wave vector. These regions, or points, are known as critical points in the phonon dispersion. At a critical point on a branch the phonon frequency as a function of wave vector has vanishing slope or changes the sign discontinuously in one or more directions. The number of phonons in the crystal, which can participate in optical processes, is the sum of products of the numbers of critical points for that space group and the numbers of distinct branches at each critical point. Each of these phonons must be assigned to one of the irreducible representations of the crystal space group; i.e., it must belong to the so-called crystal species. Therefore, by using the space group theory it is possible to determine the optical activity of the phonons.

The first Brillouin zone of Zn_3P_2 crystal due to its symmetry D_{4h}^{15} is formed as a parallelepiped presented in Fig. 4b. The high symmetry points and lines in the irreducible part of the Brillouin zone are marked in this figure. According to general rules (see Birman 1984), most of the critical points are those at the center and close to the boundaries of the Brillouin zone, and they are placed at the high symmetry points. Γ point, as well as Z, A and M points possess the highest symmetry, while X, R points and Σ , Λ and Δ lines possess the lower symmetry.

We start from the Γ point. At this point there exist only infinite wavelength phonons. Distribution of the total number of 120 phonon branches between irreducible representations of the D_{4h}^{15} space group can be performed basing on the factor group analysis proposed by Fateley et al. (1971). The total irreducible representation of the crystal is the combined irreducible representation of each equivalent set of atoms. Starting from the site symmetry group of the constituent elements one correlates the irreducible representations of the site symmetry groups with those of the crystal factor group. For Zn_3P_2 crystal, D_{4h} point group is a factor group. According to Stackelberg and Paulus (1935), and Pistorius et al. (1977) the phos-

phorous atoms occupy two sets of the equivalent positions of C_{2v} symmetry position, each of multiplicity 4; and one set of the C_2 with multiplicity 8. Zinc atoms occupy three sets of C_s (C_{1h}) symmetry position with multiplicity 8. Performing the correlation procedure, we obtain the total distribution of the Zn_3P_2 crystal lattice modes among the irreducible representation of the factor group as follows:

$$\Gamma = 9\Gamma_1^+ + 4\Gamma_1^- + 5\Gamma_2^+ + 10\Gamma_2^- + 10\Gamma_3^+ + 5\Gamma_3^- + 4\Gamma_4^+ + 9\Gamma_4^- + 16\Gamma_5^+ + 16\Gamma_5^-$$

according to the Bouckart (1936) notation, and (9)

$$\Gamma = 9A_{1g} + 4A_{1u} + 5A_{2g} + 10A_{2u} + 10B_{1g} + 5B_{1u} + 4B_{2g} + 9B_{2u} + 16E_g + 16E_u,$$

according to the Mulliken (1933) notation.

The first notation will be used hereafter. For infrared dipole interaction, the ∇ operator of the transition matrix element transforms in D_{4h}^{15} structure as

$$\Gamma_2^- + \Gamma_5^-, \quad (10)$$

so, representation of infrared active one phonon is found to be

$$\Gamma^{IR} = 9\Gamma_2^- + 15\Gamma_5^-. \quad (11)$$

The pure translations, i.e., acoustic modes possess also $\Gamma_2^- + \Gamma_5^-$ symmetry but they vanish at Γ point. The polarizability tensor, responsible for the Raman scattering process in D_{4h}^{15} structure consists of the following components (Loudon 1964):

$$\begin{pmatrix} a & . & . \\ . & a & . \\ . & . & b \end{pmatrix} \begin{pmatrix} a & . & 0 \\ . & -c & . \\ . & . & . \end{pmatrix} \begin{pmatrix} . & d & . \\ d & . & . \\ . & . & . \end{pmatrix} \underbrace{\begin{pmatrix} . & . & e \\ . & . & . \\ e & . & . \end{pmatrix}}_{\Gamma_5^+} \begin{pmatrix} . & . & . \\ . & . & e \\ . & e & . \end{pmatrix}, \quad (12)$$

so we obtain Raman active one phonon modes

$$\Gamma^R = 9\Gamma_1^+ + 10\Gamma_3^+ + 4\Gamma_4^+ + 16\Gamma_5^+. \quad (13)$$

Group theory analysis allows us to evaluate the phonon branches through the Brillouin zone. The 120 one-phonon modes we can distribute between irreducible representations of the symmetry points and lines. For the high symmetry points we obtain:

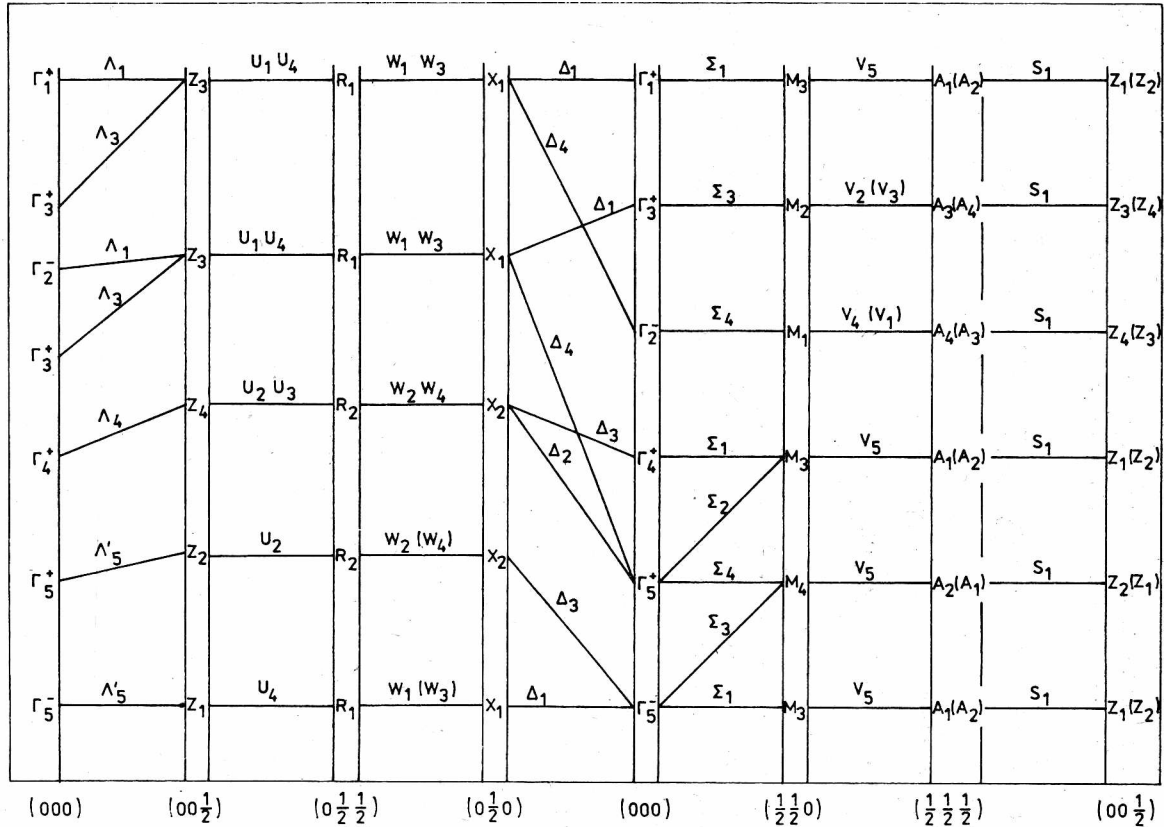


Fig. 18. Schematic model of the phonon branches symmetry of Zn_3P_2 crystal determined for the symmetry points and lines of the Brillouin zone. Coordinates of the symmetry point in $2\pi\left(\frac{1}{a} \frac{1}{a} \frac{1}{c}\right)$

Rys. 18. Schematyczny model symetrii gałęzi fononowych wzdłuż linii i punktów o wysokiej symetrii w strefie Brillouina. Współrzędne punktów symetrii podano w jednostkach $2\pi\left(\frac{1}{a} \frac{1}{a} \frac{1}{c}\right)$

$$\begin{aligned}
 Z &= 16Z_1 + 16Z_2 + 9Z_3 + 19Z_4, \\
 A &= 14A_1 + 14A_2 + 16A_3 + 16A_4, \\
 M &= 16M_1 + 16M_2 + 14M_3 + 14M_4, \\
 R &= 25R_1 + 35R_2, \\
 X &= 25X_1 + 35X_2.
 \end{aligned}
 \tag{14}$$

All of these irreducible representations are doubly degenerated. By means of the compatibility relations determined according to the standard procedure of representations decomposition (see, e.g., Streitwolf 1967, Birman 1984), a schematic model of the phonon branches symmetry evaluated through the Brillouin zone is proposed in Fig. 18. The Kovalev (1965) tables of irreducible representations were used. In this figure, only infrared or Raman active modes are included. The branches are developed from Γ to Γ point through X, R, Z points ($\Gamma \Delta X W R U Z \Delta \Gamma$) and from Γ to Z point ($\Gamma \Sigma M V A S Z$), see also Fig. 4b. It should be mentioned that group theory does not allow to choose between representations A_i and A_j at A point and Z_i and Z_j at Z point (going from M to Z). The same ambiguity takes place at W line, see Fig. 18.

4.1.2. Two-phonon transition selection rules

The general wave vector conservation rule requires that both for the sum and the difference of phonons their wave vectors should be equal to zero. This condition is fulfilled at Γ point and due to symmetry properties at the above listed critical points. Regarding a two-phonon process, if the two modes belong to different irreducible representations, one has a combination state, but if they are partners of the same space group of irreducible representations, one has an overtone state. For combination states the transition is allowed if the Kronecker product of the irreducible representations is common with the ∇ vector one (for the infrared dipole allowed transitions) or the polarizability tensor one (for the Raman allowed transitions) For overtone states, the symmetrized Kronecker square of the phonon irreducible representations should be used to derive the selection rules (see Birman 1984, and Streitwolf 1965).

As the first result we obtain that all two-overtones are infrared dipole forbidden and Raman allowed. Such a situation is typical in crystals possessing inversion symmetry, see Birman (1984) and Streitwolf (1967). The list of infrared dipole allowed combinations as well as overtones and combinations allowed in Raman scattering processes

Table 7

Two-phonon processes in Zn_3P_2 crystal at Γ point

| Infrared allowed | | | | | | |
|------------------|---------------------------------|--------------------------------------|---------------------------------|---------------------------------|---|--|
| Combinations | | | | | | |
| Species | $\Gamma_2^- \otimes \Gamma_1^+$ | $\Gamma_2^- \otimes \Gamma_5^+$ | $\Gamma_5^- \otimes \Gamma_5^+$ | $\Gamma_5^- \otimes \Gamma_1^+$ | $i = 1, 3, 4$ | |
| Polarization | Γ_2^- | Γ_5^- | Γ_2^- | Γ_5^- | | |
| Raman allowed | | | | | | |
| Overtones | | | Combinations | | | |
| Species | $[\Gamma_2^-]_2$ | $[\Gamma_5^-]_2$ | $[\Gamma_1^+]_2$ | $i = 1, 3, 4, 5$ | $\Gamma_1^+ \otimes \Gamma_1^+ \quad i = 3, 4, 5$ | $\Gamma_5^+ \otimes \Gamma_1^+ \quad i = 3, 4$ |
| Polarization | Γ_1^+ | $\Gamma_1^+, \Gamma_3^+, \Gamma_4^+$ | Γ_1^+ | | Γ_1^+ | Γ_5^+ |

Two-phonon processes in Zn_3P_2 crystal at high symmetry points

| Infrared allowed | | | | | | | |
|------------------|--------------------------|-------------------|--------------------------|--------------------------|--------------------------------------|--------------------------|---------------------------------|
| Overtones | | | | | | | |
| Species | $[Z_1](2)$ | $i = 3, 4$ | $[M_1](2)$ | $i = 1, 2$ | $[Q_1](2)$ | $Q = R, X$ | $i = 1, 2$ |
| Polarization | Γ_2^- | | Γ_2^- | | Γ_2^-, Γ_5^- | | |
| Combinations | | | | | | | |
| Species | $Q_1 \otimes Q_2$ | $P_3 \otimes P_4$ | $K_1 \otimes K_2$, | $K = R, X$ | $Q_1 \otimes Q_j$ | $Q = Z, A, M$; | $P = A, M$ |
| Polarization | Γ_2^- | Γ_2^- | Γ_5^- | | Γ_5^- | $i = 1, 2$; | $j = 3, 4$ |
| Raman allowed | | | | | | | |
| Overtones | | | | | | | |
| Species | $[Z_1](2)$ | $[A_1](2)$ | $[A_j](2)$ | $[M_1](2)$ | $[Q_1](2)$ | $Q = R, X$ | |
| Polarization | Γ_1^+, Γ_3^+ | Γ_1^+ | Γ_3^+, Γ_4^+ | Γ_1^+, Γ_4^+ | $\Gamma_1^+, \Gamma_3^+, \Gamma_5^+$ | | |
| | $i=1,2,3,4$ | $i=1,2$ | $j=3,4$ | $i=1,2,3,4$ | $i=1,2$ | | |
| Combinations | | | | | | | |
| Species | $Z_3 \otimes Z_4$ | $A_3 \otimes A_4$ | $M_3 \otimes M_4$ | $K_1 \otimes K_2$ | $P_1 \otimes P_2$ | $Q_1 \otimes Q_2$ | $Q_1 \otimes Q_j$ |
| Polarization | Γ_4^+ | Γ_1^+ | Γ_3^+ | Γ_4^+ | Γ_3^+ | Γ_4^+, Γ_5^+ | Γ_5^+ |
| | | | | $K=Z,A$ | $P=A,M$ | $Q=R,X$ | $Q=Z,A,M$ $i=1,2$ $j=3,4$ |

are tabulated in Table 7. By means of the same method the selection rules for two-phonon processes at Z, A, M, R and X critical points are collected in Table 8.

At Γ point from the 60 possible transitions only 6 of them are infrared and 13 are Raman allowed by the group theory selection rules. At the high symmetry points we obtain the numbers of two-phonon optical active modes as: 16 infrared and 29 Raman allowed. The other combinations between the branches from the different critical points are not considered in this work.

4.2. Experimental results of the optical lattice modes investigations

Reflectivity spectra were measured at room temperature and at 10 K in the $40\text{--}450\text{ cm}^{-1}$ energy range (see Misiewicz et al. 1988, Misiewicz 1988, and Wrobel and Misiewicz 1989). Absorption spectra in the $380\text{--}1200\text{ cm}^{-1}$ energy range at the same temperatures were determined using transmission and reflectivity values. Measurements were done by using a Bruker model Fourier interferometer and Beckman spectrophotometer. Unpolarized light was applied in these measurements. Samples of high resistivity and low carrier concentration ($p < 10^{13}\text{ cm}^{-3}$) were used in these measurements.

4.2.1. Reflectivity spectra in the far infrared region

Figure 19 presents reflectivity spectra in the reststrahlen region at 295 K and 10 K. As it was expected, a complex reflectivity structure is observed. In the whole energy range three regions of the reflectivity plot can be found. The first ($40\text{--}115\text{ cm}^{-1}$) consists of 6 peaks visible at room temperature. At low temperatures the structure becomes more clear. Relatively broad peak around 100 cm^{-1} splits into two independent ones. The second set of very prominent features is located at $240\text{--}360\text{ cm}^{-1}$. We observed 5 relatively broad maxima at room temperature and 7 sharper peaks at 10 K. Within these ranges relatively flat reflectivity plot is noticed. At room temperature only a few weak transitions in the range of $150\text{--}185\text{ cm}^{-1}$ can be found (see also previous paper (Misiewicz et al. 1988)). The temperature lowering causes the increase of these two maxima.

4.2.2. Dielectric constants spectra and one-phonon energies

By means of Kramers-Kronig method the analysis of the measured reflectivity spectra was performed and spectral dependences of dielec-

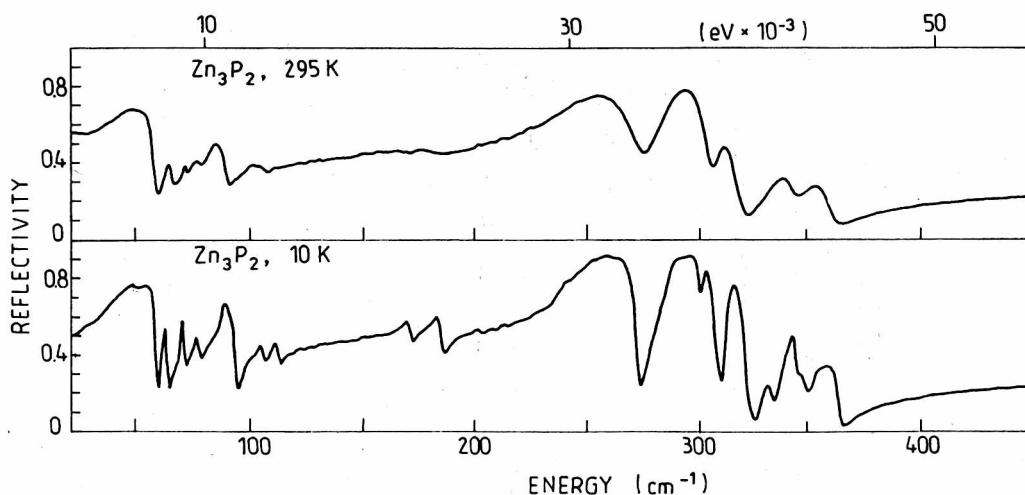


Fig. 19. Reflectivity spectra of Zn_3P_2 crystal in the reststrahlen region (Misiewicz et al. 1988a,b; Wrobel and Misiewicz 1989)

Rys. 19. Widma odbicia Zn_3P_2 w obszarze fundamentalnych wzbudzeń jednofononowych (Misiewicz i in. 1988a,b; Wrobel i Misiewicz 1989)

tric constants were determined. Figure 20 presents (as example) the spectra of real and imaginary parts of dielectric constant of Zn_3P_2 in the range of optical vibration modes, at room temperature. In Figure 21, the energy loss function ($\text{Im}(-1/\epsilon)$) plot also at 295 K is shown. As calculated from these results, the absorption coefficient approaches the value of 10^5 cm^{-1} . The refractive index, n , is calculated to be 3.2 for 500 cm^{-1} . Following Barker (1970), energies of the transverse and longitudinal optic modes are determined from the maxima positions in the imaginary parts of the dielectric constant and the energy loss function. Table 9 collects the TO and LO phonon energies adequate to Brillouin zone center. 13 pairs of phonons at 295 K and 16 pairs at 10 K in accordance with the numbers of reflectivity peaks were found.

4.2.3. Absorption spectra in the multiphonon transition region

Absorption coefficient was determined for energies higher than 385 cm^{-1} at 295 K and 450 cm^{-1} at 10 K. At room temperature (RT) in the range $385\text{--}550 \text{ cm}^{-1}$ a sequence of bands is visible (see Fig. 22). In the ranges close to 580 and 680 cm^{-1} , the local absorption maxima are located. This structure, in general, is reproduced at low temperatures

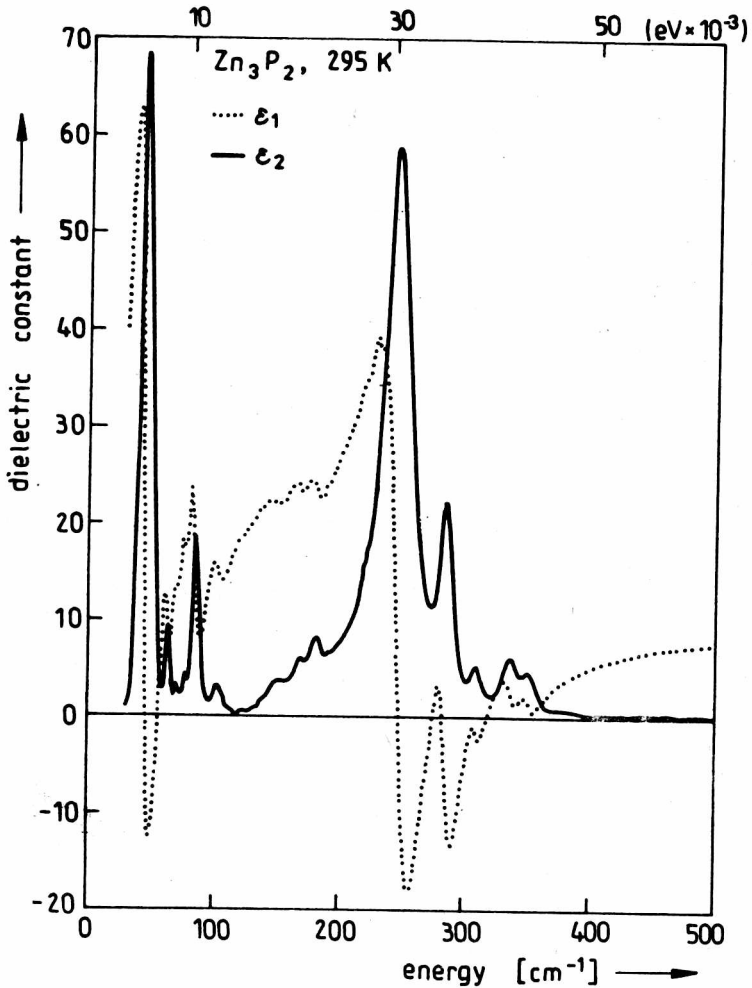


Fig. 20. Real and imaginary parts of the dielectric constant for Zn_3P_2 in the range of lattice vibrations, at room temperature (Misiewicz et al. 1988b)

Rys. 20. Rzeczywista i urojona część stałej dielektrycznej Zn_3P_2 w obszarze drgań sieci w temperaturze pokojowej (Misiewicz i in. 1988b)

but the absorption background is much weaker than at 295 K (see Fig. 23). In the $454\text{--}720\text{ cm}^{-1}$ range, there are 14 transitions visible at 295 K but at least 25 at 10 K. The main maxima, close to 580 and 680 cm^{-1} are, at low temperature, shifted towards the higher energy, in comparison with RT spectra. Figure 24 presents the higher energy part of the multiphonon transition region. The fine structure of the absorp-

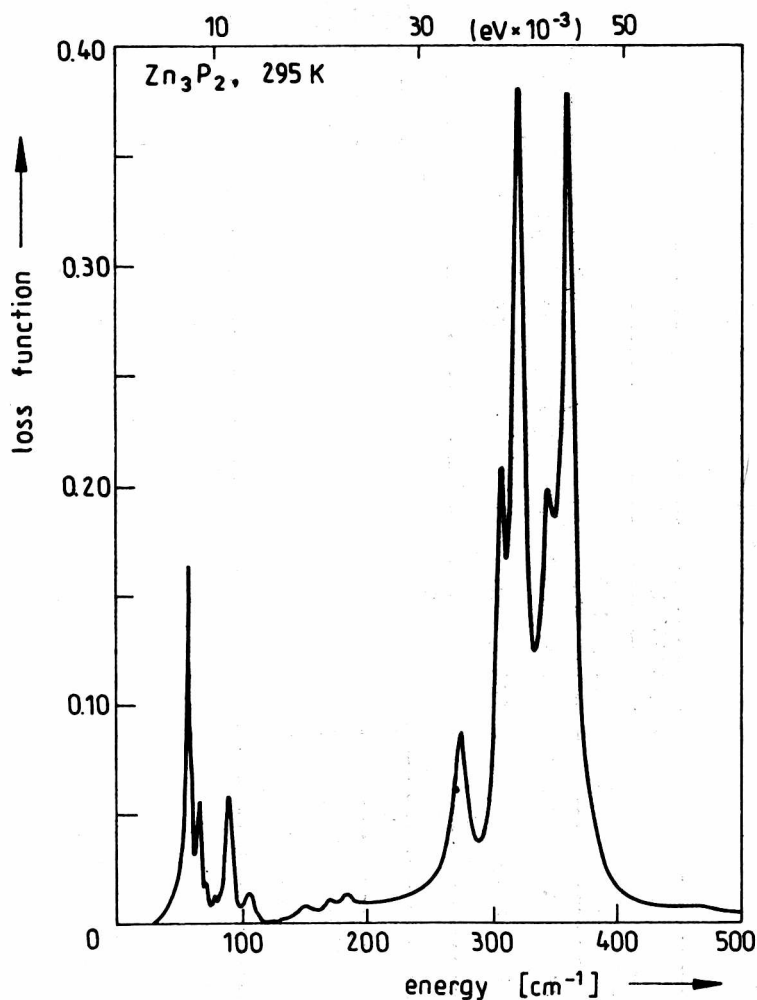


Fig. 21. Energy loss function for Zn₃P₂ crystal in the range of lattice vibrations, at room temperature (Misiewicz et al. 1988b)

Rys. 21. Funkcja strat dla Zn₃P₂ w obszarze drgań sieci w temperaturze pokojowej (Misiewicz i in. 1988b)

tion spectrum in this region is visible only for the high quality and low concentration samples. The spectra at RT and 10 K are similar. The weaker absorption background and more distinct absorption features are noticed at 10 K. Shift of the prominent structures towards higher energies, with temperature lowering is also observed. For the energies higher than 1250 cm⁻¹ an acceptor photoionization process begins (see Section 5).

Table 9

Zone center infrared active phonons in Zn_3P_2 crystal (in cm^{-1})

| Temperature 295 K | | | | | | | | | | | | | | | | |
|-------------------|------|------|------|------|------|-------|-------|-------|-----|-----|-------|-------|-------|-------|-------|-----|
| No. | 1 | 2 | 3 | 4 | 5 | 6 | 7 | 8 | 9 | 10 | 11 | 12 | 13 | | | |
| TO | 44 | 64 | 70.5 | 78 | 86 | 103 | 168.5 | 182.5 | 246 | 285 | 309.5 | 338 | 351 | | | |
| LO | 57 | 66 | 71 | 78.5 | 89 | 104.5 | 169 | 184 | 276 | 307 | 320 | 345 | 360 | | | |
| Temperature 10 K | | | | | | | | | | | | | | | | |
| No. | 1 | 2 | 3 | 4 | 5 | 6 | 7 | 8 | 9 | 10 | 11 | 12 | 13 | 14 | 15 | 16 |
| TO | 46.5 | 62 | 71 | 77 | 87.5 | 104 | 110.5 | 170.5 | 184 | 243 | 285 | 301.5 | 312.5 | 331.5 | 340 | 354 |
| LO | 58.5 | 63.7 | 71.5 | 78 | 94 | 105.5 | 112.5 | 172 | 186 | 274 | 309.5 | 301.5 | 323 | 333 | 348.5 | 363 |

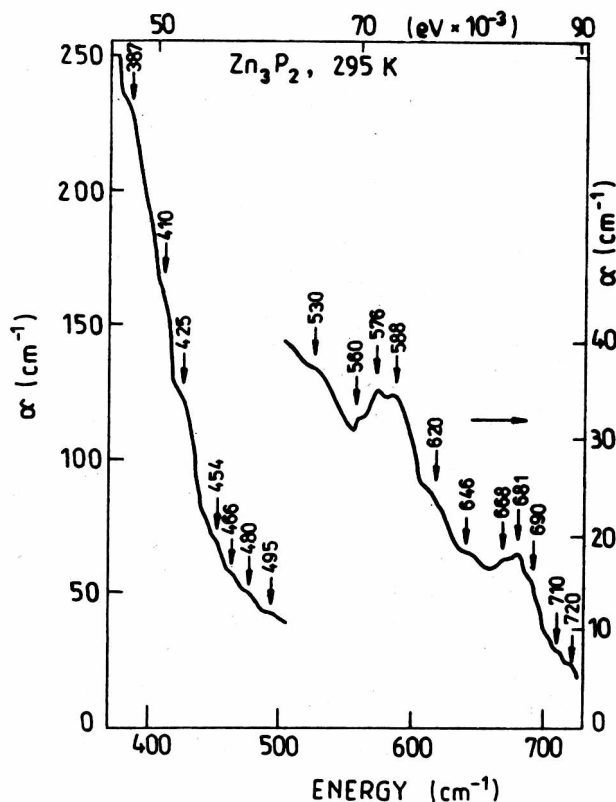


Fig. 22. Absorption coefficient spectrum of Zn_3P_2 crystal in the two-phonon transition range at room temperature (Misiewicz et al. 1988b)

Rys. 22. Widmo współczynnika absorpcji Zn_3P_2 w obszarze przejść dwu-fononowych dla temperatury pokojowej (Misiewicz i in. 1988b)

4.2.4. Raman scattering spectra

Raman scattering spectra of Zn_3P_2 were measured in backscattering geometry at room temperature using the polarized light. A krypton ion laser beam with 0.5 W at 676 nm wavelength was applied. A 3/4 m double-grating SPEX spectrometer, cooled GaAs photomultiplier and photon counting system was used for recording the spectra. The scattered light was detected in the 25-500 cm^{-1} range. Measurements were performed under the following conditions: $E \perp c \perp E$ and $E \perp c \parallel E$. These notations are equivalent to the following ones: $y(xx)\bar{y}$ or $x(yy)\bar{x}$ (VV), and $y(xz)\bar{y}$ or $x(yz)\bar{x}$ (VH); there is no difference in x and y directions in Zn_3P_2 unit cell. After careful analysis of the measured spectra,

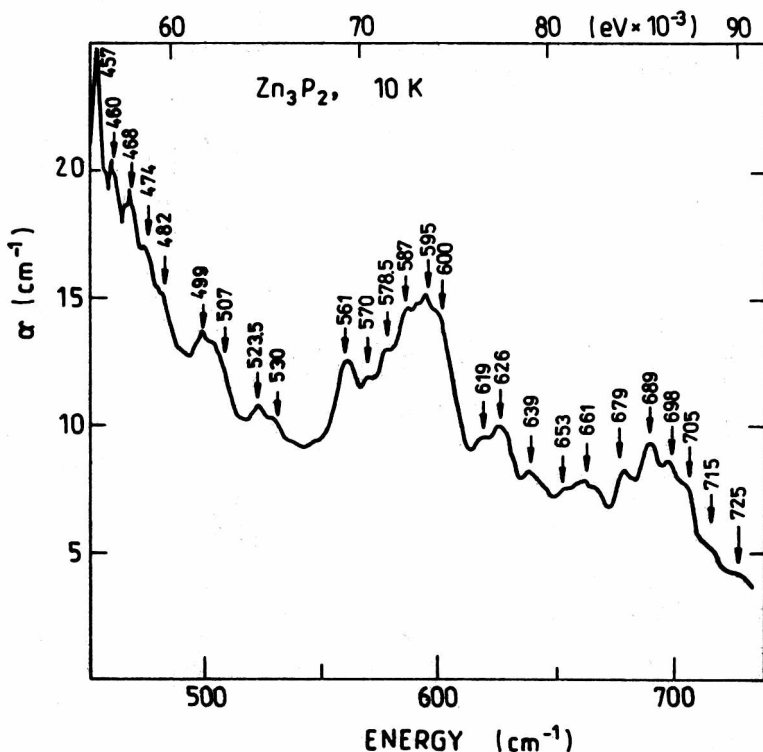


Fig. 23. Absorption coefficient spectrum of Zn_3P_2 crystal in the two-phonon transition range at 10 K (Misiewicz et al. 1988b)

Rys. 23. Widmo współczynnika absorpcji Zn_3P_2 w obszarze przejść dwufononowych w temperaturze 10 K (Misiewicz i in. 1988b)

large number of of transition was found. In the VV case, 33 peaks were observed as well as 43 for the VH configuration, see Figs. 25–27. In the VV configuration, the prominent 20 transitions are located in the 26–360 cm^{-1} energy range. In this region, 4 weaker peaks are also found. At VH configuration the 28 prominent and 5 weaker peaks are found in the same energy region. Energies of the prominent transitions are given in Table 10.

4.3. Analysis of the observed lattice modes in terms of selection rules for the optical vibrations

According to the distribution of the Zn_3P_2 modes among the irreducible representation (Eqs. (8), (9)), we should expect 9 single one-phonon transitions and 15 doubly degenerated ones, as infrared

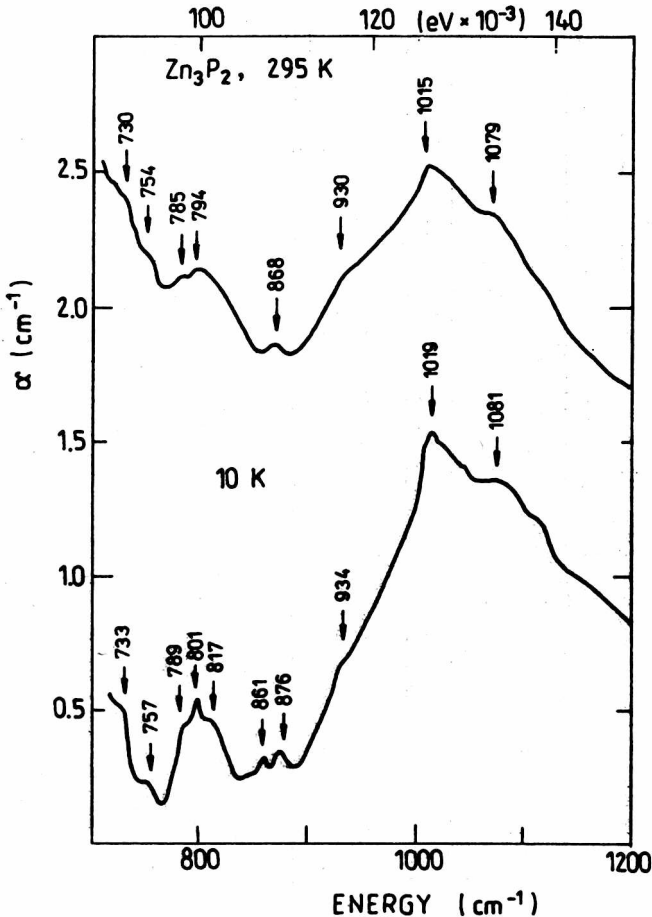


Fig. 24. Absorption coefficient spectra of Zn_3P_2 crystal in the three-phonon transition range at room temperature and 10 K

Rys. 24. Widma współczynnika absorpcji Zn_3P_2 w obszarze przejść trójfononowych w temperaturze pokojowej i w 10 K

active. From the analysis of reflectivity spectra we obtain as least 26 one-phonon transitions at room temperature and 32 one-phonon transitions at 10 K (see Tab. 9). Assuming that some of the one-phonon transitions are broadened at room temperature, the total number of 32 zone-centered phonons is in agreement with the total number of allowed phonons. Also it is assumed that some of the doubly degenerated (theoretically) modes are splitted.

Raman tensor (12) analysis shows that in VV configuration only $9\Gamma_1^+$ and $10\Gamma_3^+$ one-phonons should be visible and $16\Gamma_5^+$ doubly degenerated

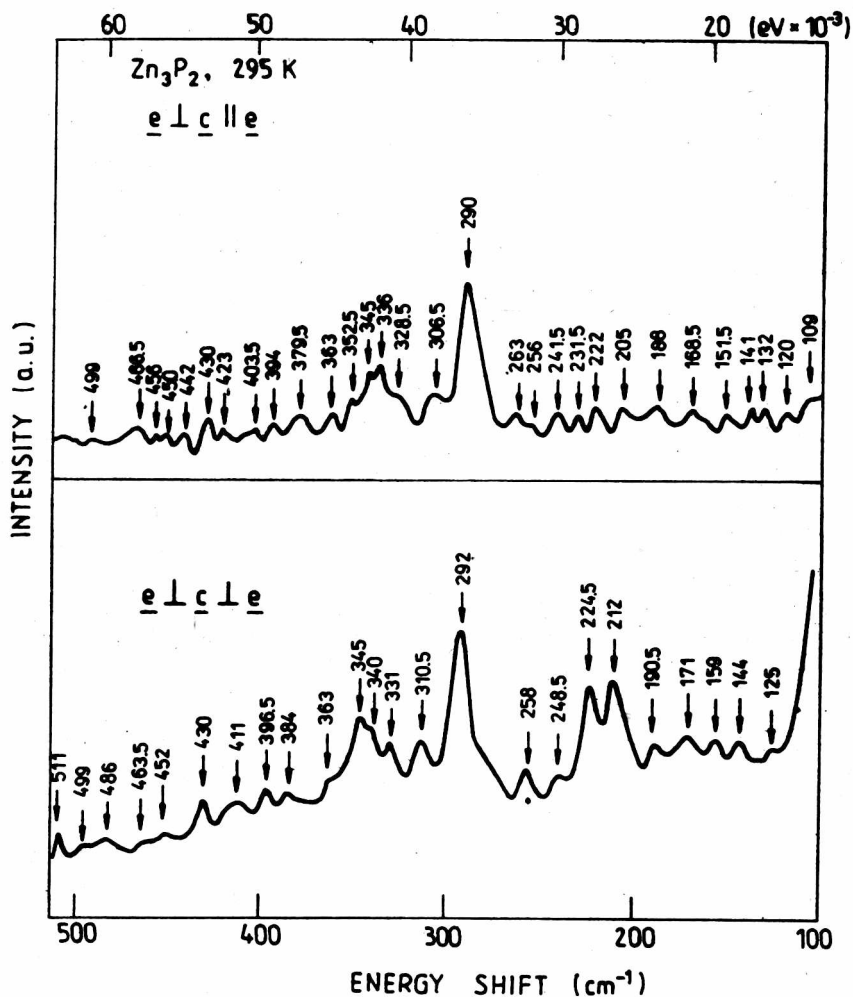


Fig. 25. Raman scattering spectra of Zn_3P_2 crystal at room temperature in two configurations: $E \perp c \parallel E$ (VH), $(y(xz)\bar{y})$, and $E \perp c \perp E$ (VV), $y(xx)\bar{y}$

Rys. 25. Widma rozpraszania Ramana Zn_3P_2 w temperaturze pokojowej dla dwóch konfiguracji: $E \perp c \parallel E$ (VH), $(y(xz)\bar{y})$ i $E \perp c \perp E$ (VV), $(y(xx)\bar{y})$

ones in VH configuration. In the VV configuration spectra it is easy to find out 20 distinct peaks and ascribe them to one-phonon branches at Γ point. To understand the number of prominent transitions observed in VH configuration one has to assume a splitting of the doubly degenerated (in the light of group theory analysis) one-phonon branches at Γ point. If we do this, we will obtain the agreement between the-

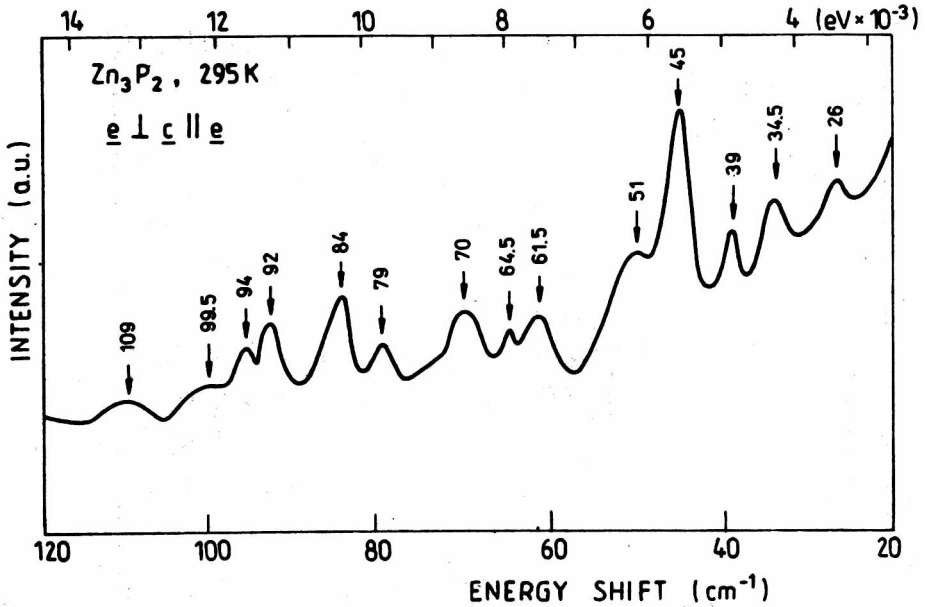


Fig. 26. Raman scattering spectrum of Zn_3P_2 crystal at room temperature in the low energy range for configuration: $E \perp c \parallel E$ (VH), $(y(xz)\bar{y})$

Rys. 26. Widmo rozpraszania Ramana Zn_3P_2 w temperaturze pokojowej w obszarze niskich energii dla konfiguracji $E \perp c \parallel E$ (VH), $(y(xz)\bar{y})$

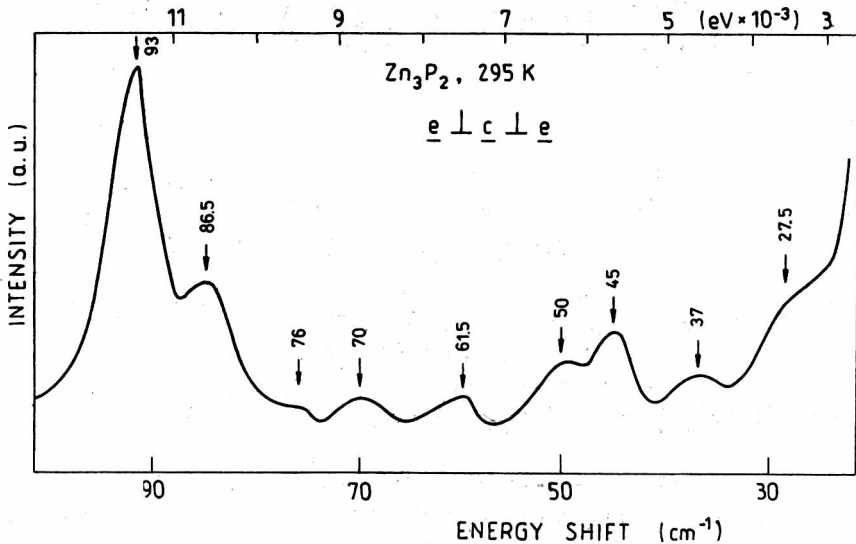


Fig. 27. Raman scattering spectrum of Zn_3P_2 crystal at room temperature in the low energy range for configuration: $E \perp c \perp E$ (VV), $(y(xx)\bar{y})$

Rys. 27. Widmo rozpraszania Ramana Zn_3P_2 w temperaturze pokojowej w obszarze niskich energii dla konfiguracji $E \perp c \perp E$ (VV), $(y(xx)\bar{y})$

oretical predictions and experimental results. As we can see in Table 10, nine modes are observed both at VV and VH configurations; most of them are located in low energy region of $26-79 \text{ cm}^{-1}$.

Mutual exclusion rules require, in the case of the crystal with inversion symmetry, that the one-phonon modes observed in infrared and Raman spectra should be different. Zn_3P_2 crystal possesses inversion symmetry so the same transitions should not be observed. Almost 60 from the total number of 74 one-phonon energies in Raman scattering and reflectivity spectra are different (compare Tables 9 and 10) so this rule seems to be well satisfied.

Group theory predicts no overtones of infrared active phonons at Γ , allowed in infrared, see Table 7. Neglecting only a few energy coincidences this condition is well fulfilled both at 295 and 10 K.

The next theoretical prediction that all infrared overtones should be Raman active in VV configuration, is fulfilled quite reasonably in the measured energy range ($80-500 \text{ cm}^{-1}$). Only a few from the infrared Γ overtones are not consistent with the transitions observed in Raman spectrum, see Tab. 11.

All Raman active Γ overtones should be Raman active at VV configuration also, as is indicated in Tab. 7. In the measured spectra, we can find most of the expected overtones (see Tab. 12) so this configuration is quite well fulfilled.

All combinations between infrared active and Raman allowed transitions at Γ point should be visible in infrared, see Tab. 7. As presented in Tables 13 and 14, all transitions observed in two-phonon absorption range may be ascribed to some combinations of the infrared and Raman permitted one-phonon.

The other transitions observed in Raman spectra at configurations VV 4 and VH -15 might be explained in terms of one-phonon combinations allowed in VV or VH configurations. However, it seems more probable to take into account the transitions at other critical points predicted by group theory, see Tab. 8.

For the energies higher than two-phonon overtones and combinations calculated by using the data from reststrahlen and Raman spectra (Tab. 9 and Tab. 10), one expects three-phonon transitions. In this term we may explain spectra presented in Fig. 12. No detailed study of three-phonon transition selection rules was performed. Nevertheless, by means of symmetrized Kronecker cube calculations, we obtain that there are infrared-active three-phonon overtones $[\Gamma_5^-]_{(3)}$ in Γ_5^- and $[\Gamma_2^-]_{(3)}$ in Γ_2^- polarizations, respectively (we remember that two-phonon overtones are forbidden in infrared, see Tab. 7). Using this result we can assign most of the transitions in Fig. 24, see Tab. 15.

Table 11

Infrared overtones at Γ point, calculated from the data of Table 9 compared with transitions observed in VV Raman scattering, at 295 K (in cm^{-1})

| | | | | | | | | | |
|----------------|------|-----|-----|-----|-----|-----|-----|-----|-----|
| | 88 | 128 | 141 | 156 | 172 | 206 | 337 | 365 | 492 |
| IR calculated | 114 | 122 | 142 | 157 | 178 | 209 | 338 | 368 | |
| Raman observed | 86.5 | 125 | 144 | 159 | 171 | 212 | 340 | 363 | 499 |

Table 12

Energies of Raman overtones calculated using Table 10 correlated with transitions observed in Raman spectra at VV configuration, at 295 K (in cm^{-1})

| | | | | | | | | | | | | | | | |
|------------|-----|-----|-----|-----|-----|-----|-----|-----|-----|--|-----|-----|-------|-----|-----|
| Calculated | 52 | 69 | 78 | 90 | 102 | 123 | 140 | 158 | 168 | | 184 | 218 | 240 | 264 | 282 |
| | 55 | | 74 | 90 | 100 | 123 | 140 | | | | 173 | 186 | | | |
| Observed | 50 | 70 | 76 | 93 | | 125 | 144 | 159 | | | 171 | 190 | 222 | | 258 |
| Calculated | | 303 | | | 337 | | 376 | | 410 | | 444 | | 463 | 483 | |
| | 288 | | 318 | | | 342 | | 381 | 424 | | 449 | | | | 516 |
| Observed | 292 | | | 340 | 340 | | | 384 | 411 | | | 452 | 463.5 | 486 | 511 |

Table 13

Energies of the transitions observed in two-phonon absorption range (at 295 K) and calculated combinations of the infrared (TO, LO) and Raman (R) zone centered one-phonons (from Table 9 and 10)

| | 387 | 410 | 425 | 454 | 466 | 480 |
|-----------------------------------|-------|---|---|---|---|---|
| LO ₁ +R ₃₅ | 388 | LO ₁₃ +R ₅ 410 | TO ₂ +R ₃₉ 427 | TO ₆ +R ₃₈ 455 | TO ₆ +R ₃₆ 466 | LO ₁₃ +R ₁₃ 480 |
| LO ₁₁ +R ₇ | 388 | TO ₂ +R ₃₇ 409 | LO ₅ +R ₃₆ 425 | LO ₁₃ +R ₁₁ 453 | LO ₁₂ +R ₁₃ 465 | TO ₁₂ +R ₁₅ 479 |
| TO ₁₂ +R ₅ | 388 | LO ₁ +R ₃₈ 409 | TO ₁₂ +R ₁₀ 424.5 | | LO ₁₀ +R ₁₈ 466 | TO ₁₁ +R ₂₀ 480.5 |
| | 495 | 530 | 560 | 576 | 588 | 620 |
| TO ₁₃ +R ₁₆ | 495 | LO ₁₁ +R ₂₄ 532 | TO ₁₂ +R ₂₆ 562 | TO ₉ +R ₃₅ 577 | TO ₉ +R ₃₇ 591 | LO ₉ +R ₃₇ 621 |
| LO ₁₀ +R ₂₁ | 495 | LO ₈ +R ₃₇ 529 | LO ₁₂ +R ₂₄ 557 | TO ₁₀ +R ₃₁ 575 | LO ₁₂ +R ₂₈ 586.5 | TO ₁₀ +R ₃₆ 621 |
| LO ₈ +R ₃₃ | 494.5 | LO ₁₀ +R ₂₆ 531.5 | TO ₁₃ +R ₂₄ 563 | TO ₁₃ +R ₂₆ 575.5 | LO ₉ +R ₃₃ 586.5 | LO ₁₃ +R ₃₇ 618 |
| | 646 | 668 | 681 | 690 | 710 | 720 |
| TO ₁₁ +R ₃₆ | 646 | LO ₁₀ +R ₃₉ 670 | LO ₁₁ +R ₃₉ 683 | LO ₁₂ +R ₃₇ 690 | LO ₁₂ +R ₃₉ 708 | LO ₁₃ +R ₃₉ 723 |
| TO ₁₀ +R ₃₉ | 648 | TO ₁₂ +R ₃₅ 669 | LO ₁₂ +R ₃₆ 681 | TO ₁₂ +R ₃₈ 690 | LO ₁₃ +R ₃₈ 712 | |
| TO ₁₂ +R ₃₂ | 644.5 | LO ₁₃ +R ₃₂ 666.5 | TO ₁₃ +R ₃₅ 682 | LO ₁₃ +R ₃₁ 691 | | |

Table 14

Energies observed in two-phonon absorption range at 10 K correlated with calculated combinations of the infrared (TO, LO) at 10 K and Raman (R) at 295 K zone centered one-phonons (from Tables 9 and 10)

| | | | | | | | | | | | |
|-----------------------------------|-------|-----------------------------------|-------|-----------------------------------|-------|-----------------------------------|-------|-----------------------------------|-------|-----------------------------------|-------|
| | 457 | | 460 | | 468 | | 474 | | 482 | | 499 |
| LO ₅ +R ₃₉ | 457 | TO ₁₅ +R ₁₃ | 460 | TO ₁₀ +R ₂₆ | 467.5 | LO ₁₄ +R ₁₅ | 474 | LO ₈ +R ₃₃ | 482.5 | TO ₈ +R ₃₄ | 499 |
| TO ₁₁ +R ₂₀ | 456 | TO ₈ +R ₃₁ | 461 | LO ₁₁ +R ₁₈ | 469.5 | TO ₉ +R ₃₁ | 474 | TO ₁₃ +R ₁₉ | 481 | LO ₁₀ +R ₂₆ | 498.5 |
| TO ₁₃ +R ₁₆ | 456.5 | LO ₁₁ +R ₁₇ | 461 | LO ₁₃ +R ₁₆ | 467 | TO ₁₀ +R ₂₇ | 474.5 | LO ₁₃ +R ₁₈ | 482 | TO ₁₄ +R ₁₉ | 500 |
| LO ₁₃ +R ₁₄ | 457 | LO ₁₂ +R ₁₈ | 460.5 | LO ₁₅ +R ₁₃ | 468.5 | LO ₁₃ +R ₁₇ | 474.5 | TO ₁₅ +R ₁₅ | 481 | TO ₁₅ +R ₁₈ | 499 |
| | 507 | | 523.5 | | 530 | | 561 | | 570 | | 578.5 |
| TO ₁₁ +R ₂₅ | 507 | TO ₈ +R ₃₈ | 522.5 | TO ₉ +R ₃₇ | 529 | TO ₁₅ +R ₂₅ | 562 | TO ₁₃ +R ₂₉ | 570.5 | LO ₁₅ +R ₂₇ | 580 |
| TO ₁₂ +R ₂₃ | 506.5 | LO ₈ +R ₃₈ | 524 | LO ₉ +R ₃₇ | 531 | LO ₁₅ +R ₂₄ | 560.5 | TO ₁₅ +R ₂₇ | 571.5 | TO ₁₆ +R ₂₆ | 578.5 |
| LO ₁₅ +R ₁₈ | 507.5 | LO ₁₂ +R ₂₅ | 523.5 | TO ₁₅ +R ₂₂ | 530.5 | TO ₁₆ +R ₂₃ | 559 | LO ₁₅ +R ₂₅ | 570.5 | | |
| LO ₁₆ +R ₁₆ | 507 | LO ₁₄ +R ₂₂ | 523.5 | LO ₁₆ +R ₁₉ | 531.5 | | | LO ₁₆ +R ₂₃ | 568 | | |

| 587 | | 595 | | 600 | | 619 | | 626 | | 639 | |
|-----------------------------------|-------|-----------------------------------|-------|-----------------------------------|-------|-----------------------------------|-------|-----------------------------------|-----|-----------------------------------|-------|
| LO ₁₃ +R ₃₀ | 586 | TO ₁₄ +R ₃₀ | 594.5 | LO ₁₁ +R ₃₁ | 600.5 | LO ₁₁ +R ₃₃ | 620 | LO ₁₀ +R ₃₈ | 626 | LO ₁₁ +R ₃₄ | 638 |
| TO ₁₆ +R ₂₇ | 585.5 | LO ₁₄ +R ₃₀ | 596 | TO ₁₃ +R ₃₁ | 602.5 | TO ₁₃ +R ₃₂ | 619 | LO ₁₄ +R ₃₁ | 625 | TO ₁₄ +R ₃₂ | 637.5 |
| LO ₁₆ +R ₂₆ | 587.5 | TO ₁₆ +R ₂₈ | 595.5 | TO ₁₅ +R ₂₉ | 598 | TO ₁₆ +R ₃₀ | 617 | LO ₁₆ +R ₃₀ | 626 | LO ₁₄ +R ₃₂ | 639.5 |
| | | LO ₁₆ +R ₂₇ | 594.5 | | | LO ₁₆ +R ₂₉ | 621 | | | LO ₁₅ +R ₃₁ | 638.5 |
| 653 | | 661 | | 679 | | 689 | | 698 | | 705 | |
| LO ₁₃ +R ₃₄ | 651.5 | LO ₁₃ +R ₃₆ | 359 | TO ₁₄ +R ₃₇ | 676.5 | LO ₁₆ +R ₃₄ | 671.5 | TO ₁₆ +R ₃₇ | 699 | TO ₁₅ +R ₃₉ | 703 |
| LO ₁₂ +R ₃₈ | 653.5 | TO ₁₄ +R ₃₄ | 660 | LO ₁₄ +R ₃₇ | 678 | TO ₁₆ +R ₃₆ | 690 | LO ₁₆ +R ₃₆ | 699 | TO ₁₆ +R ₃₈ | 706 |
| TO ₁₅ +R ₃₃ | 650.5 | LO ₁₄ +R ₃₄ | 661.5 | LO ₁₅ +R ₃₄ | 677 | | | | | LO ₁₆ +R ₃₇ | 708 |
| LO ₁₆ +R ₃₁ | 653 | TO ₁₆ +R ₃₂ | 660.5 | | | | | | | | |
| 715 | | 725 | | | | | | | | | |
| TO ₁₆ +R ₃₉ | 717 | LO ₁₆ +R ₃₉ | 726 | | | | | | | | |
| LO ₁₆ +R ₃₈ | 715 | | | | | | | | | | |

Three-phonon infrared overtones observed
in infrared absorption spectrum at 10 K (energy in cm^{-1})

| | | | | | | | | |
|--------------------------|------|-------------------|------|-------------------|-----|-------------------|-------|-------------------|
| Measured | 733 | | 817 | | 861 | | 934 | |
| Calculated from Tab.9 | 729 | 3TO_{10} | 822 | 3LO_{11} | 855 | 3TO_{11} | 928.5 | 3LO_{11} |
| Measured | 1019 | | 1081 | | | | | |
| Calculated from Tab.9 | 1020 | 3TO_{15} | 1089 | 3LO_{16} | | | | |

4.4. Conclusions of the lattice vibrations in Zn_3P_2

On the base of group theory, the symmetry of infrared and Raman active one-phonon branches for Zn_3P_2 was determined. Critical point analysis and compatibility relations allowed us to find the symmetry of phonon branches through the symmetry lines and points in Brillouin zone. The selection rules of the overtones and combinations for all high symmetry points were led out. The theoretical results were applied to explain the experimental results.

The Raman scattering spectra of Zn_3P_2 , reflectivity and absorption spectra in the whole fundamental vibrations range are presented. From the reflectivity results the set of infrared active zone centered one-phonons was determined. The main transitions in Raman spectra were ascribed to one-phonon branches at Γ point as well. The other Raman transitions and singularities in absorption spectra were interpreted in terms of overtones and two-phonon combination bands. Most of the theoretical predictions are well matched to the experimental results, leading to the conclusion that Zn_3P_2 crystal symmetry cannot be simplified to any cubic structure analysing the lattice dynamic of this crystal.

There are no theoretical calculations of phonon spectrum in Zn_3P_2 . Therefore, we cannot interpret the obtained results in more details. By using polarized light in infrared measurements, we will be able to show which branches belong to LO and TO types and give more information on the Raman active phonons.

There is also necessary to measure Raman scattering spectra at low temperature to get much sharper structure than at the room temperature and discriminate between one phonon and multi-phonon transitions. The understanding of the physical reason of the splitting of doubly degenerated modes at Γ point is very important. A cause of this lifting might be connected with the displacements of the atomic positions in the ideal antiferrofluoride cell. The other explanation might base on the fact that in Zn_3P_2 unit cell the same atoms are located in a few different crystallographic positions. It may also give some perturbation in the lattice dynamics.

5. OPTICAL TRANSITIONS RELATED TO IMPERFECTION LEVELS

Absorption measurements were performed by using a Cary-14 spectrophotometer in the 0.6-1.5 eV energy range, and Beckman-10 spectrophotometer in the 0.08-0.6 eV energy range (only for the unpolarized light). Four types of Zn_3P_2 samples were investigated depending on their room temperature resistivity and hole concentration. The samples of the first type denoted as A had resistivity higher than $\rho \approx 10^4 \Omega \text{ cm}$ and holes concentration was estimated at $p \leq 10^{13} \text{ cm}^{-3}$. The second one, denoted as B was characterized by $\rho = 5 \times 10^2 - 10^3 \Omega \text{ cm}$ and $p = 10^{14} - 10^{15} \text{ cm}^{-3}$, the third one, C, by $\rho \approx 10 - 10^2 \Omega \text{ cm}$ and $p \approx 10^{16} \text{ cm}^{-3}$, and the last, fourth one, called D had $\rho \leq 10 \Omega \text{ cm}$ and $p \geq 1 \times 10^{17} \text{ cm}^{-3}$.

5.1. Absorption within 0.1-0.5 eV energy range

Figures 28 and 29 present absorption spectra in the 0.15-0.6 eV energy range for all the sample types at room (Fig. 28), and at the liquid nitrogen temperatures (Fig. 29). For the samples with hole concentration not higher than 10^{16} cm^{-3} , i.e., types A, B, C, only lattice absorption below energy 0.15 eV is observed (see Sect. 4.2). At the energies higher than 0.15 eV there is visible increase of the absorption coefficient for the samples with middle hole concentration $10^{14} < p \leq 10^{16} \text{ cm}^{-3}$. For these samples, two additional slope changes in the absorption plots within 0.15-0.5 eV energy range were found: the first at about 0.25-0.28 eV, and the second one at 0.35-0.38 eV. For high resistivity samples (type A) almost flat absorption curve in the range of 0.15-0.45 eV was observed. Only very small changes of the absorption curve slope are visible.

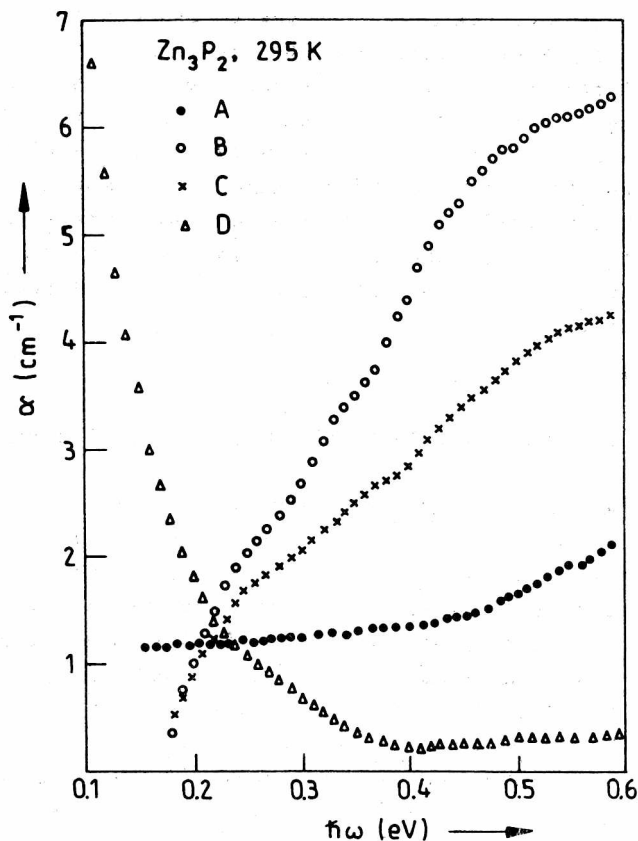


Fig. 28. Absorption spectra of the Zn_3P_2 samples of different hole concentration: A - $p \leq 10^{13} \text{ cm}^{-3}$, B - $p = 10^{14} - 10^{15} \text{ cm}^{-3}$, C - $p \approx 10^{16} \text{ cm}^{-3}$ and D - $p \geq 1 \times 10^{17} \text{ cm}^{-3}$, after background subtraction

Fig. 28. Widma współczynnika absorpcji w temperaturze pokojowej próbek o różnej koncentracji dziur: A - $\leq 10^{13} \text{ cm}^{-3}$, B - $p = 10^{14} - 10^{15} \text{ cm}^{-3}$, C - $p \approx 10^{16} \text{ cm}^{-3}$ i D - $p \geq 1 \times 10^{17} \text{ cm}^{-3}$ (po odjęciu tła)

For samples with the highest hole concentration, completely different behaviour of the absorption spectrum was found. A monotonic increase of absorption coefficient with the photon energy decreasing below 0.4 eV was found (see curve D in Figs. 28 and 29).

Cooling the samples down to 80 K did not give distinct changes of the measured spectra (see Fig. 29). For the high concentration samples (D type) the absorption became weaker in comparison with that observed at room temperature. For the other sample types, a small increase

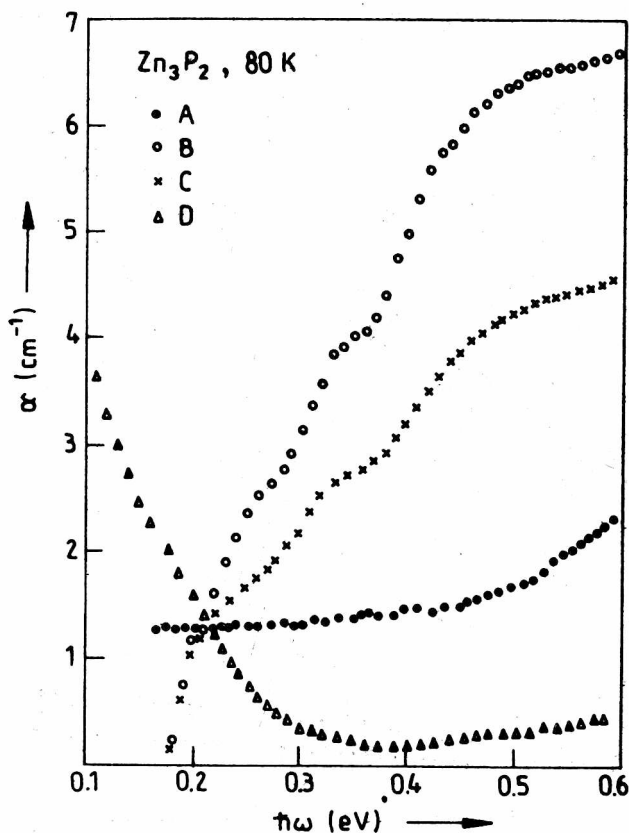


Fig. 29. Absorption spectra of the Zn_3P_2 samples of different hole concentration: A - $p \leq 10^{13} \text{ cm}^{-3}$, B - $p = 10^{14}-10^{15} \text{ cm}^{-3}$, C - $p \sim 10^{16} \text{ cm}^{-3}$ and D - $p \geq 1 \times 10^{17} \text{ cm}^{-3}$, after the background subtraction

Rys. 29. Widma współczynnika absorpcji w temperaturze pokojowej próbek o różnej koncentracji dziur: A - $\leq 10^{13} \text{ cm}^{-3}$, B - $10^{14}-10^{15} \text{ cm}^{-3}$, C - $p \approx 10^{16} \text{ cm}^{-3}$ i D - $p \geq 1 \cdot 10^{17} \text{ cm}^{-3}$ (po odjęciu tła)

of the average values of absorption coefficient at low temperatures was found. The changes in the absorption curve slopes are more prominent at low temperatures in comparison with those measured at 295 K.

5.2. Absorption and photoconductivity within 0.5-1.5 eV energy range

In Figures 30 and 31, absorption plots for 0.55-1.44 eV energy region are presented. The samples of high resistivity (type A) show in

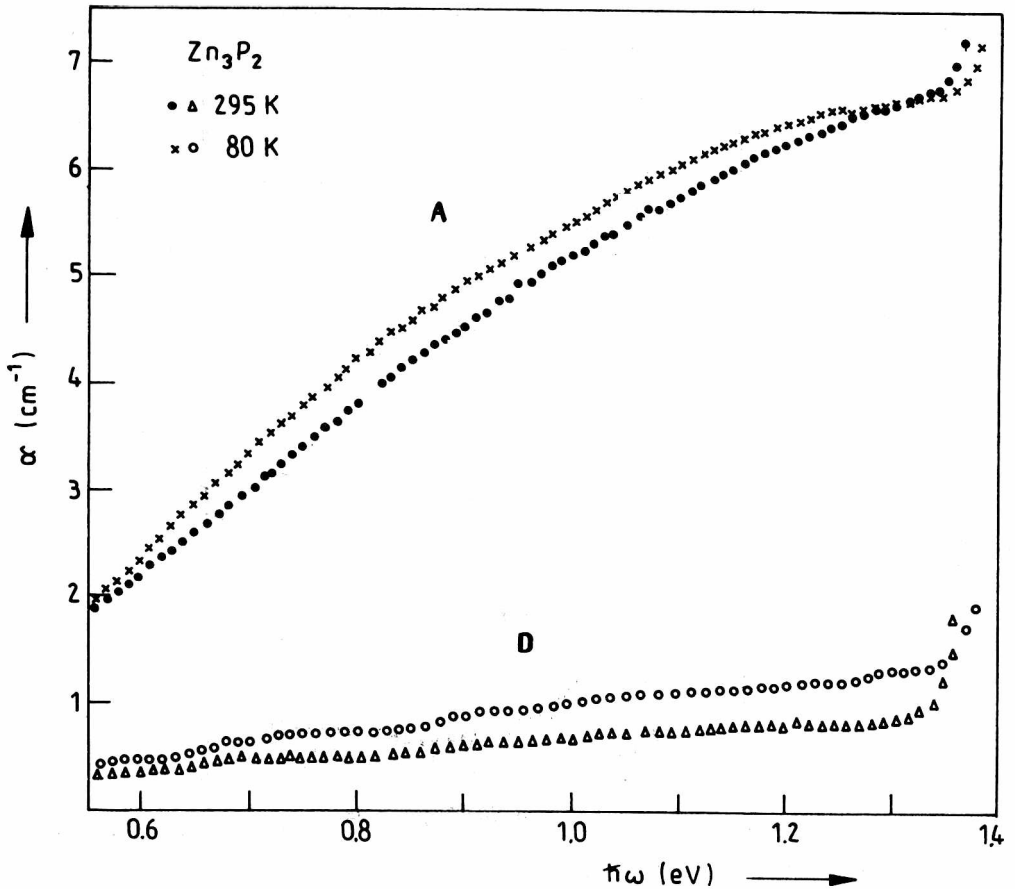


Fig. 30. Absorption spectra of the Zn_3P_2 samples with lowest - A, $p < 10^{13} \text{ cm}^{-3}$ and highest - D, $p \geq 1 \times 10^{17} \text{ cm}^{-3}$ hole concentrations

Rys. 30 Widma współczynnika absorpcji próbek o najniższej (A) $p < 10^{13} \text{ cm}^{-3}$ i najwyższej (D) $p \geq 1 \times 10^{17} \text{ cm}^{-3}$ koncentracji dziur

this region the very broad absorption band only. The beginning of this band is located at 0.45 eV (± 0.05 eV). Completely opposite behaviour is observed for low resistivity samples (D-type). In energy region of 0.55-1.4 eV only slight increase of absorption value is visible. Absorption curves for the samples with middle hole concentration are collected in Fig. 31. For the B-type samples ($p = 10^{14}$ - 10^{15} cm^{-3}) a distinct absorption band in 0.55-1.30 eV was found. C-type samples ($p \approx 10^{16} \text{ cm}^{-3}$) have (in this region) the absorption plot with three distinct changes in its slope. They are located at 0.66, 0.87 and 1.28 eV.

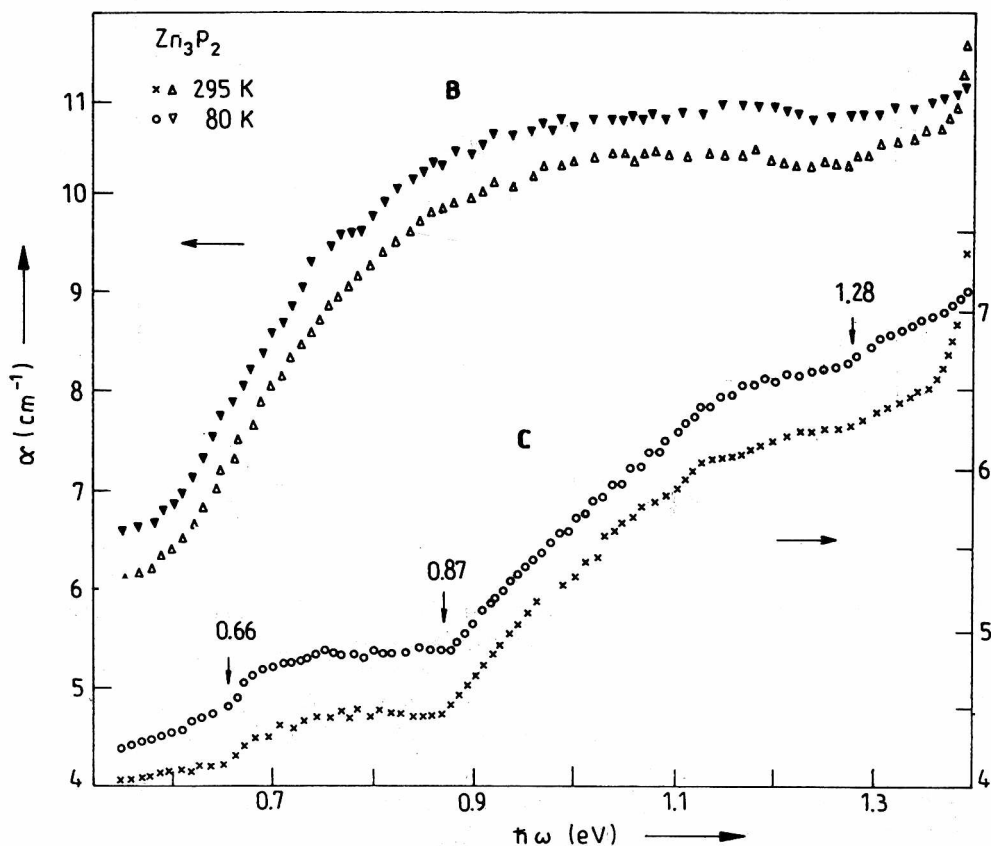


Fig. 31. Absorption spectra of the Zn_3P_2 samples with middle hole concentrations: B - $p = 10^{14}-10^{15} \text{ cm}^{-3}$ and C - $p \approx 10^{16} \text{ cm}^{-3}$. Characteristic energies are marked

Rys. 31. Widma współczynnika absorpcji próbek o średniej koncentracji dziur: B - $p = 10^{14}-10^{15} \text{ cm}^{-3}$ i C - $p \approx 10^{16} \text{ cm}^{-3}$. Zaznaczono energie charakterystyczne

The temperature decreasing down to 80 K does not change substantially any of the above-presented spectra (see Figs. 30 and 31).

For the C-type samples, a.c. photoconductivity measurements were done in the 0.65-1.5 eV energy range and at 295 K. Photoconductivity plot in the range of 0.65-1.3 eV is presented in Fig. 32. A broad maximum is placed at 0.87-1.26 eV, similarly to absorption maximum. The highest photoconductivity signal is found at energy about 1.15 eV. Ex-

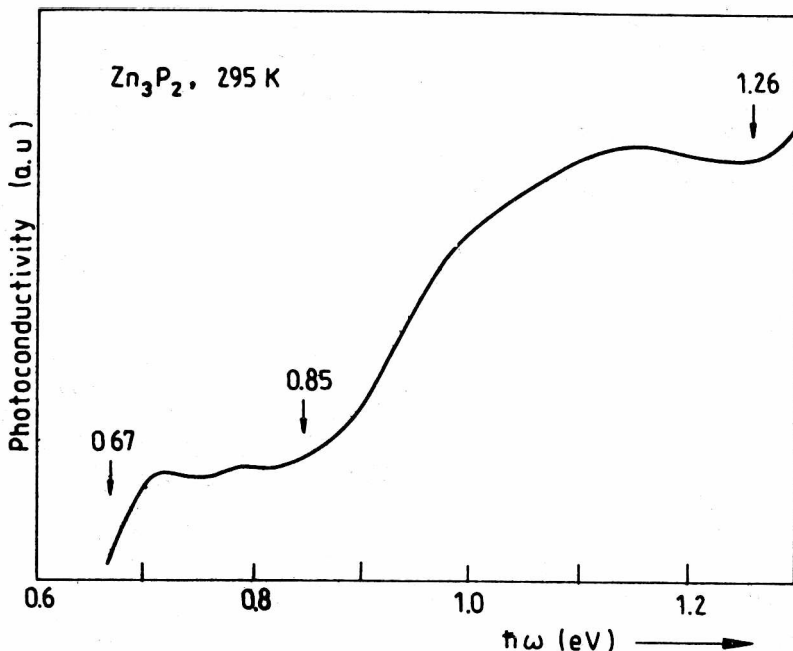


Fig. 32. Photoconductivity spectrum for the Zn_3P_2 samples with hole concentration in the range of 10^{16} cm^{-3} . Characteristic energies are marked

Rys. 32. Widmo fotoprzewodnictwa próbek o koncentracji w zakresie 10^{16} cm^{-3} . Zaznaczono energie charakterystyczne

tensions of the photoconductivity and absorption spectra towards higher energies are presented in Fig. 33. Small changes in absorption plot at the energies of 1.28, 1.34, 1.38–1.40 and 1.41–1.43 eV become more distinct in photoconductivity spectra. For the higher energies and at room temperature, there is a sharp fundamental absorption edge (see Sect. 3.2.1). In Figure 33 absorption curve at temperature 80 K in the 1.25–1.54 eV energy region is also presented. The singularities in absorption plot at 80 K are found at 1.28, 1.32, 1.36, 1.41, 1.435 and the strongest one at 1.51 eV. Experimental uncertainty of the energy values presented above does not exceed ± 0.02 eV.

5.3. Absorption derivative spectra

The region of energies higher than 1.40 eV was investigated also by means of wavelength modulation techniques. This method is a very use-

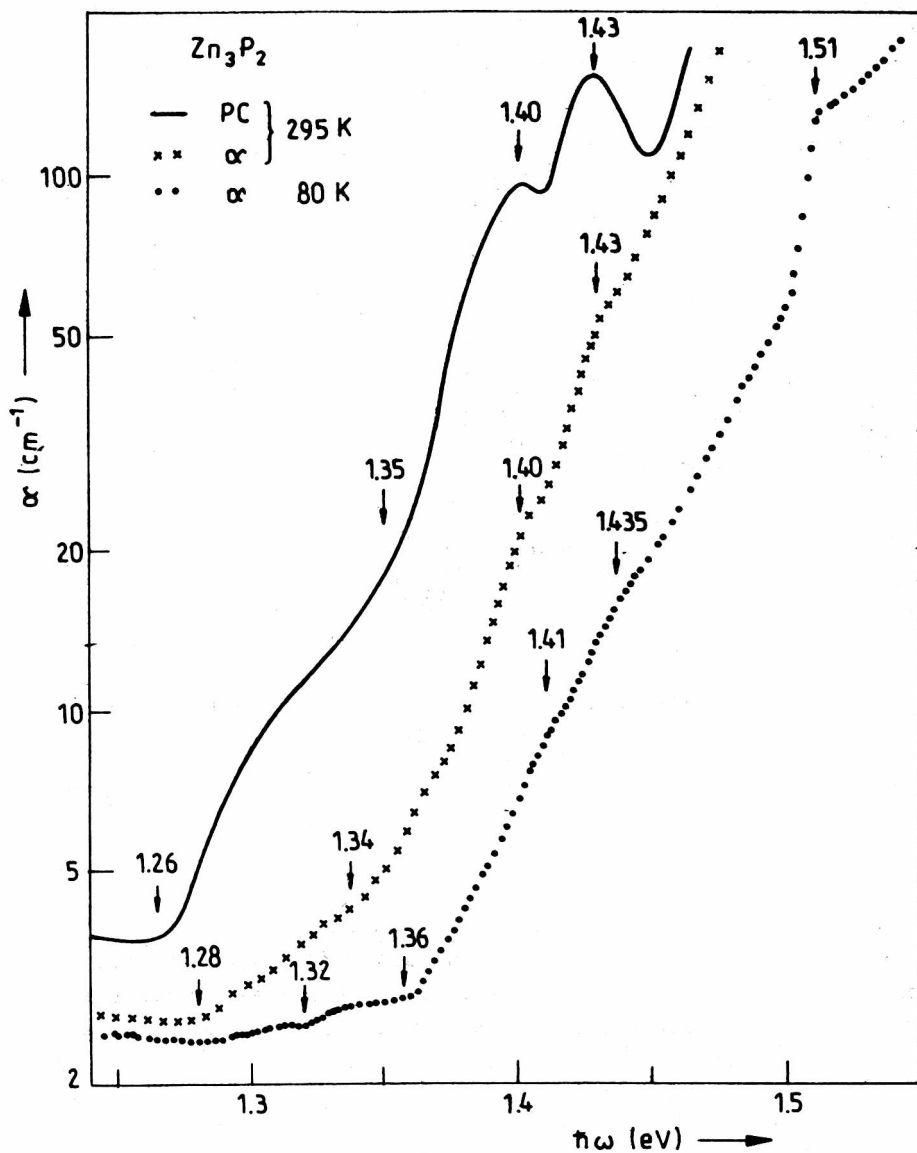


Fig. 33. Absorption and photoconductivity spectra of the Zn_3P_2 samples with hole concentration $p \approx 10^{16} cm^{-3}$. Arrows denote characteristic energies

Rys. 33. Widma absorpcji i fotoprzewodnictwa próbek o koncentracji dziur $p \approx 10^{16} cm^{-3}$. Strzałki oznaczają energie charakterystyczne

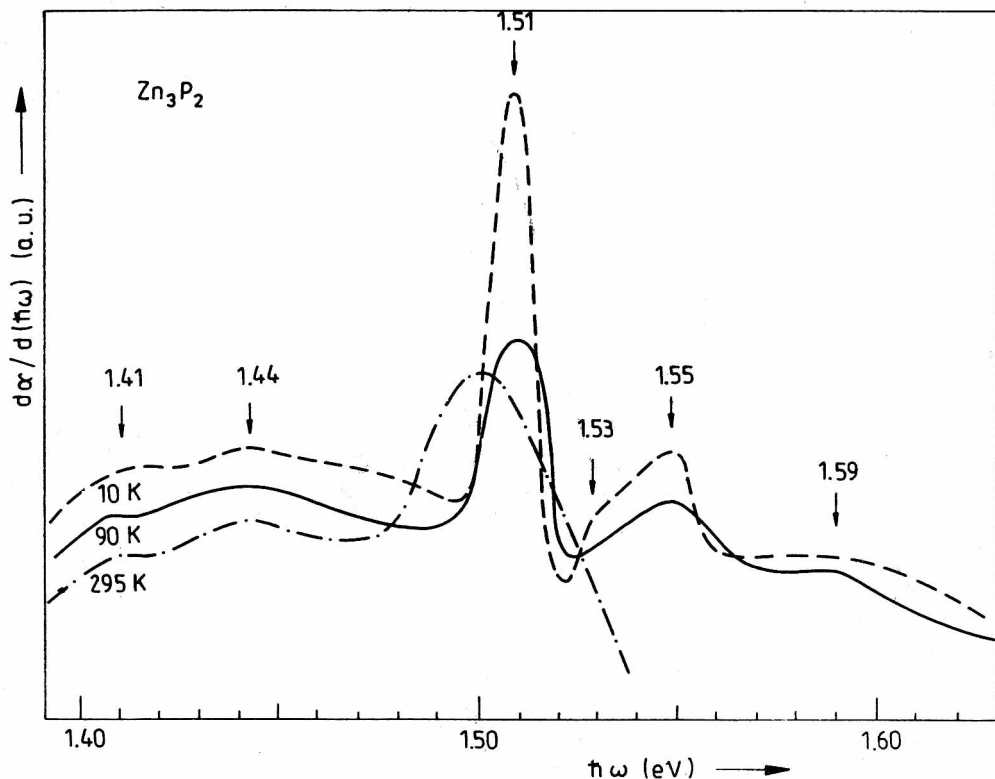


Fig. 34. Absorption derivative spectra at three different temperatures of the Zn_3P_2 samples with hole concentration $p \approx 10^{16} \text{ cm}^{-3}$. Arrows denote characteristic energies (Misiewicz and Gumienny 1987)

Rys. 34. Widma pochodnej współczynnika absorpcji w trzech temperaturach dla próbek o koncentracji $p \approx 10^{16} \text{ cm}^{-3}$. Strzałki oznaczają energie charakterystyczne (Misiewicz i Gumienny 1987)

ful tool for investigation of weak optical transitions in semiconductors. The measuring set-up was based on the GDM-1000 as well as SPM-2 Zeiss monochromators and a plane parallel vibration plate technique was used. Details were extensively described previously (Gumienny and Misiewicz 1986, Misiewicz and Gumienny 1987). The absorption derivative was determined in the 1.39–1.63 eV energy at several temperatures. Figure 34 presents plots obtained at 295, 90 and 10 K.

The main maximum at 1.503 eV at room temperature corresponds to the sharpest part of the fundamental absorption edge (see Sect.3.2.1).

For lower energies, two weak maxima at 1.41 and 1.44 eV are found. They are present also at lower temperatures without significant changes of their energy positions. At low temperatures, at which the fundamental absorption edge is shifted to the region of 1.65–1.7 eV (Pawlikowski et al. 1979), rich structure of the absorption derivative is shown. Maxima at 1.51, 1.55 and 1.59 eV are seen for 90 K. At liquid helium temperature additional peak is visible at 1.53 eV.

Very interesting part of the spectra extends over the range of 1.49–1.60 eV. Figure 35 taken from the paper of Misiewicz and Gumienny (1987) presents recorded plots at several temperatures allowing to recognize the evolution of the main transition. At temperatures around 260 K only a broad maximum exists which is slightly shifted to the higher energies. This shift is connected with the

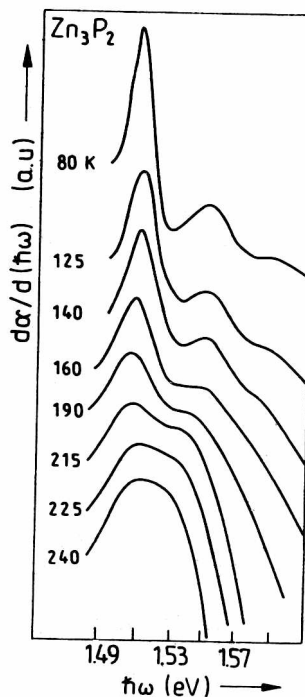


Fig. 35. Temperature evolution of the main transitions in Zn_3P_2 within 1.49–1.60 eV energy range (Misiewicz and Gumienny 1987)

Rys. 35. Zależność przejść absorpcyjnych od temperatury w zakresie 1.49–1.60 eV (Misiewicz i Gumienny 1987)

energy gap increase when the temperature is lowered. Below 240 K main maximum is fixed at energy 1.51 eV (± 0.01 eV). At 215 K a second peak at 1.55 eV becomes visible. Both of them are more distinct at lower temperatures. At about 120 K a third smaller peak appears at 1.59 eV. Below 40 K a fourth singularity is observed at 1.53 eV.

The influence of the crystal anisotropy on the defect related optical transitions was found to be negligible. As an example we see absorption curve and its derivative measured nearby the strongest transition at low temperatures, i.e., 1.51 eV. In Figure 36 (Gumienny and Misiewicz 1986) there are both plots presented for the two light polarizations. The transition at 1.51 eV occurs at both of light polarization and within the experimental accuracy (± 0.01 eV) no change in the energy position of the peak in derivative curve was found.

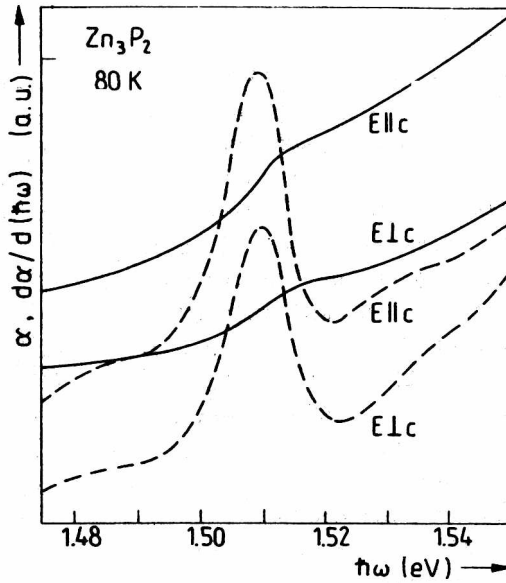


Fig. 36. Absorption and its derivative of Zn_3P_2 crystal for two light polarizations in the range of the strongest defect related transition (Gumienny and Misiewicz 1986)

Rys. 36. Widma współczynnika absorpcji i jego pochodnej dla dwóch polaryzacji światła w zakresie najsilniejszego przejścia w Zn_3P_2 swiętanego z defektami (Gumienny i Misiewicz 1987)

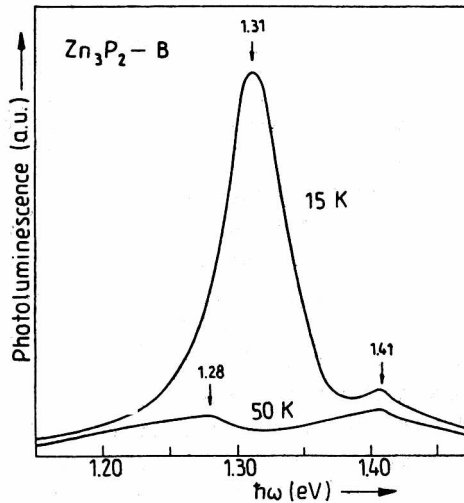


Fig. 37. Photoluminescence spectra of the Zn_3P_2 samples with the concentration $p = 10^{14} - 10^{15} \text{ cm}^{-3}$ at two different temperatures. Arrows denote maxima positions (Misiewicz et al. 1988)

Rys. 37. Widma fotoluminescencji próbek o koncentracji $p = 10^{14} - 10^{15} \text{ cm}^{-3}$ w różnych temperaturach. Strzałki oznaczają położenia maksimów (Misiewicz i in. 1988)

5.4. Low-temperature photoluminescence spectra

To perform photoluminescence measurements, two different equipments were used. In the 1.15–1.48 eV range the set-up consisted of IIA-120 argon laser with 488 nm line, grid monochromator SPM-2 a cooled MIO FD29 photomultiplier, lock-in and a multichannel analyser (for details, see Misiewicz et al. 1988). To perform the photoluminescence measurements in the 1.48–1.70 eV range, the samples were excited by krypton ion

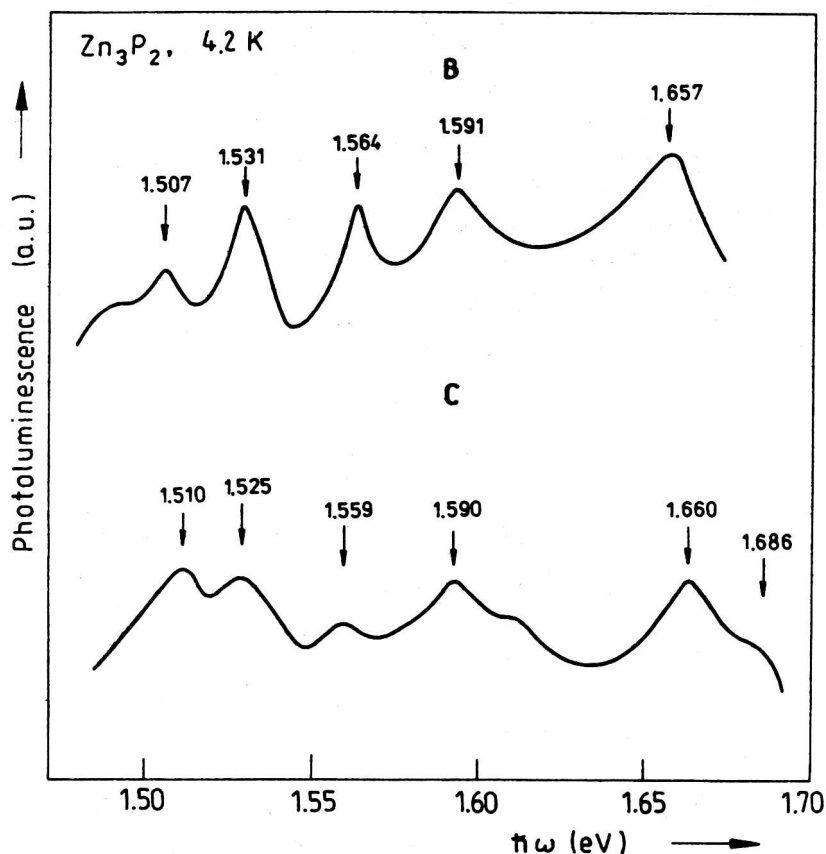


Fig. 38. Photoluminescence spectra of two different types of Zn₃P₂ samples: B - $p = 10^{14}-10^{15} \text{ cm}^{-3}$ and C - $p \approx 10^{16} \text{ cm}^{-3}$. Arrows denote peak positions

Rys. 38. Widma fotoluminescencji dwóch typów próbek: B - $p = 10^{14}-10^{15} \text{ cm}^{-3}$ i C - $p \approx 10^{16} \text{ cm}^{-3}$. Strzałki oznaczają położenia maksimów

laser at 676 nm line. A double-grating SPEX spectrometer, cooled GaAs photomultiplier and photon counting system were used.

Representative photoluminescence curves in the 1.15–1.47 eV range are presented in Fig. 37. The prominent band is placed within 1.24–1.36 eV energy range at temperature of 15 K, with the maximum at 1.31 eV. Besides the main maximum, there is a smaller one at 1.41 eV. The temperature increase up to 50 K causes the decrease of the main peak intensity and its shift towards the lower energy. No changes of the small peak at 1.41 eV position and intensity with increasing temperature were observed.

Typical curves for samples of B- and C-types are presented in Fig. 38. The obtained spectra are similar to the above ones, with only small discrepancies in the energies of maxima and in the shape.

We can try to explain the photoluminescence investigations results taking as a starting point the energy gap value at liquid helium temperature obtained by Pawlikowski et al. (1979), i.e., 1.69 eV. It seems that a small feature observed in Fig. 38 on C-type sample at 1.686 eV may be connected with the band-to-band recombination process. To explain the other features, we assume the predominant role of Donor-Acceptor Pair (DAP) recombination in observed photoluminescence spectra. Features attributed to the DAP recombination have energies given by

$$\hbar\omega = E_g - (E_A + E_D) + \frac{e^2}{\epsilon r} \quad (15)$$

where E_A and E_D are acceptor and donor ionization energies, respectively, and $r \sim (\pi N_A)^{1/3}$ is the main pair separation distance. For N_A close to 10^{17} cm^{-3} we obtain $e^2/\epsilon r \approx 10 \text{ meV}$ which is within the energy uncertainty of the peaks. Thus, from the photoluminescence spectra, we may determine the energies of $(E_A + E_D)$ sums as follows: 0.04, 0.11, 0.14, 0.17, 0.19, 0.29, 0.39 eV. Transitions connected with these energies will be discussed in Sect. 5.6.

5.5. Description of the transitions observed in absorption spectra by means of Quantum Defect Method

5.5.1. Transitions within 0.1–0.5 eV energy range

The increase of absorption value in the 0.15–0.5 eV energy range for the samples with middle hole concentration, i.e., B- and C-types, may be explained as a sum of few photoionization processes, assuming that the absorption steps are connected with the valence band - acceptor level transitions.

The problem of acceptor photoionization, including the central cell correction was solved theoretically by Beeb (1969) using the Quantum Defect Method (QDM).

According to this method, the photoionization cross-section is expressed in the form of

$$\sigma(\hbar\omega) = (4\pi\alpha_0 a^{*2}/3n) \left[v^3 2^{2v} f(y) / \sqrt{y} (1+y)^v \right], \quad (16)$$

where: v is the effective principal quantum number, $\hbar\omega$ is the photon energy, $\alpha_0 = 1/137$, $a^* = (\epsilon/m_h^*)a_H$ is the effective Bohr radius ($a_H = 0.53 \text{ \AA}$), n - the refractive index, ϵ is the static dielectric constant

$$f(y) = \left\{ \frac{\sin[(v+1)\arctan\sqrt{y}]}{\sqrt{y}} - \frac{(v+1)\cos[(v+1)\arctan\sqrt{y}]}{\sqrt{1+y}} \right\}^2 \quad (17)$$

and $y = (\hbar\omega - E_I)/E_I$. E_I is the observed ionization energy and $E_I = E_0/v^2$, where E_0 is the hydrogenic-like ($v = 1$) ionization energy

$$E_0 = R a_H^2 / m_h^* a^{*2}, \quad (18)$$

and $R = 13.6 \text{ eV}$. The effective Bohr radius a^* , v and E_I are related through the dependence

$$a^{*2} = \frac{R a_H^2}{m_h^* v^2 E_I} \quad (19)$$

Bebb's formula was fitted to the experimental absorption spectra, assuming the total absorption is a sum of three photoionization transitions, i.e.

$$\alpha_{\text{meas}} = \alpha_1 + \alpha_2 + \alpha_3. \quad (20)$$

Three adjustable parameters were used here: the effective principal quantum number v , the ionization energy E_I , and the concentration of neutral acceptors N_A (the latter could be obtained from the absorption cross-section). Taking the hole effective mass value $m_h^* = 0.4 m_0$ and refractive index $n = 3.2$ (see Sect. 4.2.2), the set of fitting parameters was obtained for the B- and C-type of samples

* Exact value of effective mass both for the holes and electrons in Zn_3P_2 is unknown.

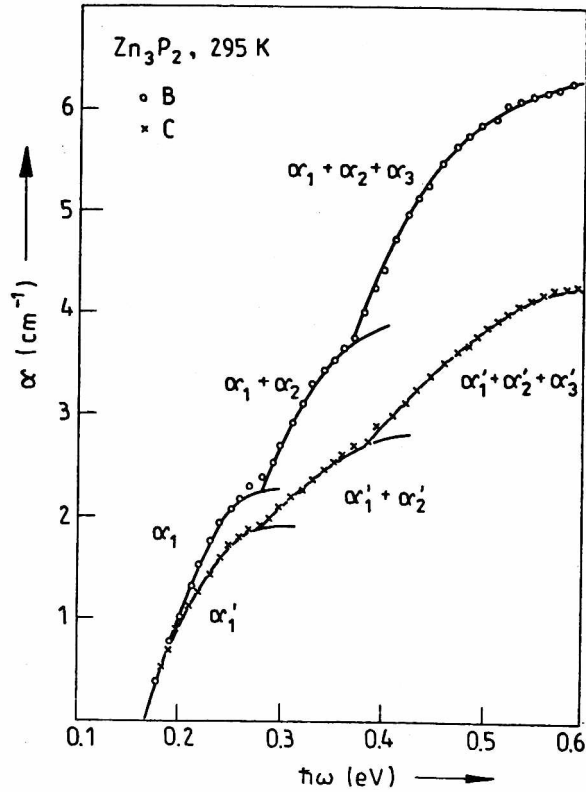


Fig. 39. Quantum Defect Method application to describe absorption curves for the Zn_3P_2 samples with middle hole concentration; lines - theoretical model (see Tab. 16)

Rys. 39. Zastosowanie metody defektu kwantowego do opisu krzywych absorpcji próbek o średniej koncentracji dziur, linie ciągłe - model teoretyczny

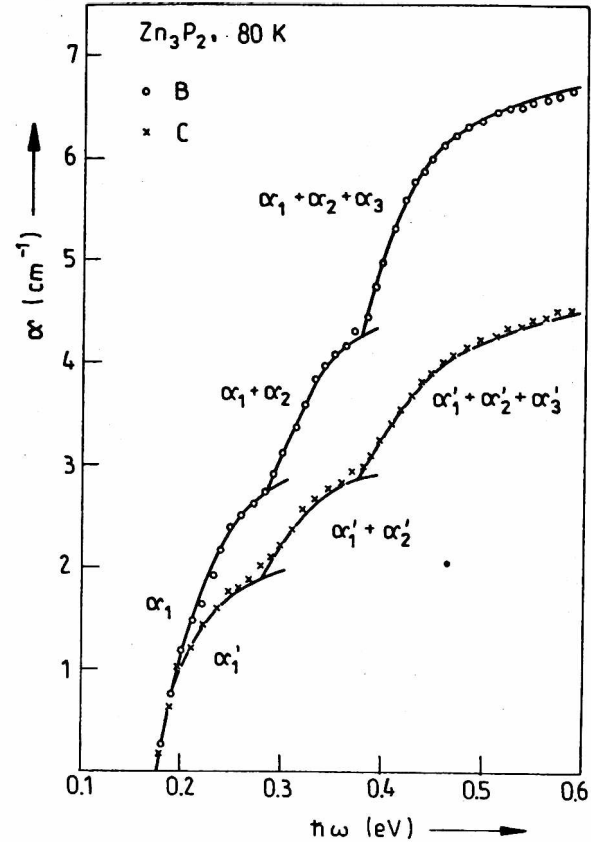


Fig. 40. Quantum Defect Method application to describe absorption curves for the Zn_3P_2 samples with middle hole concentration; lines - theoretical model (see Tab. 17)

Rys. 40. Zastosowanie metody defektu kwantowego do opisu krzywych absorpcji próbek o średniej koncentracji dziur, linie ciągłe - model teoretyczny

Table 16

Fitting parameters for the sample of B-type with $p = 10^{14} - 10^{15} \text{ cm}^{-3}$

| | 295 K | | | 80 K | | |
|-------------------------------------|------------|------|------|------|-------|-------|
| | E_I (eV) | 0.17 | 0.27 | 0.36 | 0.175 | 0.275 |
| ν | 0.56 | 0.46 | 0.39 | 0.56 | 0.46 | 0.39 |
| N_A (10^{17} cm^{-3}) | 1.8 | 6 | 15 | 2.5 | 6 | 13 |

Table 17

Fitting parameters for the sample of C-type with $p \approx 10^{16} \text{ cm}^{-3}$

| | 295 K | | | 80 K | | |
|-------------------------------------|------------|------|------|------|-------|------|
| | E_I (eV) | 0.17 | 0.28 | 0.38 | 0.175 | 0.28 |
| ν | 0.55 | 0.44 | 0.37 | 0.55 | 0.44 | 0.37 |
| N_A (10^{17} cm^{-3}) | 1.5 | 4 | 9 | 1.6 | 4.3 | 9 |

(Tables 16 and 17). The solid lines in Figs. 39 and 40 present the curves obtained by fitting of the above formula to the experimental results. The above presented data have exemplary character in the sense that the determined acceptor concentrations change from sample to sample in the range of $2-3 \times 10^{17} \text{ cm}^{-3}$, quantum defect numbers within the range of ± 0.05 and ionization energies within the range of ± 0.02 eV.

In the case of the samples with the smallest hole concentration, i.e., A-type, we can only notice increase of the absorption value at 0.45 eV.

Samples with the highest hole concentration (D-type) exhibit absorption increase when the photon energy is lowering, starting from 0.4 eV. Trying to explain this behaviour, it was assumed that the high energy tail of some photoionization process in this region is seen. An attempt to describe observed spectrum within the frame of QDM was made. Figure 41 presents a fitting of absorption cross-section plot (solid line) to the experimental points. A few experimental points for energies lower than 0.1 eV were not presented in Fig. 28. To determine the position of the assumed acceptor level of the energy smaller than 0.1 eV, it was necessary to extract lattice absorption, using high

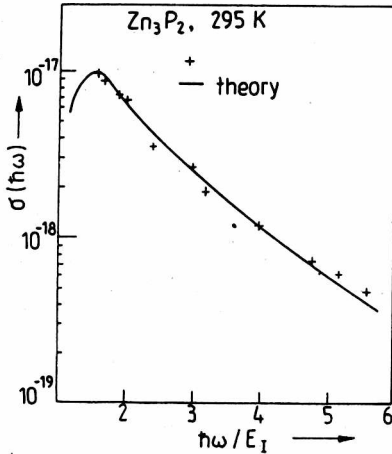


Fig. 41. Theoretical fit of the absorption cross-section for the quasi-hydrogenic acceptor model to the low energy part of the absorption plot measured for the highest hole concentration sample, $p \approx 1 \times 10^{17} \text{ cm}^{-3}$ (see Fig. 28), $E_I = 0.05 \text{ eV}$

Rys. 41. Dopasowanie teoretycznego modelu przekroju czynnego na absorpcję dla wodoropodobnego akceptora do niskoenergetycznej części widma absorpcji zmierzonej dla przykładowej próbki o najwyższej koncentracji dziur $p \approx 1 \times 10^{17} \text{ cm}^{-3}$ (rys. 28), $E_I = 0.05 \text{ eV}$

resistivity samples, from the total absorption of the sample of D-type. The best result of this fitting procedure was achieved for the ionization energy $E_I = 0.05 \text{ eV}$, quantum defect number $\nu = 0.97$ and neutral acceptor concentration $N_A = 6 \times 10^{17} \text{ cm}^{-3}$. Small ionization energy and high value (very close to the hydrogenic limit $\nu = 1$) indicate that this level is very similar to the typical hydrogenic-like acceptor

5.5.2. Transitions for the energies higher than 0.5 eV

Samples with hole concentration in the range of $p = 10^{14} - 10^{15} \text{ cm}^{-3}$ have characteristic absorption spectra with a broad photoionization band. Assuming that valence band-acceptor level transitions dominate and by using QDM approach we obtain the best fitting (Fig. 42) with the following parameters: ionization energy $E_I = 0.55 \text{ eV} \pm 0.03 \text{ eV}$, quantum defect number $\nu = 0.3$ and neutral acceptor concentration $N_A = 9 \times 10^{18} \text{ cm}^{-3}$, at 295 K. Decrease of temperature does not change the result significantly. Attempts to describe (in terms of QDM) the broad absorption band observed for the samples with the lowest hole concentration (A-type) as well as the steps in absorption and photoconductivity spectra for the samples with $p \approx 10^{16} \text{ cm}^{-3}$ (C-type), did not succeed. Nevertheless, the existence of some deep levels is very probable with the energy $E_I \approx 0.45 \text{ eV}$ for the A-type samples and with $E_I = 0.66 \text{ eV}$ and 0.87 eV for C-type samples.

Transitions observed at 1.28 eV and at higher energies will be discussed in the next part of this monograph. Only a distinct threshold at 1.51 eV and at low temperatures is discussed now. This transition may be described within the frame of QDM, assuming acceptor level-

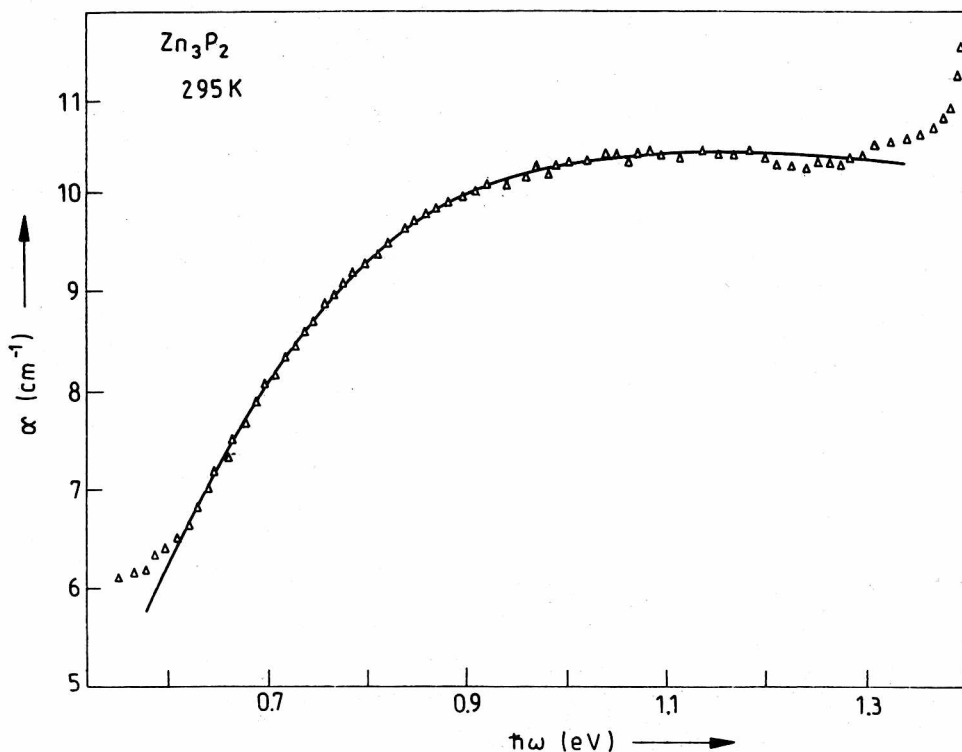


Fig. 42. Quantum Defect Method application to describe absorption spectra of the sample with hole concentration $p = 10^{14}-10^{15} \text{ cm}^{-3}$.
solid line - theoretical model

Rys. 42. Zastosowanie metody defektu kwantowego do opisu absorpcji przykładowej próbki o koncentracji dziur $p = 10^{14}-10^{15} \text{ cm}^{-3}$,
Linia ciągła - model teoretyczny

conduction band transitions process. In this case, absorption cross-section is described by the relation

$$\sigma(\hbar\omega) = \frac{32\pi a^*{}^2 \alpha_0}{n \hbar\omega} \frac{E_g (m_0 - m_e^*)}{m_0} S(\nu, x_0). \quad (21)$$

Function S has the following form:

$$S(\nu, x_0) = \frac{\nu^2 2^{2\nu} \sin^2[(\nu + 1) \arctan(x_0^{1/2})]}{16 x_0^{1/2} (1 + x_0)^{\nu+1}}, \quad (22)$$

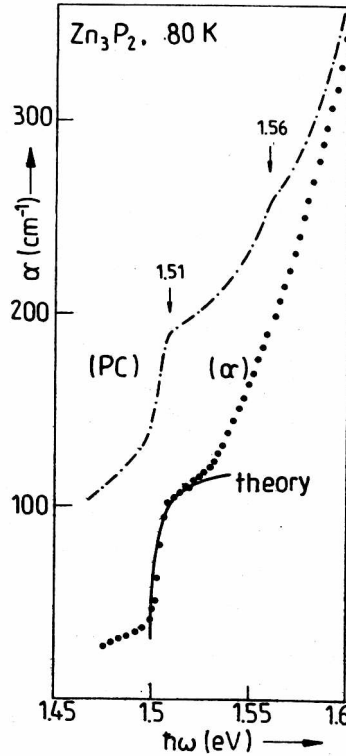


Fig. 43. Absorption and photoconductivity plots at low temperature in the high energy region. Solid line presents theoretical fit of the Quantum Defect Method, for transition from the acceptor level to the conduction band

Rys. 43. Widma absorpcji i fotoprzewodnictwa w niskiej temperaturze w obszarze wysokich energii. Linia ciągła oznacza teoretyczne dopasowanie metody defektu kwantowego przejść z poziomu akceptorowego do pasma przewodnictwa

where

$$x_c = \frac{m_e^*/m_h^*}{m_h^*} \frac{E_c(k)}{E_I}, \quad (23)$$

and m_e^*/m_h^* is the ratio of the carrier effective masses, E_g - energy gap, $E_c(k)$ - momentum dependence of the conduction band energy, E_I - ionization energy of the acceptor. Since the effective masses are not precisely determined for Zn_3P_2 , the ratio of the masses was taken as a parameter of fitting procedure. The best fitting presented in Fig. 42 by continuous line was obtained for $m_e^* = 0.35 m_0$ and $m_h^* = 0.45 m_0$, effective quantum number $\nu = 0.5$, $E_I = 0.19$ eV and $N_A = 2 \times 10^{17} \text{ cm}^{-3}$. The energy gap value at 80 K of 1.69 eV was taken from paper of Pawlikowski et al. (1979). The above discussed results are representative

for the samples with hole concentrations close to 10^{16} cm^{-3} . The transition at 1.51 eV was observed for all investigated samples with various intensity. Discrepancy between the determined E_I values was smaller than 0.02 eV.

Photoconductivity plot at 80 K is also presented in Fig. 43. This spectrum corresponds well with the absorption curve in the vicinity of 1.51 eV. In photoconductivity plot, there is also a small step at 1.56 eV. This transition is consistent with those observed in photoluminescence and absorption derivative spectra.

5.6. Origin and features of acceptor levels

Basing on the presented above results and their discussion, we can state the existence of the row of acceptor-like energy levels. In the high concentration sample, there is one important 0.05 eV level only. This value determined from fitting of quasi-hydrogenic model to the absorption plot is in a very good accordance with value determined from electrical transport measurements (see Tab. 18). Almost flat absorption spectra in the 0.4-1.36 eV energy range indicate that the deep levels, if they exist in these samples, play a neglecting role. For the samples of concentration from 10^{14} to 10^{16} cm^{-3} , three low energy levels were found at about 0.17, 0.27 and 0.36 eV. Additional level at 0.55 eV existing in the samples of concentration of $p = 10^{14}$ - 10^{15} cm^{-3} probably plays an important role in the control of the low hole concentration in these samples. Absorption process connected with this level is strong enough to cover any other processes in the 0.6-1.3 eV energy region. Such possible processes occur in the samples with $p \approx 10^{16} \text{ cm}^{-3}$, where the onsets are positioned at 0.65, 0.87 and 1.28 eV. Excitation of energy levels located within 0.87-1.28 eV energy range, with the maxima near 1.15 eV, may correspond with broad photoluminescence band observed in the same region by Sundström (1980) and Huldt et al. (1979).

The characteristic energies determined in the 0.05-0.9 eV energy range may be interpreted as energies of acceptor levels. Table 18 presents all values of acceptor energies determined from the electrical transport measurement in this work, and the data from the literature. Appropriate set of energies obtained from optical measurements is presented in Tab. 19.

For the highest hole-concentration samples, the QDM fitting to the measured absorption plot led to the concentration of the neutral acceptor of the 0.05 eV level equal to $N_A = 6 \times 10^{17} \text{ cm}^{-3}$. Taking the hole

Table 18

Energies of the transitions obtained from electrical transport measurements (in eV)

| | | | | | | |
|-------------|-----------|-----------|------------|-----------|-----|---------------------------------|
| 0.034 | | | | 0.51 | | Żdanowicz and Henkie (1964) |
| | 0.18 | | 0.44 | | 0.8 | Shevchenko et al. (1975) |
| | | | | 0.59 | | Möller et al. (1979) |
| 0.02, 0.034 | 0.14 | 0.25 | 0.47 | | | Catalano and Hall (1980) |
| | | 0.20 | 0.36, 0.48 | 0.73 | | Wang et al. (1982) |
| | 0.13 | 0.20 | 0.36, 0.48 | | | Suda and Bube (1984) |
| 0.04-0.045 | 0.14 | | | 0.54-0.67 | | Suda and Kuronayagi (1986) |
| | | | | | | Sierański and Szatkowski (1986) |
| 0.034 | | 0.27 | | 0.6 | | Szatkowski and Sierański (1987) |
| 0.015-0.04 | 0.14-0.19 | 0.25-0.30 | 0.36-0.42 | 0.55-0.72 | | Misiewicz (1989) |

Table 19

Energies (in eV) of the transitions observed in optical measurements for the energies lower than 1.0 eV

| Temperature 295 K | | Temperature 80-100 K | | |
|-------------------|------|----------------------|-----------|------|
| This work | | a | This work | b |
| α | PC | α | α | PL |
| 0.05 | | | 0.05 | |
| 0.17 | | 0.17 | 0.175 | |
| 0.27 | | 0.26 | 0.28 | |
| 0.36 | | 0.36 | 0.37 | |
| 0.45 *) | | | 0.45 *) | |
| 0.55 | | 0.55 | 0.55 | 0.52 |
| 0.66 | 0.67 | 0.65 | 0.67 | 0.64 |
| 0.87 | 0.85 | 0.87 | 0.87 | 0.80 |

*) Only for the highest resistivity samples.

a - Misiewicz et al. (1986a), b - Sundström et al. (1980).

α - absorption, PC - photoconductivity, PL - photoluminescence

concentration value from electrical measurements, equal to $p = 1 \times 10^{17}$ cm^{-3} and $m_h^* = 0.4$ one can determine N_A values by using the dependence

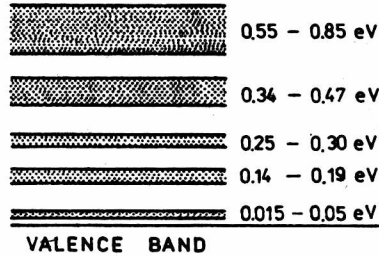
$$\frac{p^2}{N_A - p} = \frac{N_V}{2} \exp(-E_A/kT); \quad (24)$$

where $N_V = 2(2\pi m_h^* kT/h^2)^{3/2}$ is the effective density of states in the valence band. From Eq. (24) we get $N_A = 2.1 \times 10^{17} \text{ cm}^{-3}$. The compensation ratio of this level is determined as $\frac{N_A - N_D}{N_A} = \frac{p}{N_A} = 0.48$

using N_A from (24) and 0.16 value for N_A obtained from optical absorption fitting.

For the samples with hole concentration $p \approx 1 \times 10^{16} \text{ cm}^{-3}$ the energy of the shallowest acceptor level was determined as 0.17 eV. By means of relation (24) we obtain neutral acceptor concentration $N_A = 1.1 \times 10^{17} \text{ cm}^{-3}$ which is in good agreement with that determined from absorption cross-section ($N_A = 1.5 \times 10^{17} \text{ cm}^{-3}$). For these samples com-

CONDUCTION BAND

Fig. 44. Common acceptor levels in Zn_3P_2 Rys. 44. Poziomy akceptorowe zaobserwowane w Zn_3P_2

compensation ratio is equal to 0.09-0.07. For samples with $p = 10^{14}-10^{15} \text{ cm}^{-3}$ the compensation ratio of the 0.17 eV acceptor is equal to $10^{-2}-10^{-3}$.

In the case of highest resistivity samples absorption curve is almost flat up to 0.45 eV with small absorption value which indicates that the possible acceptor levels lying below 0.45 eV are fully compensated.

The Fermi level in Zn_3P_2 seems to be located in the vicinity of the top of valence band in the case of D-type samples, within 0.14-0.20 eV energy range for B- and C-types of samples and near to 0.4 eV for A-type samples. The common observed acceptor levels in Zn_3P_2 crystal are schematically marked in Fig. 44, together with appropriate energy values.

Tables 20 and 21 present the data referring to the transitions observed in the 1.2-1.67 eV energy range. The explanation of the nature of the transitions observed in the 1.2-1.5 eV energy region is not easy (ambiguous) due to the uncertainty of the nature of fundamental band-to-band transitions. An indirect band gap in Zn_3P_2 equal to 1.315 eV at room temperature was proposed by Pawlikowski et al. (1979) basing on the changes of the absorption curve slope in the range of 1.28-1.4 eV. Similar model was used by Źdanowicz et al. (1980). Developed model with more complicated indirect structure was proposed by Pawlikowski (1982a). Unfortunately, no strict evidence of such models was obtained up to now.

Using indirect fundamental energy gap model, the steps observed in 1.28-1.4 eV energy range (see Fig. 33) may be interpreted as a reflection of the phonon assisted transitions.

Optical transitions within the energy range of 1.2-1.5 eV at 295 K
(energy in eV)

| This work $d\alpha/dE$ | | Absorption | | | Photoconductivity | | |
|---------------------------|------|------------|------|------|-------------------|------|------|
| | | a | b | c | This work | d | e f |
| 1.28 | | 1.28 | 1.28 | | 1.26 | 1.27 | 1.25 |
| 1.34 | | 1.34 | 1.34 | 1.35 | 1.35 | 1.32 | |
| 1.40 | 1.41 | 1.38 | | 1.42 | 1.40 | 1.41 | 1.40 |
| 1.43 | 1.44 | 1.40 | | | 1.43 | 1.43 | 1.44 |

- a - after Pawlikowski et al. (1979),
 b - after Mislewicz et al. (1986a),
 c - after Żdanowicz et al. (1980),
 d - after Wang and Bube (1982),
 e - after Radautsan et al. (1976),
 f - after Volodina et al. (1977).

Alternative explanation may be based on the impurity-defect involved transitions. To perform such analysis, the direct energy gap value equal to 1.60 eV at 295 K is assumed (see Sect. 3.4). Taking this value into account, we may connect transitions at 1.4-1.43 eV with the electron excitation from acceptor levels at 0.19 and 0.16 eV to the conduction band and transitions at 1.34 eV with the excitation of the electron from 0.26 eV acceptor to the conduction band. Transitions occurring at 1.26-1.28 eV may be correlated with 0.32-0.34 eV acceptor excitation. A scheme of these transitions is presented in Fig. 45a. This model needs an assumption that all acceptor levels which participate in transitions marked in Fig. 45a are occupied by electrons. This is only possible if Fermi level is located around 0.35 eV above the valence band.

In Figure 45b, an alternative model is proposed. In this model, it is assumed that Fermi level is located within 0.14-0.20 eV energy range. Transitions at 1.41 and 1.44 eV are the same as in previous model but transition at 1.26 eV is explained as occurring between the valence band and the donor level and transition at 1.34 eV takes place between acceptor and donor levels. The last model seems to be more probable be-

Optical transitions within the 1.2-1.67 eV energy range at low temperatures (energy in eV)

| Temperature 77-100 K | | | | | | Temperature 4-20 K | | | | |
|----------------------|--------------|------|----------|------------|------|--------------------|-------------------|-------|------|---|
| This work | | | a | b | c | This work | | d | e | f |
| α | $d\alpha/dE$ | PC | α | $d(PV)/dE$ | PL | $d\alpha/dE$ | Photoluminescence | | | |
| 1.28 | | | | | | | | | | |
| 1.32 | | | 1.315 | | | 1.31 | | 1.32 | 1.33 | |
| 1.36 | | | 1.36 | | | | | 1.36 | 1.37 | |
| 1.41 | 1.41 | | | 1.41 | | 1.41 | 1.41 | | | |
| 1.435 | 1.44 | | | | | 1.44 | | | | |
| 1.51 | 1.51 | 1.51 | 1.51 | 1.49 | | 1.51 | 1.51 | 1.51 | | |
| | | | | 1.52 | | 1.53 | 1.53 | | | |
| | 1.55 | 1.56 | | | 1.56 | 1.55 | 1.56 | | | |
| | 1.59 | | | 1.62 | 1.62 | 1.59 | 1.59 | | | |
| | | | | | | 1.66 | | 1.665 | | |

a - after Pawlikowski et al. (1979),
 b - after Syrbu et al. (1980),
 c - after Sundström et al. (1981),

d - after Huldt et al. (1979),
 e - after Briones et al. (1981),
 f - after Kurbatov et al. (1976).

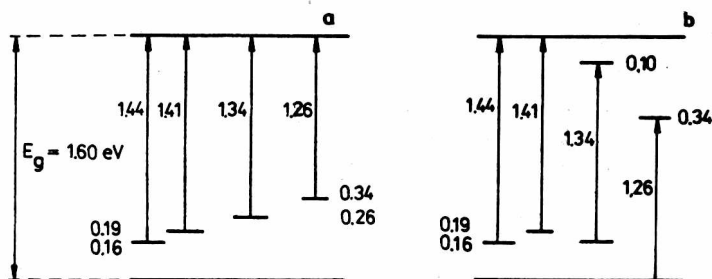


Fig. 45. Diagram of the optical transitions related to the defect levels at 295 K: for the Fermi level close to 0.35 eV above the valence band (a), and for the Fermi level located within 0.14–0.20 eV energy range (b). Energies in eV

Rys. 45. Przejścia optyczne związane z poziomami defektowymi w 295 K: a - gdy poziom Fermiego jest położony ok. 0.35 eV ponad pasmem walencyjnym, b - poziom Fermiego jest położony w zakresie energii 0.14–0.20 eV ponad pasmem walencyjnym. Energia w eV

cause the energy of Fermi level assumed in this case is more reasonable. (Unfortunately, there is no independent data on the Fermi level energy in Zn_3P_2).

The absorption bands occurring within 0.9–1.4 eV energy range may also result from the transitions from valence band and/or acceptor level to the unresolved ionized donor levels.

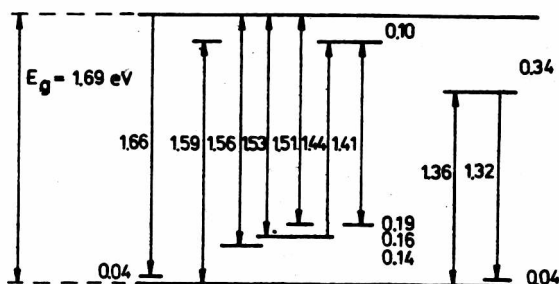


Fig. 46. Diagram of the optical transitions related to the defect levels for low temperatures (4–20 K). Fermi level is located close to 0.2 eV above the valence band. Arrows up denote transitions observed in excitation processes and arrows down denote the transitions visible in recombination processes. Energy in eV

Rys. 46. Schemat przejść optycznych związanych z poziomami defektowymi w niskich temperaturach (4–20 K). Poziom Fermiego jest zlokalizowany ok. 0,2 eV ponad pasmem walencyjnym. Strzałki w górę oznaczają przejścia zaobserwowane w procesach wzbudzenia, strzałki w dół natomiast oznaczają przejścia widoczne w procesach rekombinacyjnych. Energia w eV

Taking the low temperature direct energy gap value to be 1.69 eV (Pawlikowski et al. 1979) we may propose a scheme of defect related optical transitions at low temperatures (4–20 K). Energies of these transitions are collected in Table 21.

Almost all the transitions observed in photoluminescence spectra are also present in absorption derivative spectrum. It is possible that the transitions observed in absorption spectrum correspond with those observed in photoluminescence spectra forming pairs of absorption-luminescence transitions between the acceptor levels and residual donor levels. Such interpretation needs the assumption that electron-lattice coupling effect is small, because the differences between the energies of absorption and emission processes are small.

In our discussion concerning the nature of the transitions observed, apart from the acceptor levels at 0.04, 0.14, 0.16 and 0.19 eV active role of two donor levels with the same as at 295 K activation energies, i.e., 0.10 and 0.34 eV is assumed. Fermi level energy is expected to be close to 0.2 eV above the valence band maximum. In Fig. 46 a diagram proposed to describe transitions observed at temperatures 4–20 K is presented.

The room-temperature resistivity values and transitions observed in the optical spectra of Zn_3P_2 crystals may originate from some impurity levels. Nevertheless, no correlation between the presence of Si, Sb, Fe, Pb, Al, Mg, Cu, Cd and Ag atoms in Zn_3P_2 crystals with concentration in the range of 10^{16} – 10^{17} cm^{-3} and crystal properties of Zn_3P_2 was found. Müller et al. (1979) have found that the incorporation of the impurities such as S, Si, Cu, Ga and Al gave no change in Zn_3P_2 crystal properties. No resistivity changes were also found by Wang et al. (1982), and Masumoto et al. (1971) as a result of Ag, Au, Cu and Fe doping.

In our investigations of some Zn_3P_2 crystals doped with Ag or Cd atoms of concentrations higher than 10^{17} cm^{-3} , the samples showed low resistivity and hole concentration $p \geq 1 \times 10^{17}$ cm^{-3} . Some of the iodine transport grown crystals indicated highest resistivity.

Thus, it seems very probable that both resistivity values and the presence of optical transitions within the energy gap are connected with some crystal defect related mechanism. Three possible simplest defects acting as acceptors may be taken into account:

- i) phosphorous interstitials, P_1 ,
- ii) singly ionized zinc vacancies, V_{Zn}^- , and
- iii) doubly ionized zinc vacancies, $\text{V}_{\text{Zn}}^{2-}$.

The activity of the first type of defects as a predominant source of holes in Zn_3P_2 was suggested by Catalano and Hall (1980). We may

assume that phosphorous interstitial give an acceptor level in the range of 0.015-0.05 eV. In the same energy region, there may be placed also an acceptor created by substitution of zinc atom by a silver one, although the ionic radius of Ag is slightly larger than that of Zn. The question is if this element really gives simple Ag_{Zn} acceptor. Less probable is the creation of a simple acceptor by cadmium atom. Perhaps, the presence of Ag or Zn atoms facilitates creation of simple P_1 defect in the crystal.

Zinc vacancy levels may give acceptors with higher energies, for example, at 0.17 and 0.26 eV. The presence of Zn vacancies in Zn_3P_2 crystal was established by Arushanov et al. (1981). The deep levels may be created in Zn_3P_2 crystal by some complexes and/or standard deep oxygen-related states, but it is very probable that Zn interstitials and/or phosphorous vacancies create such levels.

It might be expected that crystals grown by iodine transport would show appreciable compensation. Nevertheless, such behaviour was not commonly observed.

Till now, the intensive efforts to obtain n-type Zn_3P_2 have not been successful. A self-compensation effect is likely to occur in Zn_3P_2 crystal similarly as, e.g., in ZnSe (Pawlikowski 1985a). In such a case, any donor impurity is compensated by native defects generated in the crystal lattice.

5.7. Conclusions on the optical transitions related to imperfection levels

In this part, the defect related optical properties of Zn_3P_2 crystals with hole concentration from 10^{13} cm^{-3} up to 10^{17} cm^{-3} were investigated. Optical measurements were performed in the 0.08-1.3 eV energy range for four types of Zn_3P_2 samples. For the samples with the lowest hole concentration ($p \leq 10^{13} \text{ cm}^{-3}$) the absorption is controlled by deep levels lying in the 0.45-1.2 eV energy range. Samples with middle hole concentration ($10^{14} \leq p \leq 10^{16} \text{ cm}^{-3}$) possess acceptor levels manifesting themselves in absorption spectra at energies as follows: 0.17 eV, 0.27 eV and 0.36 eV. Additionally, for the samples with $p = 10^{14}-10^{15} \text{ cm}^{-3}$, the deep level at 0.55 eV with high concentration ($N_A \approx 10^{19} \text{ cm}^{-3}$) was found. Two weaker transitions at 0.66 and 0.85 eV were found in the samples with $p \approx 10^{16} \text{ cm}^{-3}$ both in the absorption and photoconductivity spectra. Samples with the highest hole concentration ($p \geq 1 \times 10^{17} \text{ cm}^{-3}$) show the existence of one main acceptor level at energy of 0.05 eV, while the deep levels play no es-

sential role. Quantum defect method gave a very good theoretical description of the absorption spectra leading to the conclusion of hydrogen-like 0.05 eV acceptor level and reasonable value of neutral acceptor concentrations.

Absorption and its wavelength derivative, photoconductivity and photoluminescence measurements were used to investigate optical transitions in the 1.25-1.66 eV energy region. Energies of optical transitions identified in the spectra investigated were consistent with those expected. Very good agreement between our experimental results and the literature data was found (see Tabs. 18-21).

The influence of Zn_3P_2 crystal anisotropy on the defect related optical transitions was found to be negligible.

It was suggested that the native defects are responsible for the main acceptor levels in Zn_3P_2 crystal, i.e., phosphorous interstitial as a shallow acceptor, and zinc vacancies as a deeper ones. Deep, compensating levels may be correlated with the presence of phosphorous vacancies and zinc interstitials.

6. FINAL CONCLUSIONS AND REMARKS

In this work, the results of investigations on the electromagnetic wave interaction with Zn_3P_2 crystal within whole 0.003-11 eV energy range are presented.

Absorption and reflectivity measurements were applied as main experimental tools in these examinations. The following methods were used in some energy ranges:

- birefringence in 0.5-1.45 eV energy range,
- photoluminescence, at low temperatures, in 1.1-1.7 eV energy range,
- photoconductivity in 0.65-2.6 eV energy range,
- Raman scattering in 0.003-0.062 eV energy range.

Additionally, the absorption derivative within 1.4-1.6 eV energy range was measured at several temperatures.

Optical excitations observed within energy range of 0.003-0.150 eV ($25-1200\text{ cm}^{-1}$) were interpreted as phonon and multiphonon transitions.

By means of group theory methods the symmetry of phonon branches through the symmetry lines and points in Zn_3P_2 Brillouin zone was determined. The selection rules for the phonon overtones and combinations allowed in infrared and/or Raman scattering spectra have been derived and used to successful interpretation of the observed multiphonon transitions.

Significant influence of the crystal anisotropy on the lattice modes was theoretically predicted and partially confirmed by the analysis of Raman scattering spectra.

Additional reflectivity and absorption measurements performed in far infrared region and at the polarized light should enable resolving LO and TO phonon branches, as well as confirming other theoretical predictions.

To discriminate between different types of multiphonon lattice transitions, the detailed temperature dependences both of the infrared and Raman scattering spectra should be measured within multiphonon transitions range.

The understanding of the physical nature of the splitting of doubly degenerated modes at Γ point is also very important.

Optical transitions within 0.15-1.45 eV energy range (at room temperature) and 0.15-1.66 eV (at low temperatures) were analysed assuming the existence of defect related levels in forbidden energy gap. Energies of acceptor levels were determined to be 0.05 eV, 0.17 eV, 0.27 eV and 0.36 eV. The deep levels were found at 0.55 eV, 0.66 eV and 0.85 eV.

The absorption processes connected with acceptor levels were successfully described by means of the Quantum Defect Method. Native defects, namely, phosphorous interstitials and zinc vacancies were assumed to be responsible for the acceptor levels in Zn_3P_2 crystal. Deep compensating levels were proposed to be the result of phosphorous vacancies and zinc interstitials.

Diagrams of the optical transitions observed within 1.25-1.45 eV (at room temperature) and 1.25-1.66 eV energy range (at low temperatures) were proposed obtaining reasonable self-consistence of the energies of transitions observed.

On the base of measurements performed, no influence of the crystal anisotropy on the defect related optical transitions was found.

To understand the nature and creation mechanism of the found levels, additional investigations should be performed. Especially, there is a problem of finding the simple method of control the carrier concentration in Zn_3P_2 crystal and correlation between carrier concentration and Fermi level position.

The band structure of Zn_3P_2 was verified by means of the optical spectra measurements within 1.5-11 eV energy range at room temperature.

Lin-Chung pseudocubic band structure model was successfully adopted to describe transitions of the energies higher than 4.5 eV.

Additional crystal field potential with tetragonal symmetry was necessary to introduce into Lin-Chung model to obtain qualitative agreement between theoretical model and experimental results within 2-4.5 eV energy range. Anisotropy in the optical spectra in this region was not significant.

Lin-Chung model, as a pseudocubic one, was useless in interpretation of the transitions lying nearby energy gap. By using selection rules and optical spectra at polarized light an anisotropic model of the band structure at Γ point was proposed. Direct energy gap of Zn_3P_2 crystal was determined as 1.60 eV (at $E \perp c$ polarization), whereas crystal field and spin-orbit splitting of the valence band as equal to 0.03 eV and 0.11 eV, respectively. A second conduction band was found at 0.28 eV above the conduction band bottom.

Except energy gap value, the band structure is not very sensitive to the temperature changes. Nevertheless, it seems to be important to verify the model proposed for Γ point at the low temperatures, where excitonic transitions should be clearly visible.

The problem of the energy band structure calculations for Zn_3P_2 crystal should arise again. Now, there is much easier to solve such problem for real crystal structure - D_{4h}^{15} (with 40 atoms in unit cell) due to the intensive progress in computer calculations techniques. Experimental data as well as group theory analysis performed in the present work may be a good basis of such calculations.

The photoemission techniques as XPS, UPS and angle resolved PS should be used as sources of band structure parameters.

Useful and important data enabling determination of band structure of Zn_3P_2 crystal may be also taken from magneto-optics and magnetotransport experiments, which have not been performed hitherto.

ACKNOWLEDGEMENTS

Special thanks are directed to Prof. J.M. Pawlikowski for his permanent encouragements, very fruitful discussion and critical reading of the manuscript.

Author is deeply indebted to Drs P. Becla and D. Heiman from Francis Bitter National Magnet Laboratory, MIT, Cambridge, USA, who made it possible for him to perform important part of the measurements.

Drs J.M. Wrobel and B.P. Clayman from Simon Fraser University, Burnaby, Canada, are deeply acknowledged for their help in the far-infrared measurements.

This work was done under the Research Programme CPBP 01.04.I.2.7 from the Institute of Physics, Polish Academy of Sciences.

REFERENCES

- ADHYAPAK S.V., and NIGAVEKAR A.S., (1978), *J. Phys. Chem. Solids* 39, 171-173.
- ARUSHANOV E.K., (1981), *Prog. Crystal Growth Charact.* 3, 211.
- BARKER A.S., (1970), [in] *Far Infrared Properties of Solids*, Eds.: S.S.Mitra and S. Nudelman, Plenum Press, New York, p. 247.
- BEBB H.B., (1969), *Phys. Rev.* 185, 1116-1124.
- BECLA P., GUMIENNY Z., and MISIEWICZ J., (1979), *Opt. Appl.* 9, 143-150.
- BENDETT M.P., and HUNGSPREGER R.G., (1981), *J. Electron. Mater.* 10, 559-64.
- BIRMAN J.L., (1984), *Theory of Crystal Space Groups and Lattice Dynamics*, Ed. L. Genzel, Springer-Verlag, Berlin, Heidelberg.
- BOUCKAERT L.P., SMOLUCHOWSKI R., and WIGNER E., (1936), *Phys. Rev.* 50, 58-66.
- BRIONES F., WANG. F.C., and BUBE R.H., (1981), *Appl. Phys. Lett.* 39, 805-807.
- CARDONA M., (1967), [in] *Semiconductors and Semimetals*, Ed. R.K. Willardson and A.C. Beer, Academic Press, New York, Vol. 3, p. 142.
- CATALANO A., and HALL R.B., (1980), *J. Phys. Chem. Solids* 41, 635.
- CISOWSKI J., (1982), *Phys. Status Solidi (b)* 111, 289-293.
- DOMASHEVSKAYA E.P., TEREKHOV V.A., UGAI Ya.A., (1980), *Proc. 1st Int. Symposium of the Physics and Chemistry of II-V Compounds*, Eds.: M.J. Gelten and L. Żdanowicz, Mogilany, Poland, p. 225-235.
- DOW J.D., and REDFIELD D., (1972), *Phys. Rev. B* 5, 594-98.
- DOWGIAŁO-PLENKIEWICZ B., and PLENKIEWICZ P., (1978), *Phys. Status Solidi (b)* 87, 309-315.
- ELLIOT R.J., (1957), *Phys. Rev.* 108, 1384-1389.
- FAGEN E.A., (1979), *J. Appl. Phys.* 50, 6505-6615.
- FATELEY W.G., McDEVITT N.T., and BENTLEY F.F., (1971), *Appl. Spectrosc.* 25, 155-173.
- GAJ J.A., (1973), *Proc. 4th Conf. Phys. Semicond.*, Institute of Physics Polish Academy of Sciences, 39, 260-65.
- GUMIENNY Z., and MISIEWICZ J., (1982), *Opt. Appl.* 12, 37-47.
- GUMIENNY Z., and MISIEWICZ J., (1985), *Opt. Appl.* 15, 63-68.
- HULDT L., NILSSON N.G., SUNDSTRÖM B.O., and ŻDANOWICZ W., (1979), *Phys. Status Solidi (a)*, 53, K15-K18.
- JEZIERSKI K., and MISIEWICZ J., (1985), *Acta Phys. Pol. A* 67, 489-93.
- KOVALEV V., (1965), *Irreducible Representations for Space Groups*, Eds.: Gordon and Breach, New York, p. 46-84.
- KURBATOV L.N., DIROCHKA A.I., SINITSYN E.V., LAZAREV V.B., SHEVCHENKO

- V. YA., and KOZLOV S.E., (1976), Sov. J. Quant. Electron. 6, 166-168.
- LIN-CHUNG P.J., (1971), Phys. Status Solidi (b) 47, 33-39.
- LOFERSKI J.J., (1956), J. Appl. Phys. 27, 777-87.
- LOUDON R., (1964), Adv. Phys. 13, 423-82.
- MASUMOTO K., ISOMURA S., and SASAKI K., (1971), Phys. Status Solidi (b) 6, 515-519.
- MISIEWICZ J., and GAJ J.A., (1981), Phys. Status Solidi (b), K23-K25.
- MISIEWICZ J., and GAJ J.A., (1980), Proc. 1st Int. Symposium of the Physics and Chemistry of II-V Compounds, Eds. M.J. Gelten and L. Żdanowicz, Mogilany, Poland, p. 163-167.
- MISIEWICZ J., WROBEL J., SUJAK-CYRUK B., and KRÓLICKI F., (1980), Opt. Appl. 10, 75-78.
- MISIEWICZ J., MIROWSKA N., and GUMIENNY Z., (1984), Phys. Status Solidi (a) 83, K51-K56.
- MISIEWICZ J., WROBEL J., and JEZERSKI K., (1984a), J. Phys. C.: Solid State Phys. 17, 3091-99.
- MISIEWICZ J., and KRÓLICKI F., (1985), Mater. Sci. 11, 39-55.
- MISIEWICZ J., KRÓLICKI F., LEWICKI M., and KASPRZAK J.F., (1986), Acta Phys. Pol. A 67, 1127-30.
- MISIEWICZ J., SUJAK-CYRUL B., and BARTCZAK A., (1986a), Solid State Commun. 58, 677-679.
- MISIEWICZ J., SUJAK-CYRUL B., SZATKOWSKI J., SIERAŃSKI K., and KRÓLICKI F., (1986b), Acta Phys. Pol. A 67, 125-28.
- MISIEWICZ J., GUMIENNY Z., (1987), Phys. Status Solidi (a), 104, K37-K40.
- MISIEWICZ J., GUMIENNY Z., CYWIŃSKI R., and MUGEŃSKI E., (1989), Phys. Status Solidi (a) 111, K249-K253.
- MISIEWICZ J., (1988), Phys. Status Solidi (a) 107, K65-K68.
- MISIEWICZ J., WROBEL J., CLAYMAN B.P., and KRÓLICKI F., (1988a), Acta Phys. Pol. A 73, 405-409.
- MISIEWICZ J., (1988a), Infrared Phys. 28, 215-218.
- MISIEWICZ J., WROBEL J.M., and CLAYMAN B.P., (1988b), Solid State Commun. 66, 747-750.
- MISIEWICZ J., KOWALSKI B., and ORŁOWSKI B.A., (1989), Acta Phys. Pol., A 75, 67-70.
- MISIEWICZ J., and JEZERSKI K., (1989), Solid State Commun., 70, 465-469.
- MISIEWICZ J., (1989), J. Phys. Chem. Solids, will be published.
- MÖLLER A., ELROD U., MUNZ P., HÖNIGSCHMID J., CLEMEN C., and BUCHER E., (1979), Inst. Phys. Conf. Ser. 43, 825-828.
- MULLIKEN R.S., (1933), Phys. Rev. 43, 279-282.

- MURALI K.R., GOPALAM B.S.V., and SOBHANADRI J., (1986), *Thin Solid Films* 136, 275-280.
- NAUKA K., and MISIEWICZ J., (1981), *Phys. Status Solidi (a)*, 65, K95-K97.
- OLBRYCHSKI K., (1963), *Phys. Status Solidi* 3, 214-49.
- PAWLIKOWSKI J.M., MISIEWICZ J., and MIROWSKA N., (1979), *J. Phys. Chem. Solids* 40, 1027-33.
- PAWLIKOWSKI J.M., (1982), *Phys. Rev. B* 26, 4711-13.
- PAWLIKOWSKI J.M., (1982a), *J. Appl. Phys.* 53, 3639-3643.
- PAWLIKOWSKI J.M., (1985), *J. Phys. C.: Solid State Phys.* 18, 5605-5116.
- PAWLIKOWSKI J.M., (1985a), *Proc. Int. Conf. Phys. Techn. Compens. Semicond.*, Madras, Vol. 1, p. 105-113.
- PAWLIKOWSKI J.M., (1988a), *Infrared Phys.* 28, 177-182.
- PAWLIKOWSKI J.M., (1988b), *Rev. Solid State Sci.* 2, 581-602.
- PISTORIUS C.W.F.T., CLARK J.B., COETZNER J., KRUGER G.J., and KUNZE O.A. (1987), *High-Temp.-High Pressures* 9, 471-82.
- PHILLIPS J.C., (1966), *Solid State Phys.* 18, 55-164.
- PLENKIEWICZ P., and DOWGIAŁŁO-PLENKIEWICZ B., (1979), *Phys. Status Solidi (b)* 95, 2937-2945.
- RADAUTSAN S.J., SYRBU N.N., VOLODINA V.J., and KIOSSEV V.K., (1976), *Sov. Phys. Dokl.* 21, 193-196.
- RADAUTSAN R.S., SYRBU N.N., NEBOLA J.J., VOLODINA V.J., (1977), *Sov. Solid State Phys.* 19, 1290.
- SELL D.D., (1972), *Proc. Int. Conf. Physics of Semiconductors*, Ed. PWN, Warszawa, p. 800-806.
- SHEVCHENKO V.Ya., BABARINA L.R., KOZLOV S.E., and LAZAREV V.B., (1975), *Izv. Akad. Nauk SSSR, Neorgan. Mater.* 11, 1719.
- SIERAŃSKI K., and SZATKOWSKI J., (1986), *Phys. Status Solidi (a)*, 94, K113-K116.
- SOBOLEV V.V., and SYRBU N.N., (1974), *Phys. Status Solidi (b)*, 64, 423-29.
- STACKELBERG M., and PAULUS R., (1935), *Z. Phys. Chem. B* 24, 427-60.
- STREITWOLF H.W., (1967), *Gruppentheorie in der Festkörperphysik*, Akademische Verlagsgesellschaft, Geest und Portig. K.-G., Leipzig, p. 143-146.
- STURGE M.D., (1962), *Phys. Rev.* 127, 768-773.
- SUDA T., and BUBE R.H., (1984), *Appl. Phys. Lett.* 45, 775-778.
- SUDA T., and KUROYANAGI A., *Jpn. J. Appl. Phys.* 25, L993-996.
- SUNDSTRÖM B.O., NILSSON N.G., HULDT L., and ŻDANOWICZ W., (1980), *Proc. Ist Int. Symp. Phys. Chem. II-V Compounds, Mogilany*, Eds.: M.J. Gelten and L. Żdanowicz, Eindhoven, Netherlands, p. 175-178.
- SUNDSTRÖM B.O., (1981), *Physica Scripta* 24, 444-5.

- SYRBU N.N., STAMOV I.G., MOROZOVA V.I., KIOSSEV V.K., and PEEV L.G., (1980), Proc. Ist Int. Symp. Phys. Chem. II-V Compounds, Mogilany, Eds.: M.J. Gelten and L. Żdanowicz, Eindhoven, Netherlands, p. 237-242.
- SZATKOWSKI J., and SIERANKI K., (1987), Acta Phys. Pol. A 71, 297-301.
- URBACH F., (1953), Phys. Rev. 92, 1324-28.
- VOLODINA V.J., RADAUTSAN S.J., KADYGROB V.J., and SYRBU N.N., (1977), Sov. Phys. Semicond. 11, 609-610.
- WANG F.C., FAHRENBUCH A.L., and BUBE R.H., (1982), J. Electron. Mater. 11, 75-79.
- WANG F.C., and BUBE R.H., (1982), J. Appl. Phys. 53, 3335-3338.
- WARDZYŃSKI W., (1970), J. Phys. C.: Solid State Phys. 3, 1251-63.
- WROBEL J.M., and MISIEWICZ J., (1989), in preparation.
- ZYUBINA T.A., TOROPSEV V.P., TOROPSEV Yu.P., and SHCHUKIN O., (1977), Izv. Akad. Nauk.SSSR, Neorg. Mater., Vol. 13, p. 355-57.
- ŻDANOWICZ L., ŻDANOWICZ W., PETELENZ D., and KLOC K., (1980), Acta Phys. Pol. A 57, 159-165.
- ŻDANOWICZ W., and ŻDANOWICZ L., (1975), Ann. Rev. Mater. Sci. 5, 301-327.

Pracę złożono 10 stycznia 1989 r.,
w ostatecznej formie 14 marca 1989 r.

AppendixA REVIEW OF PAPERS ON APPLICATION STUDIES OF Zn_3P_2

The main interest connected with Zn_3P_2 arises from its usefulness to produce solar energy converters. Thus, there is a number of papers devoted to this problem.

A high photosensitivity of simple metal- Zn_3P_2 junctions was found ten years ago (see Pawlikowski et al. (1978), and Catalano et al. (1979)). Photoelectric properties of Zn_3P_2 were studied by Pawlikowski et al. (1980), Mirowska et al. (1981). Barrier heights of evaporated metal contacts on Zn_3P_2 were examined by Convers Weyth and Catalano (1979). Minority-carrier diffusion length in Zn_3P_2 was investigated by Convers Wyeth and Catalano (1979), and Nauka and Misiewicz (1981). In the first paper, spectral responses of (Al, Mg, or Be)- Zn_3P_2 junctions were also measured. The first Schottky-type solar cells were prepared by sputter depositing a thin transparent film of Mg on Zn_3P_2 (Bhushan and Catalano 1981) obtaining solar energy conversion efficiency of 4-6% under AM1 illumination.

Thin Zn_3P_2 films were applied for photovoltaic solar cell, firstly, by Catalano et al. (1980), and followed by Bhushan (1982), obtaining energy conversion efficiency of 4% and 4.3%, respectively.

Properties of Mg- Zn_3P_2 junctions after different heat treatments to improve the solar energy conversion in such junctions were investigated by Catalano and Bhushan (1980a) and by Bhushan (1982a) indicating the possibility to formate p-n junction in Zn_3P_2 . Such junction should indicate energy conversion efficiency as high as $\eta = 18.5\%$.

$ZnO-Zn_3P_2$ heterojunctions were extensively investigated by Nayar and Catalano (1981), and Nayar (1982). Such devices indicated energy conversion of 2%. Promising properties of $ZnSe/Zn_3P_2$ heterojunctions were found by Bhushan et al. (1982) and by Bhushan and Pawlikowski (1987), and of Zn_3P_2 -ITO (indium-tin oxide) by Suda et al. (1982,1983), Zn_3P_2/CdS heterojunctions were produced and investigated by Suda et al. (1984). Solar cell made of such type heterojunctions indicated energy conversion efficiency of 1-2%.

Studies on the electrical properties and transport mechanisms for Mg- Zn_3P_2 junctions were performed by Wang et al. (1982), and Mirowska et al. (1985), Rao et al. (1987), Szatkowski and Sierański (1988), and Szatkowski et al. (1988).

Solar energy conversion efficiency was found to be equal to 1% for simple Mg- Zn_3P_2 contacts (Misiewicz et al. 1986), and 2.5% for the

junctions made of Cd-doped Zn_3P_2 , without any antireflection coating (Szatkowski et al. 1988).

Interfacial properties of the Mg- Zn_3P_2 solar cells were investigated by Kazmerski et al. (1981), Casey et al. (1987), as well as by Szatkowski and Sierański (1988a, 1988b).

Surface properties of Zn_3P_2 single crystals were analysed by AES and XPS technics by Elrod et al. (1987), and Suda et al. (1986).

Photochemical solar cells made of the Zn_3P_2 thin films were investigated by Singh and Singh (1987).

Photon collection efficiency, carrier collection efficiency and fill-factor - three important factors of solar cell quality - were calculated, extensively discussed, and finally, compared with experimental data for prototype Zn_3P_2 -bases solar cell devices by Pawlikowski (1985, 1985a, 1986).

It was shown in these papers that after some optimization procedure solar energy conversion efficiency on Zn_3P_2 -based solar cell may reach 16%.

Current status of Zn_3P_2 -based solar cells is extensively reviewed by Pawlikowski (1988) and (1988a).

Zn_3P_2 may be also used to produce ultraviolet photoconductive detectors as it was shown by Irwin et al. (1979) and Bendett and Hungsperger (1981).

A distinct photodichroism observed on metal- Zn_3P_2 (oriented single crystal) junctions may be applied in high quality light polarization step indicator (Misiewicz et al. 1984).

Near infrared detectors based in Mg- Zn_3P_2 junctions were investigated by Popko et al. (1988).

Thin Zn_3P_2 films play a very important role in the applications, so, papers on the main techniques of obtaining such films are mentioned below.

Vapour Phase Deposition method was applied by: Żdanowicz et al. (1980), Fagen (1979), Murali and Rao (1981), and Murali et al. (1986), Deiss et al. (1985, 1987), Von Sacken et al. (1985), Arsenault and Brodie (1985), Singh and Singh (1987a), and Suda et al. (1988).

Chemical Vapour Deposition method was used by: Long (1983), Papazoglou et al. (1987), and Kato et al. (1987).

Close Space Vapour Transport was applied by Catalano et al. (1980), and Bhushan (1982).

Modifications and combinations of different methods were presented in the papers by Sberverglieri and Romero (1981), Suda et al. (1983), Chu et al. (1983), Lousa et al. (1985), Fuke et al. (1987), and Suda et al. (1988a).

- ARSENAULT C.J., and BRODIE D.E., (1987), *Can. J. Phys.* 65, 756-9.
- BENDETT M.P., and HUNGSPERGER R.G., (1981), *J. Electron. Mater.* 10, 559-69.
- BHUSHAN M., and CATALANO A., (1981), *Appl. Phys. Lett.* 38, 39-41.
- BHUSHAN M., (1982), *Appl. Phys. Lett.* 40, 51-53.
- BHUSHAN M., (1982a), *J. Appl. Phys.* 53, 514-19.
- BHUSHAN M., PAWLIKOWSKI J.M., and PEREYRA I., (1982), *Proc. 161st Electrochemical Society Meeting, Montreal 1982, Vol. 82-8, p. 505-13.*
- BHUSHAN M., and PAWLIKOWSKI J.M., (1987), *Electron. Technology* 20,
- CASEY M., FAHRENBUCH A.L., and BUBE R.H., (1987), *J. Appl. Phys.* 61, 2941-46.
- CATALANO A., MASI J.V., and WYETH N.C., (1979), [in] *Proc. 2nd E.C., Photovoltaic Solar Energy Conference, Berlin, Ed. Reidel, Dordrecht, Holland 1979, p. 440.*
- CATALANO A., BHUSHAN M., and CONVERS WYETH N., (1980), *Proc. 14th IEEE Photovoltaic Conference (San Diego 1980), p. 641-46.*
- CATALANO A., BHUSHAN M., (1980a), *Appl. Phys. Lett.* 37, 567-69.
- CONVERS WYETH N., and CATALANO A., (1979), *J. Appl. Phys.* 50, 1403-07.
- CONVERS WYETH N., and CATALANO A., (1980), *J. Appl. Phys.* 51, 2286-88.
- CHU T.L., CHU SHIRLEY S., MURTHY K., STOKES E.D., and RUSSELL P.E., (1983), *J. Appl. Phys.* 54, 2063-68.
- DEISS J.L., ELIDRISSI B., ROBINO M., and WEIL R., (1985), *Appl. Phys. Lett.* 49, 969-70.
- DEISS J.L., ELIDRISSI B., ROBINO M., TAPIERO M., ZIELINGER J.P., and WEIL R., (1987), *J. Non-Cryst. Solids* 97-98, 678-82.
- ELROD U., LUX-STEINER M.Ch., OBERGFELL M., BUCHER E., and SCHLAPBACH L., (1987), *Appl. Phys. B* 43, 197-201.
- FAGEN E.A., (1979), *J. Appl. Phys.* 50, 6505-15.
- FUKE S., IMAI T., OKUYAMA S., and KUWAHARA K., (1987), *J. Appl. Phys.* 62, 1127-29.
- IRWIN K.G., KOPEIKA N.S., HUNGSPERGER R.G., (1979), *Electron. Lett.* 718.
- KATO Y., KURITA S., and SUDA I., (1987), *J. Appl. Phys.* 62, 3733-39.
- KAZMERSKI L.L., IRELAND P.J., and CATALANO A., (1981), *J. Vac. Sci. Technol.* 18, 363-71.
- LONG J., (1983), *J. Electrochem Soc.* 130, 725-27.
- LOUSA A., BERTRAN E., VARELA M., and MORENZA J.L., (1985), *Solar Energy Materials* 12, 51-56.
- MIROWSKA N., MISIEWICZ J., NAUKA K., and PAWLIKOWSKI J.M., (1981), *Acta Phys. Pol. Ser A* 60, 233-39.

- MIROWSKA N., MISIEWICZ J., and JEZIERSKI K., (1985), *Acta Phys. Pol. Ser. A* 67, 233-36.
- MISIEWICZ J., MIROWSKA N., and GUMIENNY Z., (1984), *Phys. Status Solidi (a)* 83, K51-56.
- MISIEWICZ J., SZATKOWSKI J., MIROWSKA N., JEZIERSKI K., GUMIENNY Z., and KRÓLICKI F., (1986), *Acta Phys. Pol. Ser. A* 69, 1131-35.
- MURALI K.R., and RAO D.R., (1981), *Thin Solid Films* 86, 283-286.
- MURALI K.R., GOPALAM B.S.V., and SOBHANADRI J., (1986), *Thin Solid Films* 136, 275-280.
- NAUKA K., and MISIEWICZ J., (1981), *Phys. Status Solidi (a)* 64, K95-99.
- NAYAR P.S., and CATALANO A., (1981), *Appl. Phys. Lett.*, 39, 105-7.
- NAYAR P.S., (1982), *J. Appl. Phys.* 53, 1069-75.
- PAPAZOĞLOU E., and RUSSELL T.W.F., (1987), *J. Vac. Sci. Technol.* 5, 3378-82.
- PAWLIKOWSKI J.M., MIROWSKA N., and KRÓLICKI F., (1978), *Infrared Phys.* 18, 343-46.
- PAWLIKOWSKI J.M., MIROWSKA N., BECLA P., and KRÓLICKI F., (1980), *Solid State Electron.* 23, 755-58.
- PAWLIKOWSKI J.M., (1985), *Opt. Appl.* 15, 3-19.
- PAWLIKOWSKI J.M., (1985a), *Proc. Int. Conf. Physics and Technology of Compensated Semiconductors (Madras)*, p. 97-103.
- PAWLIKOWSKI J.M., (1986), *Electron. Technol.* 19, 75-89.
- PAWLIKOWSKI J.M., (1988), *Infrared Phys.* 28, 177-182.
- PAWLIKOWSKI J.M., (1988a), *Rev. Solid State Sci.* 2, 581-602.
- POPKO E., MIROWSKA N., SZATKOWSKI J., SIERAŃSKI K., and MISIEWICZ J., (1988), *Proc. 2nd Conf. on Surface Physics (Wrocław)*, p. 207-211.
- RAO V.J., SAMUEL V., NAGESWARA RAO N.B.S., and SINHA A.P.B., (1987), *Thin Solid Films* 149, 1-7.
- Von SACKEN U., and BRODIE D.E., (1985), *Can. J. Phys.* 63, 757-761.
- SBERVEGLIERI G., and ROMERO N., (1981), *Thin Solid Films* 83, L133-36.
- SINGH R.P., and SINGH S.L., (1987), *Phys. Status Solidi (a)*, 101, 129-135.
- SINGH R.P., and SINGH S.L., (1987a), *Phys. Status Solidi (a)* 100, 493-500.
- SUDA T., KOBAYASHI M., KUROYANAGI A., and KURITA S., (1982), *Jpn J. Appl. Phys.* 21, Suppl. 21-2, 63-65.
- SUDA T., SUZUKI M., and KURITA S., (1983), *Jpn J. Appl. Phys.* 22, L656-L658.
- SUDA T., KANNO T., and KURITA S., (1983), *Jpn J. Appl. Phys.* 22, L777-L779.
- SUDA T., KUROYANAGI A., and KURITA S., (1984), *Proc. Int. Photovoltaic Sci. and Eng. Conf. (Kobe)*, p. 381-84.

- SUDA T., MURATA Y., and KURITA S., (1986), Jpn J. Appl. Phys. 25, L162-164.
- SUDA T., NISHIMOTO T., and KURITA S., (1988), J. Cryst. Growth 86, 430-438.
- SUDA T., MIRAKAWA T., and KURITA S., (1988a), J. Cryst. Growth 86, 423-429.
- SZATKOWSKI J., and SIERAŃSKI K., (1988), Phys. Status Solidi (a), 106, 473-477.
- SZATKOWSKI J., and SIERAŃSKI K., (1988a), Solid State Electron. 31, 257-60.
- SZATKOWSKI J., and SIERAŃSKI K., (1988b), Phys. Status Solidi (a) 106, K31-34.
- SZATKOWSKI J., SIERAŃSKI K., and MISIEWICZ J., (1988), Phys. Status Solidi (a), 106, 551-55.
- WANG FAA-CHING, FAHRENBRUCH A.L., and BUBE R.H., (1982), J. Appl. Phys. 53, 8874-79.
- ŻDANOWICZ L., ŻDANOWICZ W., PETELEŃZ D., and KLOC K., (1980), Acta Phys. Pol. Ser. A 57, 159-165.

WZBUDZENIA OPTYCZNE W FOSFORU CYNKU (Zn_3P_2)

Przedstawiono wyniki badań oddziaływania promieniowania elektromagnetycznego z półprzewodnikowym kryształem Zn_3P_2 w zakresie energii promieniowania od 0,003 do 11 eV.

Jako podstawowe techniki badawcze zastosowano absorpcję i odbicie. Ponadto w wybranych obszarach energii wykonano następujące pomiary:

- dwójłomności w zakresie 0,5-1,45 eV,
- fotoluminescencji w niskich temperaturach w zakresie energii 1,1-1,7 eV,
- fotoprzewodnictwa w zakresie energii 0,65-2,6 eV,
- rozpraszania Ramana w zakresie energii 0,003-0,062 eV.

Dodatkowo w obszarze energii 1,40-1,60 eV wykonano pomiary różniczkowych widm współczynnika absorpcji w szerokim zakresie temperatur.

Widma odbicia zmierzone w zakresie 0,003-0,050 eV, po zastosowaniu analizy Kramersa-Kroniga, umożliwiły określenie energii fononów optycznych w punkcie Γ . Widma absorpcji w zakresie 0,047-0,150 eV oraz rozpraszania Ramana posłużyły do wyznaczenia energii przejść dwu- i trójfononowych. Stosując metody teorii grup, określono symetrię gałęzi fononowych wzdłuż głównych linii i punktów symetrii strefy Brillouina. Wyznaczono reguły wyboru dla przejść wielofononowych i zastosowano je

do interpretacji wyników eksperymentalnych. Stwierdzono istotny wpływ anizotropii kryształu na widma drgań sieciowych.

Przejścia optyczne w obszarze energii 0,15–1,45 eV zostały zinterpretowane jako związane z istnieniem poziomów defektowych w obszarze przerwy energetycznej. Parametry poziomów akceptorowych zostały wyznaczone na podstawie metody defektu kwantowego. Określono energie znalezionych poziomów jako równe (w eV): 0,05; 0,17; 0,27; 0,36; 0,55; 0,66 i 0,85. Istnienie tych poziomów przejawia się w różny sposób dla próbek o różnych koncentracjach dziur. Pomiaru prowadzono dla próbek o koncentracjach w zakresie 10^{13} cm^{-3} – 10^{17} cm^{-3} . Za główną przyczynę istnienia poziomów akceptorowych uznano naturalne defekty typu P_1 , $\sqrt{V_{\text{Zn}}}$ i V_{Zn} . Głębokie, kompensujące poziomy powiązано z możliwymi wakansami fosforowymi i atomami cynku w międzywęźlach. Przejścia optyczne zaobserwowane w obszarze 1,25–1,45 eV (w temperaturze pokojowej) i 1,25–1,66 eV (w niskiej temperaturze) są satysfakcjonująco zgodne z oczekiwaniami.

Na podstawie wykonanych badań nie stwierdzono istotnego wpływu anizotropii kryształu na widma przejść optycznych związanych z defektami struktury krystalicznej.

Przejścia optyczne w zakresie energii 1,5–11 eV w temperaturze pokojowej interpretowano jako przejścia międzypasmowe. W obszarze energii 1,5–2 eV zaobserwowano wyraźną anizotropię widm optycznych (absorpcji, fotoprzewodnictwa, odbicia). Anizotropia widma odbicia w zakresie 2–5 eV jest niezbyt silna. W obszarze wyższych energii prowadzono badania jedynie w świetle niespolaryzowanym. Zaobserwowano, że najsilniejsze przejścia występują w obszarze od 4 do 7 eV. Korzystając z analizy Kramersa–Kroniga wyznaczono stałe optyczne Zn_3P_2 . Osobliwości zaobserwowane w widmach odbicia i stałych optycznych zinterpretowano na podstawie pseudokubicznego modelu struktury pasmowej, obliczonego przez Lin–Chung. Uzyskano dobre zgodności wyników eksperymentalnych z modelem teoretycznym dla przejść o energiach wyższych od 4,5 eV. Interpretacja przejść w obszarze 2–4,5 eV wymagała uwzględnienia w modelu Lin–Chung dodatkowego oddziaływania pochodzącego od pola krystalicznego o symetrii tetragonalnej. Tą drogą uzyskano jakościowy opis wyników eksperymentalnych. Model Lin–Chung jako pseudokubiczny nie znalazł zastosowania do opisu przejść w okolicy przerwy energetycznej. Opierając się na analizie teoriogrupowej otrzymano reguły wyboru dla przejść optycznych, z uwzględnieniem polaryzacji światła. Na tej podstawie oraz korzystając z wyników pomiarów absorpcji, fotoprzewodnictwa i odbicia w świetle spolaryzowanym na zorientowanych próbkach zaproponowano model struktury pasm energetycznych w punkcie Γ . Stwierdzono, że prosta przerwa energetyczna ma energię 1,60 eV. Rozszerzenie

nia pasma walencyjnego w punkcie Γ przez pole krystaliczne i oddziaływanie spin-orbita są równe odpowiednio 0,03 eV i 0,11 eV. Drugie pasmo przewodnictwa leży o 0,28 eV powyżej dna pasma przewodnictwa.

Otrzymane przez autora wyniki przedstawiono na tle rezultatów innych prac, uzyskując spójny obraz oddziaływania promieniowania elektromagnetycznego z kryształem Zn_3P_2 .

ОПТИЧЕСКИЕ ВОЗБУЖДЕНИЯ В ФОСФИДЕ ЦИНКА Zn_3P_2

Представлены результаты собственных исследований автора настоящей работы, касающиеся воздействия электромагнитной волны с полупроводниковым кристаллом Zn_3P_2 в диапазоне энергии волны от 0,003 до II эв.

В качестве исследовательской техники применяли абсорбцию и отражение. Кроме этого, в избранных областях энергии провели следующие измерения:

- двойное лучепреломление в области 0,5–1,45 эв,
- фотолуминесценцию при низких температурах в диапазоне энергии 1,1–1,7 эв,
- фотопроводимости в диапазоне энергии 0,65–2,6 эв,
- рамановское рассеяние в диапазоне энергии 0,003–0,062 эв.

Дополнительно в диапазоне энергии 1,4–1,6 эв выполнены измерения дифференциальных спектров коэффициента поглощения при широком интервале температур.

Спектры отражения, измеренные в диапазоне 0,005–0,050 эв, с применением анализа Крамера-Кронига, дали возможность определить энергию оптических фононов в точке Γ . Спектры поглощения в диапазоне 0,047–0,150 эв, а также рамановское рассеяние дали возможность определить энергии двух- и трехфононных переходов. Применяя методы теории групп, определили симметрию фононных ветвей вдоль главных линий и точек симметрии бриллюэновской зоны. Определили правила принципа отбора для многофононных переходов и применили их для интерпретации экспериментальных результатов. Установлено существенное влияние анизотропии кристалла на спектры сетевых колебаний.

Оптические переходы в диапазоне энергии 0,15–1,45 эв были истолкованы как переходы, связанные с существованием дефектных уровней в области энергетического разрыва. Параметры акцепторных уровней были определены, исходя из метода квантового дефекта. Определены энергии найденных уровней, которые составляли (в эв): 0,05; 0,17; 0,27; 0,36; 0,55; 0,66 и 0,85. Существование этих уровней проявляется разным способом для образцов с разными концентрациями дырок. Измерения проводились для образцов с концентрациями в диапазоне 10^{13} см^{-3} – 10^{17} см^{-3} . В качестве основной причины существования акцепторных уровней были предложены естественные дефекты типа P_1 , V_{Zn}^- и V_{Zn}^{--} . Глубокие, компенсирующие

уровни были связаны с возможными фосфорными вакансиями и атомами цинка в междузлиях. Оптические переходы, наблюдаемые в диапазоне 1,25–1,45 эв (при комнатной температуре) и 1,25–1,66 эв (при низких температурах), хорошо соотносятся с предполагаемыми переходами.

На основе проведенных испытаний не было установлено существенное влияние анизотропии кристалла на спектры оптических переходов, связанных с дефектами кристаллической структуры.

Оптические переходы в диапазоне энергии 1,5–11 эв при комнатной температуре можно интерпретировать как междузонные переходы. В области энергии 1,5–2 эв можно было заметить отчетливую анизотропию оптических спектров (абсорбции, фотопроводимости, отражения). Анизотропия спектра отражения в диапазоне 2–5 эв является неособенно сильной. В области высших энергий проводили испытания только в неполяризованном свете. Было замечено, что самые сильные переходы имеют место в диапазоне от 4 до 7 эв. Используя анализ Крамерса–Кронига, определили оптические постоянные Zn_3P_2 . Замеченные особенности в спектрах отражения и оптических постоянных интерпретировались, исходя из псевдокубической модели зонной структуры, которая была рассчитана Лин–Чунг. Были получены хорошие соотношения экспериментальных результатов с теоретической моделью для переходов для энергий выше 4,5 эв. Интерпретация переходов в области 2–4,5 эв требовала учета в модели Лин–Чунг дополнительного воздействия, происходящего с кристаллического поля тетрагональной симметрии. Этим путем было получено качественное описание экспериментальных результатов. Модель Лин–Чунг, как псевдокубическая, не нашла применения для описания переходов в окрестности энергетического разрыва. Исходя из анализа теории групп, были получены принципы отбора для оптических переходов с учетом поляризации света. На этой основе, а также используя результаты измерений абсорбции, фотопроводимости и отражения в поляризованном свете на ориентированных образцах, была разработана модель структуры энергетических полос в точке Г. Было установлено, что прямой энергетический разрыв имеет энергию 1,6 эв, расщепления кристаллическим полем и спин-орбитой соответственно равны 0,03 эв и 0,11 эв. Вторая полоса проводимости находится на 0,28 эв выше дна полосы проводимости.

Полученные автором результаты представлены на фоне результатов других работ, получая четкое изображение воздействия электромагнитной волны с кристаллом Zn_3P_2 .

CONTENTS

| | |
|---|----|
| 1. Introduction | 4 |
| 2. Zn_3P_2 crystal structure | 7 |
| 3. Energy band structure of Zn_3P_2 | 9 |
| 3.1. Theoretical considerations | 9 |
| 3.1.1. Bondings | 9 |
| 3.1.2. Quasi-cubic energy band structure model | 10 |
| 3.1.3. Spin-orbit and crystal field effects | 12 |
| 3.1.4. Selection rules for direct optical transitions in real crystal structure of Zn_3P_2 | 13 |
| 3.2. Interband optical transitions - experiment | 15 |
| 3.2.1. Fundamental absorption edge | 15 |
| 3.2.2. Photoconductivity spectra | 18 |
| 3.2.3. Reflectivity spectra | 19 |
| 3.3. Birefringence | 24 |
| 3.4. Interband optical transitions - a model | 26 |
| 3.4.1. Optical transitions at the center of Brillouin zone | 26 |
| 3.4.2. Analysis of the high-energy interband optical transitions | 31 |
| 3.5. Conclusions on the band structure of Zn_3P_2 | 38 |
| 4. Lattice vibrations in Zn_3P_2 | 40 |
| 4.1. Theoretical analysis of lattice modes | 40 |
| 4.1.1. Symmetry of one-phonon branches | 40 |
| 4.1.2. Two-phonon transition selection rules | 43 |
| 4.2. Experimental results of the optical lattice modes investigations | 46 |
| 4.2.1. Reflectivity spectra in the far infrared region | 46 |
| 4.2.2. Dielectric constants spectra and one-phonon energies | 46 |
| 4.2.3. Absorption spectra in the multiphonon transition region | 47 |
| 4.2.4. Raman scattering spectra | 51 |
| 4.3. Analysis of the observed lattice modes in terms of selec- tion rules for the optical vibrations | 52 |
| 4.4. Conclusions of the lattice vibrations in Zn_3P_2 | 62 |
| 5. Optical transitions related to imperfection levels | 63 |
| 5.1. Absorption within 0.1-0.5 eV energy range | 63 |
| 5.2. Absorption and photoconductivity within 0.5-1.5 eV energy range | 65 |

| | |
|--|----|
| 5.3. Absorption derivative spectra | 68 |
| 5.4. Low-temperature photoluminescence spectra | 73 |
| 5.5. Description of the transitions observed in absorption spectra by means of Quantum Defect Method | 74 |
| 5.5.1. Transitions within 0.1-0.5 eV energy range | 74 |
| 5.5.2. Transitions for the energies higher than 0.5 eV | 78 |
| 5.6. Origin and features of acceptor levels | 81 |
| 5.7. Conclusions on the optical transitions related to imperfection levels | 89 |
| 6. Final conclusions and remarks | 90 |
| References | 93 |
| Appendix | 97 |

SPIS RZECZY

| | |
|--|----|
| 1. Wprowadzenie | 4 |
| 2. Struktura krystaliczna Zn_3P_2 | 7 |
| 3. Struktura pasmowa Zn_3P_2 | 9 |
| 3.1. Rozważania teoretyczne | 9 |
| 3.1.1. Wiązania | 9 |
| 3.1.2. Pseudokubiczny model struktury pasmowej | 10 |
| 3.1.3. Wpływ oddziaływania spin-orbita i pola krystalicznego | 12 |
| 3.1.4. Reguły wyboru dla prostych przejść optycznych w rzeczywistej strukturze krystalicznej | 13 |
| 3.2. Międzypasmowe przejścia optyczne - eksperyment | 15 |
| 3.2.1. Krawędź absorpcji podstawowej | 15 |
| 3.2.2. Widma fotoprzewodnictwa | 18 |
| 3.2.3. Widma współczynnika odbicia | 19 |
| 3.3. Dwójłomność | 24 |
| 3.4. Model międzypasmowych przejść optycznych | 26 |
| 3.4.1. Przejścia optyczne w centrum strefy Brillouina | 26 |
| 3.4.2. Analiza międzypasmowych przejść optycznych w obszarze wysokich energii | 31 |
| 3.5. Wnioski dotyczące struktury pasmowej Zn_3P_2 | 38 |
| 4. Drgania sieci w Zn_3P_2 | 40 |
| 4.1. Teoretyczna analiza drgań sieci | 40 |
| 4.1.1. Symetria gałęzi jednofononowych | 40 |
| 4.1.2. Reguły wyboru dla przejść dwufononowych | 43 |

| | |
|--|----|
| 4.2. Eksperymentalne badania optycznych drgań sieci | 46 |
| 4.2.1. Widma odbicia w obszarze dalekiej podczerwieni | 46 |
| 4.2.2. Stałe dielektryczne i energie fononów | 46 |
| 4.2.3. Widma absorpcji w obszarze przejść wielofono- nowych | 47 |
| 4.2.4. Widma rozpraszania Ramana | 51 |
| 4.3. Analiza zaobserwowanych drgań sieci w oparciu o reguły wyboru dla drgań optycznych | 52 |
| 4.4. Wnioski dotyczące drgań sieci w Zn_3P_2 | 62 |
| 5. Przejścia optyczne związane z poziomami defektowymi | 63 |
| 5.1. Absorpcja w obszarze energii 0,1-0,5 eV | 63 |
| 5.2. Absorpcja i fotoprzewodnictwo w obszarze energii 0,5- -1,5 eV | 65 |
| 5.3. Widma absorpcji różniczkowej | 68 |
| 5.4. Fotoluminescencja w niskich temperaturach | 73 |
| 5.5. Opis przejść zaobserwowanych w widmach absorpcji za pomocą Metody Defektu Kwantowego | 74 |
| 5.5.1. Przejścia w zakresie energii 0,1-0,5 eV | 74 |
| 5.5.2. Przejścia w zakresie energii wyższych niż 0,5 eV | 78 |
| 5.6. Dyskusja na temat pochodzenia i natury poziomów akcep- torowych | 81 |
| 5.7. Wnioski dotyczące przejść optycznych związanych z pozio- mami defektowymi | 89 |
| 6. Wnioski i uwagi końcowe | 90 |
| Spis literatury | 93 |
| Appendix | 97 |

PRACE NAUKOWE INSTYTUTU FIZYKI
(wydane w latach 1987—1989)

- | | |
|---|-------|
| Nr 19, Monografie nr 9, J. Wiasak, <i>Magnetoabsorpcja w półprzewodnikach typu InSb</i> , Wrocław 1987 | 95,— |
| Nr 20, Monografie nr 10, R. Gonczarek, <i>Qualitative effects generated by Fermi liquid interaction in superconducting and superfluid systems</i> , Wrocław 1988 | 200,— |
| Nr 21, Monografie nr 11, L. Jacak, <i>Nonlinear topics in the theory of Fermi liquids</i> , Wrocław 1987 | 200,— |
| Nr 22, Monografie nr 12, J. Nowak, <i>Aberracje hologramów w ocenie jakości odzworowania</i> , Wrocław 1987 | 200,— |
| Nr 23, Knoferencje nr 4, <i>VIII polsko-czechosłowacka konferencja optyczna</i> , Wrocław 1988 | 70,— |
| Nr 24, Monografie nr 13, H. Pykacz, <i>Własności fizyczne monokryształów $(NH_4)_{1-x}H_{1-x}(ND_4)_xD_xSeO_4$</i> , Wrocław 1989 | 150,— |
| Nr 25, Monografie nr 14, B. Radojewska, <i>Epitaksjalne kryształy mieszane $GaAs_{1-x}Sb_x$. Wytwarzanie, własności i zastosowanie</i> , Wrocław 1989 | 200,— |
| Nr 26, Monografie nr 15, S. Kuźmiński, <i>Zjawiska fotoelektronowe na realnej powierzchni $CdTe$ i $Cd_{1-x}MnTe$</i> , Wrocław 1989 | 400,— |
| Nr 27, Monografie nr 16, R. Poprawski, <i>Wpływ zmian uporządkowania elektrycznego na własności dielektryczne i termiczne kryształów $RbHSeO_4$ i NH_4HSeO_4</i> , Wrocław 1989 | 30,— |



Cena zł 500,—

Subscription should be sent (at any time of the year) to:

„Ars Polona”

Krakowskie Przedmieście 7, 00-068 Warszawa

Bank account number: PBK XIII Oddz. W-wa 370044-1195-139-11

Zamówienia na prenumeratę można składać:

OR PAN, PKiN, 00-901 Warszawa

Nr konta bankowego: PBK IX Oddz. W-wa, 370031-4793

Wydawnictwa Politechniki Wrocławskiej
ma stałe na składzie Księgarnia Wr 49
Wybrzeże Wyspiańskiego 27, 50-370 Wrocław
oraz Wojewódzka Księgarnia Techniczna
ul. Świdnicka 8, 50-067 Wrocław

ISSN 0370-0828